# Insect flight dynamics: Stability and control

Mao Sun*

*Institute of Fluid Mechanics, Beijing University of Aeronautics and Astronautics, Beijing 100191, China*

(published 16 May 2014)

Insects can hover, fly forward, climb, and descend with ease while demonstrating amazing stability, and they can also maneuver in impressive ways as no other organisms can. Is their flight inherently stable? If so, how can they maneuver so well? In recent years, significant progress has been made in revealing the dynamic flight stability and flight control mechanisms of insects and has partially answered these questions. Here the most recent advances in this active area are reviewed. The aim is to provide the background necessary to do research in the area and raise questions that need to be addressed in the future. This review begins with an overview of the flapping kinematics and aerodynamics of insect flight. It is followed by a summary of the governing equations of insect motion and the simplified theoretical models used for analysis of dynamic stability and control. Next, the stability properties of hovering flight and forward flight are scrutinized. Then the flight control properties are explored, dealing in turn with flight stabilization control, steady-state control for changing from hovering to forward flight and from one forward-flight speed to another, and control for maneuvers near hovering. Finally, remarks are given on the state of the art of this research field and speculation is made on its outlook in the near future.

DOI: 10.1103/RevModPhys.86.615 PACS numbers: 87.85.gj, 47.85.Gj, 45.30.+s

## CONTENTS

I. Introduction 615
II. Flapping Kinematics and Aerodynamics 616
A. Flapping kinematics 616
B. Aerodynamic-force mechanisms 618
C. Aerodynamic models for flight dynamics studies 621
III. Governing Equations and Theoretical Models 622
A. Governing equations 622
B. Averaged model and linear theory 624
IV. Hovering-flight Stability Analysis 626
A. Aerodynamic derivatives and natural modes of motion 626
B. Reduced-order equations and physical interpretation of the natural modes of motion 628
C. Test of the averaged model by direct numerical simulation 631
D. Floquet stability analysis 632
E. Applicability of the linearization 632
F. The effect of wing deformation 633
V. Forward-flight Stability Analysis 633
VI. Stabilization Control Analysis 634
A. Controllability analysis 634
B. Closed-loop control analysis 635
VII. Steady-state Control 638
A. Steady-state control for changing from hovering to small-speed flight 638
B. Control for changing from one forward-flight speed to another 639
VIII. Maneuver Control 640
IX. Concluding Remarks 641
Acknowledgments 642
Appendix 642
References 642

*m.sun@buaa.edu.cn

## I. INTRODUCTION

Winged insects took to the air about $350 \times 10^6$ years ago (Wootton, 1981; Ellington, 1991). They have been experimenting with wings, kinematics, aerodynamics, sensory systems, and control since then. Natural selection has produced flies that complete 180° turns in as little as three wing strokes (Wakeling and Ellington, 1997) and species capable of landing on flowers buffeted by wind (Dudley, 2000). Besides curiosity about how these sophisticated aerodynamic feats are performed, researchers are interested in the mechanics of insect flight for the following two reasons. One is that biologists need to understand the effects of aerodynamic-force production, energy expenditure, and flight balance on the physiology, behavior, evolution, and other aspects of insects (Weis-Fogh and Jensen, 1956; Weis-Fogh, 1972; Ellington, Machin, and Casey, 1990; Dickinson *et al.*, 2000). The other reason is that engineers who desire to develop small robots with maneuverability comparable to that of flying insects are eager to understand the novel aerodynamic and control mechanisms of insects and emulate their performances in the design of small flying machines (Davis, 1996; Ellington, 1999; Shyy, Berg, and Ljungqvist, 1999; Wilson, 2001; Ma *et al.*, 2013).

The mechanics of insect flight broadly encompasses two aspects: aerodynamics and flight dynamics. Aerodynamics answers the questions of how the aerodynamic forces and moments, which support the weight of an insect, propel its motion in the air and control the motion, are produced, and what the energy expenditure is when producing these forces and moments. It also provides tools for computing the aerodynamic forces and moments and their variations as functions of wing and body motions.

Flight dynamics, on the other hand, includes dynamic flight stability and flight control. Dynamic flight stability of a flying

 © 2014 American Physical Society

body deals with the disturbed motion of the body about the equilibrium-flight state following an initial disturbance. If the disturbed motion dies out as time increases, the equilibrium flight is stable; otherwise, it is unstable. Dynamic stability is an inherent property of the flying system (no active control using sensory information is applied); it represents the natural flight dynamics of the flying body (it is also called passive stability or inherent stability). There are three types of flight control. One is stabilization control, which is used to stabilize inherently unstable flight or to augment the stability of weakly stable flight by applying time-varying control forces and moments to suppress the disturbed motion. The second is maneuver control, which is used to produce aerobatics, such as a fast turn, by applying large, time-varying control forces and moments. The third is steady-state control, which is used to change the system from one equilibrium flight to another, for example, changing from hovering flight to forward flight or from one forward-flight speed to another. For insects, stabilization control is generally performed by their reflex control systems because it requires very fast responses, while maneuver control and steady-state control are performed intentionally (Dickinson, 1999, 2006; Dudley, 2000; Bender and Dickinson, 2006; Taylor and Krapp, 2007).

Insects fly by flapping their wings (except for dragonflies and butterflies which occasionally glide). When studying insects' aerodynamics and/or flight dynamics, one needs to first know the flapping kinematics of the wings, i.e., wing motion relative to the body of the insect. Therefore, wing kinematics measurement and description are an integral part of aerodynamics and flight dynamics studies.

Historically, people studied the aerodynamics of insect flight prior to flight dynamics. This is because flight dynamics is a result of coupling between aerodynamics and motion (dynamics) of the insect and it could not be analyzed without understanding the mechanisms of aerodynamic-force production and knowing how the aerodynamic forces and moments vary as functions of wing and body motion. As a result, although aerodynamics of insect flight has been a subject of study for about 100 years (Weis-Fogh and Jensen, 1956; Ellington, 1995; Sane, 2003; Wang, 2005; Ansari, Zbikowski, and Knowles, 2006; Shyy *et al.*, 2010; Wu, 2011), only in the past 15 years or so have researchers begun to devote more effort to the area of flight dynamics.

In this review we describe the significant work done so far in the area of flight dynamics of insects. The aim is to point to unanswered questions in this area that will help in advancing knowledge on insect flight. Furthermore, it provides the background necessary to do research in the area. We begin with an overview of the flapping kinematics and aerodynamics of insect flight (Sec. II). We then summarize the governing equations of insect motion and the simplified theoretical models used for stability and control analysis (Sec. III). Next we scrutinize the stability properties of hovering flight (Sec. IV) and forward flight (Sec. V). Then we explore the flight control properties, dealing in turn with flight stabilization control (Sec. VI), steady-state controls for changing from hovering to forward flight and from one forward-flight speed to another (Sec. VII), and control for maneuvers near hovering (Sec. VIII). Finally, we remark on the state of the art of this research field and speculate on its outlook in the near future (Sec. IX).

## II. FLAPPING KINEMATICS AND AERODYNAMICS

### A. Flapping kinematics

Researchers have measured flapping kinematics of free hovering flight for more than ten species and free forward flight for a few species of insects; these insects include flies, mosquitoes, wasps, bees, moths, butterflies, beetles, and dragonflies (Weis-Fogh, 1973; Ellington, 1984c; Dudley and Ellington, 1900a, 1990b; Willmott and Ellington, 1997a, 1997b; Fry, Sayaman, and Dickinson, 2003, 2005; Altshuler *et al.*, 2005; Wang and Russell, 2007; Liu and Sun, 2008; Walker, Thomas, and Taylor, 2010). The following description of flapping kinematics follows the approach taken by Ellington (1984c) and is mainly based on the results for these insects.

Generally the flapping motion is approximately confined to a plane, termed a stroke plane (Fig. 1); the wings sweep back and forth reciprocally in the plane. The angle between the stroke plane and the horizontal is referred to as the stroke-plane angle and is denoted by $\beta$ (Fig. 1). The longitudinal axis of the body is at an angle $\chi$ from the horizontal ($\chi$ is referred to as the body angle). Let $(x_1, y_1, z_1)$ be a reference frame with the origin at the wing base and the $x_1$-$y_1$ plane coinciding with the stroke plane (Fig. 1). The position and orientation of the wing relative to the stroke plane can be described by three Euler angles when the wing is considered to be a rigid plate: positional angle ($\phi_w$), stroke deviation angle ($\theta_w$), and pitch angle ($\psi_w$) (Fig. 1), where $\phi_w$ is defined as the angle between the projection of the line joining the wing base and the wing tip onto the stroke plane and the $y_1$ axis, $\theta_w$ is defined as the angle between the line joining the wing base and the wing tip and its projection onto the stroke plane, and $\psi_w$ is defined as the angle between the local wing chord and the line $l$ ($l$ is perpendicular to the wing span and parallel to the stroke plane). $\psi_w$ is related to the angle of attack of the wing, $\alpha$ (see below).

For many insects (e.g., hoverflies, droneflies, and bumblebees), the angle between the stroke plane and the longitudinal axis of the body ($\beta + \chi$) is nearly constant (Ellington, 1984c; Ennos, 1989; Dudley and Ellington, 1900a; Liu and Sun, 2008) and for others this angle varies a little with flight conditions; e.g., for the hawk moth *Manduca sexta*, the angle increases from 55° at hovering to 75° at the highest flight speeds (Willmott and Ellington, 1997a).

The amplitude of $\phi_w$ is termed the stroke amplitude (denoted as $\Phi$) and the mean value of $\phi_w$ is termed the mean stroke angle (denoted as $\bar{\phi}$). $\Phi$ ranges from approximately 60° (for syrphid flies) to approximately 180° (for beetles and moths). For a given insect, $\Phi$ and $\bar{\phi}$ vary depending on the flight conditions, e.g., the flight speed (Ellington, 1984c; Willmott and Ellington, 1997a). In general, the stroke deviation angle $\theta_w$ is relatively small; its magnitude is below 10° (Ellington, 1984c; Ennos, 1989; Mou, Liu, and Sun, 2011), which is why one says that the flapping motion is generally approximately confined to the stroke plane. Fruit

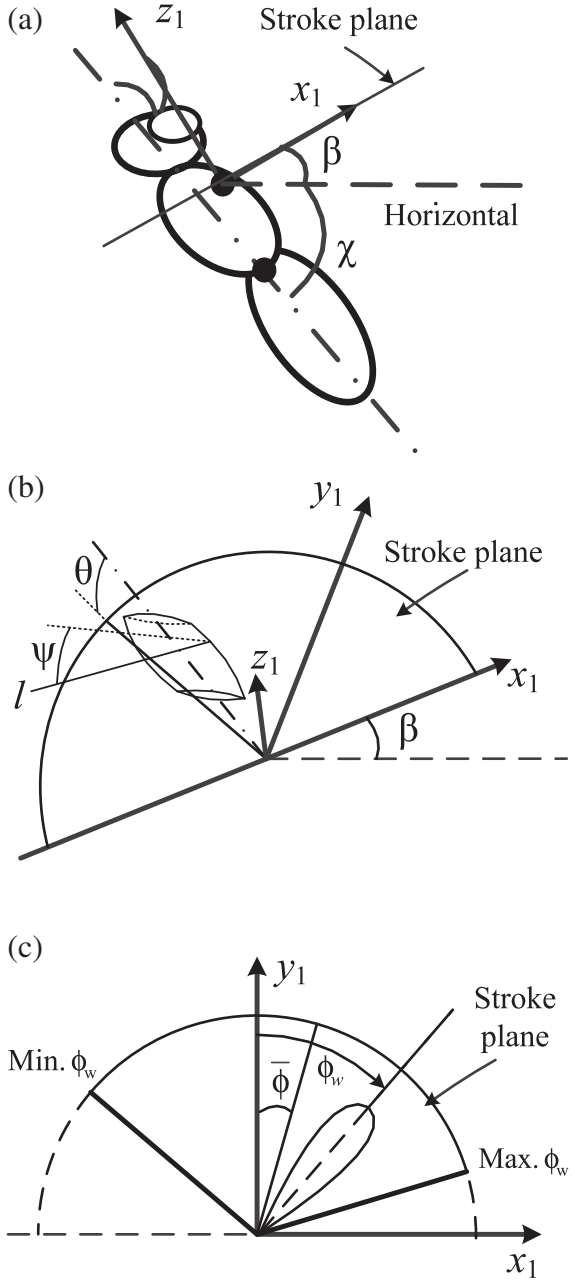


FIG. 1. (a) Sketch of insect body and stroke plane. Here $\beta$ is the stroke-plane angle; $\chi$ is the body angle. (b) Angles of a flapping wing that determine the wing orientation relative to the stroke plane. The $(x_1, y_1, z_1)$ coordinates are in a system with its origin at the wing root; the $y_1$ axis points to the side of the insect and the $x_1$-$y_1$ plane coincides with the stroke plane. $l$ is a line that is perpendicular to the wing span and parallel to the stroke plane. $\phi_w$, $\psi_w$, and $\theta_w$ are the positional angle, pitch angle, and deviation angle of the wing, respectively. $\psi_w$ is related to the angle of attack of the wing, $\alpha$, in the downstroke, $\alpha = \psi_w$, and in the upstroke, $\alpha = 180° - \psi$. (c) Sketch showing the stroke amplitude $\Phi = \max\ \phi_w - \min\ \phi_w$, and the mean stroke angle $\bar{\phi} = (\max\ \phi_w - \min\ \phi_w)/2$.

flies are an exception; for them $\theta_w$ is relatively large and can be as large as about 30° (Fry, Sayaman, and Dickinson, 2005).

During hovering flight, for some insects, the stroke plane is approximately horizontal ($\beta = 0$). Hovering with a horizontal stroke plane is referred to as normal hovering, and otherwise the hovering is referred to as inclined-stroke-plane hovering (Weis-Fogh, 1973). At normal hovering, in a forth (ventral) sweep, termed the downstroke, the wing forms an angle with the stroke plane (termed the angle of attack and denoted as $\alpha$) and lift can be produced. Near the end of the downstroke, the wing flips (rotates around a spanwise axis) and the underside of the wing becomes its top side and vice versa. In the following back (dorsal) sweep, the upstroke, the speed and angle of attack are the same as those in the downstroke and the wing produces the same amount of lift. Near the end of the upstroke, the wing flips back and starts another wing-beat cycle. The drag on the wing in the upstroke has the same magnitude as, but the opposite direction to, that in the downstroke. Thus the mean drag in a cycle is zero, i.e., the mean force vector is in the vertical direction, balancing the insect weight. $\alpha$ is related to $\psi_w$ as follows: in the downstroke $\alpha = \psi_w$; in the upstroke $\alpha = 180° - \psi_w$.

During forward flight, the stroke plane is tilted forward, which tilts the mean force vector forward; the horizontal component of the force vector overcomes the body drag of the insect (Ellington, 1984c; Dudley and Ellington, 1900a; Willmott and Ellington, 1997a). As the stroke plane tilts forward, the body angle becomes smaller (the angle between the stroke plane and the longitudinal axis of the body is generally fixed), which helps to decrease the body drag. By tilting the stroke plane backward or sideways, the insect can fly in the corresponding direction (Ellington, 1984c).

When the stroke plane is tilting forward (in forward flight and, for some insects, in hovering flight also), in the forth (ventral) sweep of the wing, the wing is actually moving forward and downward with respect to the insect body, which is the reason why the forth sweep is called a downstroke. For similar reasons, the back (dorsal) sweep is referred to as an upstroke. A downstroke or an upstroke is referred to as a half-stroke. As mentioned previously, in a half-stroke, the wing sweeps (rotates azimuthally) in the stroke plane; this motion is referred to as "translation." At stroke reversal, the wing rotates around a spanwise axis; this motion is referred to as "rotation."

In general, in the midportion of a half-stroke, the angle of attack of the wing varies relatively slowly and can be approximated by a constant, which is about 35° for many insects in normal hovering (Ellington, 1984c); at stroke reversal, the wing rotates by about 110°. The rotation time is approximately 20% of the wing-beat period. For a fruit fly, the wing-beat frequency is around 250 Hz (Ennos, 1989) and the mean rotation velocity of the wing exceeds 100 000° per second; for a hawk moth, the wing-beat frequency is around 25 Hz (Willmott and Ellington, 1997a), and the mean rotation velocity exceeds 10 000° per second. It should be noted that for some insects (e.g., dragonflies, some honeybees, and hoverflies in inclined-stroke-plane hovering) the stroke amplitude is low ($\Phi$ is 60°–90°) and the rotation time of a wing can be about 35% of the wing-beat period, i.e., the wing rotates in the bigger part (about 70%) of its translation (Norberg, 1975; Altshuler *et al.*, 2005; Mou, Liu, and Sun, 2011).

For many insects in normal hovering, the translational velocity can be closely approximated by a simple harmonic function, in which the maximum velocity occurs at the middle of the half-strokes and the maximum acceleration at the beginning of the half-strokes (Ellington, 1984c; Ennos,

1989; Liu and Sun, 2008; Mou, Liu, and Sun, 2011). For a fruit fly in tethered flight, it was observed that the translational velocity varied with time approximately according to a trapezoidal function (Zanker, 1990), i.e., the translational velocity is constant throughout a half-stroke, punctuated by rapid accelerations at stroke reversal. Compared to the simple harmonic function, the trapezoidal function exaggerates the acceleration at the beginning and the deceleration near the end of a half-stroke, and it also causes the acceleration at the beginning of the half-stroke to end earlier and the deceleration near the end of the half-stroke to start later. However, this pattern of wing translation, combined with proper wing-rotation timing, can create forces by all the mechanisms currently known to function on single wings (Dickinson, 1999). Therefore, in several experimental and computational studies, a translational velocity varying as a trapezoidal function was employed (Ramamurit and Sandberg, 2002; Sun and Tang, 2002; Birch and Dickinson, 2003; Wu and Sun, 2004).

When half the wing rotation is conducted near the end of a half-stroke and the other half at the beginning of the next half-stroke, the wing rotation is called symmetrical rotation. When the major part of rotation is conducted before the stroke reversal, it is called advanced rotation. And when the major part of rotation is conducted after the stroke reversal, it is called delayed rotation. The timing of the wing rotation can change the time course and the mean of the aerodynamic forces significantly, especially in the case of translational velocity varying as a trapezoidal function. Different timing of the wing rotation for the left and the right wings is possibly employed to provide control forces on the wings during maneuvering (Dickinson, Lehman, and Götz, 1993; Dickinson, Lehman, and Sane, 1999).

Some or all of the kinematic parameters, such as stroke amplitude, wing-beat frequency, or angle of attack of the wing, might vary with the flight speed (Vogel, 1966, 1967a; Dudley and Ellington, 1900a; Willmott and Ellington, 1997a). Bumblebees and hawk moths are the only insects for which these kinematic parameters have been measured over the entire speed range (Dudley and Ellington, 1900a; Willmott and Ellington, 1997a).

Insect wings are not rigid, and during flapping motion they deform and have small deviations from the rigid plane. From high-speed pictures of hovering and forward-flying insects, Ellington (1984c) and Ennos (1989) observed that for many insects the wings are twisted by 10º to 20º along their length, with a higher angle of attack at the wing base than at the tip (rather like the blades of a propeller), and they are gently cambered on both the downstroke and the upstroke. Fruit-fly wings, however, show negligible twist and camber; their small wings appear relatively stiffer than those of larger insects and hence more resistant to torsional twisting and camber deformation (Vogel, 1967a; Ellington, 1984c). These data are qualitative and because only one camera was used, reliable data could be obtained only for the midportion of a half-stroke. Recently, using four high-speed digital video cameras, Walker, Thomas, and Taylor (2010) obtained quantitative data on the time-varying camber and spanwise twist of wings in free-flying droneflies. Their data showed that camber and twist are approximately constant in the mid-half-stroke, similarly to the results described by Ellington (1984c) and Ennos (1989), and that around the stroke reversal the camber and twist are much larger than in the mid-half-stroke; Fig. 2 gives diagrams of wing motion showing the instantaneous wing profiles at two distances along the wing length in one half-stroke (upstroke) measured by Walker, Thomas, and Taylor (2010).

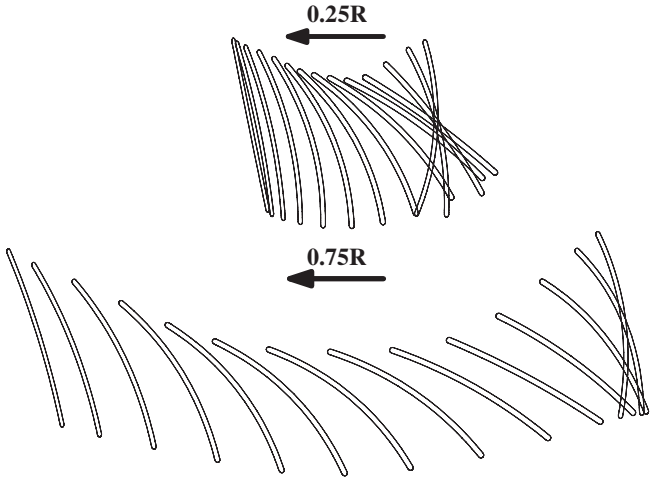


FIG. 2. Diagram of wing motion in the upstroke of a drone fly in hovering flight, showing the instantaneous wing profiles at 25% and 75% wing lengths ($R$). The arrow represents the direction of the wing motion. From Walker, Thomas, and Taylor, 2010.

### B. Aerodynamic-force mechanisms

A wing moving in the air experiences an aerodynamic force. Following the convention in aerodynamics, the force component normal to the direction of the far-field flow relative to the wing is referred to as lift ($L$), the force component in the direction of the flow is referred to as drag ($D$), and the angle between the direction of the flow and the wing is referred to as the angle of attack ($\alpha$) (Fig. 3). At the Reynolds numbers (Re) of insect wings (Re = 10 to 3000), $L$ and $D$ are proportional to $\rho U^2 S$, where $\rho$ is the air density, $U$ is the speed of the far-field flow relative to the wing, and $S$ is the wing area (for a flapping wing, Re is based on the mean chord length and the mean translational velocity at the radius of the second moment of the wing area, which is around $0.6R$ from the wing root for most insects, where $R$ is the wing length). The dimensionless $L$ and $D$ are referred to as lift ($C_L$) and drag ($C_D$) coefficients:

$$C_L(\alpha) = \frac{L}{0.5\rho U^2 S}, \qquad C_D(\alpha) = \frac{D}{0.5\rho U^2 S}. \tag{1}$$

Most of the results relevant to the aerodynamics of insect flight published before the 1950s were summarized in a critical review by Weis-Fogh and Jensen (1956). They reviewed many theories for aerodynamic analysis of insect flight, with detailed explanations for what they referred to as the most complete theories. These theories predicted that insects did not make use of unusual aerodynamic forces for their flight (that is, conventional, steady-state aerodynamic

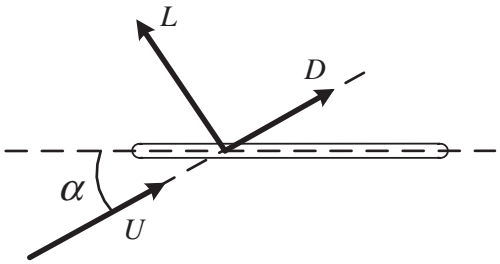


FIG. 3. Definition of aerodynamic lift and drag.

principles could explain the aerodynamic forces in insect flight). Research work on insect flight from the late 1950s to the early 1990s can be divided into three parts. One was the observation and analysis of the wing kinematics of insects in tethered and free flight (Vogel, 1966, 1967a; Ellington, 1984c; Ennos, 1989). The second part was measurements of the aerodynamic forces on real and model wings and the bodies of insects in wind tunnels in steady-state and fixed-wing conditions (Vogel, 1967b; Okamoto, Yasude, and Azuma, 1996). The third part was calculation, under the assumption of a quasisteady state, of the lift and power of insects based on the observed wing kinematics and the measured aerodynamic-force coefficients (Weis-Fogh, 1972, 1973; Ellington, 1984a, 1984d, 1984e). The calculation showed whether or not the conventional aerodynamic theory can explain the aerodynamic forces of insect flight. As an example, we considered the measured lift and drag coefficients at various angles of attack for a fruit-fly wing, as illustrated in Fig. 4 (Vogel, 1967b). The Reynolds number is 200. At $\alpha = 10°$, the $C_L$ value is only 0.23, much smaller than that of a wing at high Re. The maximum $C_L$ is around 0.6 (Fig. 4). Even if the maximum $C_L$ is used in the quasisteady-state theory, the estimated lift is not enough to support the weight of a fruit fly (Ellington, 1984a; Ennos, 1989; Zanker, 1990); this is also the case for many other insects (Ellington, 1984a, 1984d, 1984e). Typically the mean $C_L$ required to balance the weight of an

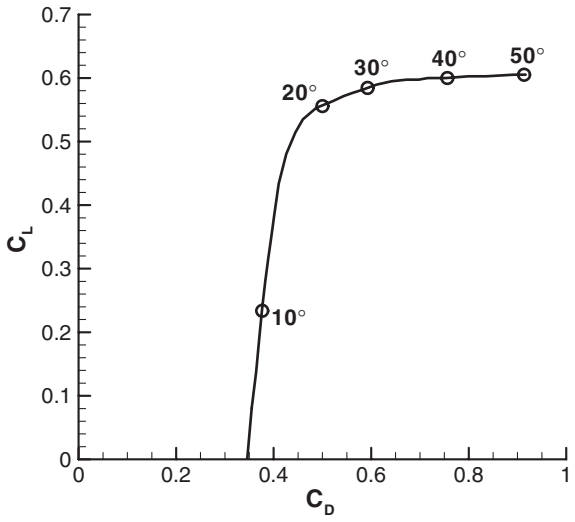


FIG. 4. Polar diagram of a fruit-fly (*Drosophila virilis*) wing. The angle of attack is given in degrees along the curve. Adapted from Vogel, 1967b.

insect is about 1.5 (Sun, Wang, and Xiong, 2007), much larger than that of an airplane at cruising flight, which is about 0.7 (the velocity relative to the air of an insect wing is small due to the small length scale of the wing and hence the required nondimensional lift is large). These works clearly showed that steady-state aerodynamic theory cannot explain the aerodynamic-force generation of most insects, and, as a result, it was concluded that unsteady aerodynamic mechanisms must be operating.

The work showing that most insects must use unsteady aerodynamics to fly was conducted in the 1980s. Earlier, in the 1970s, when studying the flight of the small wasp *Encarsia formosa*, Weis-Fogh (1973) discovered that before the downstroke the two wings "clap" together and then open like a book (referred to as the "fling"). The Reynolds number of the wing is only around 15. Weis-Fogh (1973) suggested that the fling motion of the wing pair might cause the necessary circulation to be generated immediately because one wing with its circulation acted as the starting vortex of the other wing and vice versa, avoiding the delay due to the Wagner effect (Wagner, 1925; Walker, 1931). Lighthill (1973) modeled the fling phase using two-dimensional inviscid theory. He showed that a circulation proportional to the angular velocity of the fling was generated without the delay associated with the Wagner effect. Maxworthy (1979), by a flow-visualization experiment on a pair of wings, discovered that during the fling process a leading-edge vortex is generated by each wing and its circulation is substantially larger than that calculated by Lighthill's theory. The clap and fling mechanism is a typical example of unsteady lift generation. Besides *Encarsia formosa*, the only insects known to use the clap and fling mechanism are some butterflies during their takeoff (Sunada *et al.*, 1993). Although most insects do not employ this motion (Ellington, 1984c; Ennos, 1989; Fry, Sayaman, and Dickinson, 2005; Fontaine *et al.*, 2009), its study made researchers reconsider the aerodynamics of insect flight. The studies by Lighthill (1973), Weis-Fogh (1973), and Maxworthy (1979) on the clap and fling mechanism pioneered the study of unsteady flows of insect flight and inspired researchers to continue the study in the years to come.

It could be said that, in the 1980s and before, research on insect flight was mainly on the analysis of wing kinematics and on exploring whether or not the conventional steady-state aerodynamic theory was applicable. Entering the 1990s, researchers began to put forth more effort to explore the unsteady flows in insect flight (Ellington, 1995).

Since at the beginning of each half-stroke the wing is started at a high angle of attack, dynamic stall (stall delayed for a short time) was considered as a candidate for explaining the extra lift of insect wings. Dickinson, Lehman, and Götz (1993) measured the aerodynamic forces of an airfoil started rapidly at high angles of attack in the Reynolds number range of fruit-fly wings (Re = 75–225). They showed that lift is enhanced by the presence of a dynamic-stall vortex or leading-edge vortex (LEV). After the initial start, a $C_L$ as high as 2 is maintained within approximately two to three chord lengths of travel. Afterward, $C_L$ drops due to the shedding of the LEV. But the decrease is not rapid, because the shedding of the LEV is slow at such low Re; and from three to five chord lengths of travel, the $C_L$ is still as high as approximately 1.7 (at higher

Re, $C_L$ drops faster). They considered that because the fly wing typically moved only two to four chord lengths each half-stroke, the stall-delaying behavior was more appropriate for models of insect flight than were the steady-state approximations.

Ellington *et al.* (1996) and van den Berg and Ellington (1997a, 1997b) performed flow-visualization studies on the large hawk moth *Manduca sexta* in tethered forward flight (the speed ranged from 0.4 to 5.7 $m\,s^{-1}$) and on a mechanical model of the hawk-moth wings (Re $\approx$ 3500). They found that the LEV on the wings is not shed in the translational phases of the half-strokes and that there is a spanwise flow directed from the wing base to the wing tip; Fig. 5 shows a picture of the LEV. Analysis of the momentum imparted to fluid by the vortex wake showed that the LEV could produce enough lift for weight support. In the case of hovering flight, the hawk-moth wing travels approximately three chord lengths each half-stroke; whereas, in the case of forward flight at high speeds, the wing travels twice as far. They suggested that the spanwise flow prevented the LEV from detaching.

The above studies identified delayed stall as a high-lift mechanism of some small and large insects. Dickinson (1999) measured the aerodynamic forces on a revolving model fruit-fly wing (Re $\approx$ 75) and showed that large lift and drag are maintained and stall does not occur. Usherwood and Ellington (2002a, 2002b) measured the aerodynamic forces on revolving real and model wings of various insects and a bird (quail) and, for some of the cases, flow visualization was also conducted. They found that large aerodynamic forces are maintained by the attachment of the LEV for values of Re $\approx$ 600 (mayfly) to 15 000 (quail) and for different wing plan forms. These results further showed that the delayed-stall mechanism is valid for most insects [$R$ ranging from 2 mm (fruit fly) to 50 mm (hawk moth)]. The delayed-stall mechanism was confirmed by flow-field measurements on real insects (Bomphrey *et al.*, 2005) and by computational fluid dynamics (CFD) analyses (Liu and Kawachi, 1998; Liu *et al.*, 1998; Wang, 2000a, 2000b; Lan and Sun, 2001; Sun and Wu, 2004). The flow-field measurement and CFD results also explained how the LEV attachment could be maintained.

Dickinson, Lehman, and Sane (1999) and Sane and Dickinson (2001) measured the aerodynamic forces on a mechanical model of a fruit-fly wing in flapping motion. They showed that when the translational velocity varies according to a trapezoidal function with large accelerations at stroke reversal and the wing rotation is advanced, in addition to the large lift during the translational phase of a half-stroke (which is due to the delayed-stall mechanism), large lift peaks occur at the beginning and near the end of the half-strokes. Dickinson, Lehman, and Sane (1999) suggested that the large lift peak at the beginning of the half-stroke was due to the wake-capture mechanism (see below) and that near the end of the half-stroke was due to the effect of wing rotation. Ramamurit and Sandberg (2002) and Sun and Tang (2002) simulated the flows of model fruit-fly wings using the CFD method, based on wing kinematics nearly identical to those used in the experiment of Dickinson, Lehman, and Sane (1999). They obtained qualitatively similar results to those of the experiment. Sun and Tang (2002), on the basis of the computed vorticity fields and vortex dynamics theory (Wu, 1981), showed that the large force peak near the end of the half-stroke can be explained by the generation of strong vorticity in a short time due to the fast pitching-up rotation of the wing, confirming the suggestion of Dickinson, Lehman, and Sane (1999) (the "pitching-up rotation mechanism"). Their analysis further showed that the large force peak at the beginning of the half-stroke is mainly due to the added-mass effect that resulted from the rapid translational acceleration of the wing (the "rapid-acceleration mechanism"). Birch and Dickinson (2003) measured the forces and flows of the model fruit-fly wing, and by comparing the results of the first stroke (in the absence of wake effects) with those of the fourth stroke (in the presence of the wake of the prior strokes), they showed that the force peak at the beginning of the stroke is partially contributed to by the interaction between the wing and the wake left by the previous strokes (the "wake-capture mechanism"). The wake-capture phenomenon (an increase of the effective fluid velocity due to the vortex wake shed by the previous stroke) was first shown to exist for a two-dimensional wing in a simplified flapping motion (Dickinson, 1994). A relatively small portion of the large force peak at the beginning of the half-stroke could have been produced by the wake-capture mechanism.

In the above, four unsteady high-lift mechanisms have been identified, i.e., the delayed stall, the rapid acceleration (or added mass), the rapid-pitching-up rotation, and the wake capture. However, it should be noted that the rapid-acceleration and rapid-pitching-up-rotation mechanisms are significant only in the case when acceleration at the beginning and deceleration near the end of a stroke are very large (i.e., the translational velocity varies as a trapezoidal function) and the wing rotation is advanced, and that the lift enhancement by the wake-capture mechanism is relatively small and limited to a short time (Birch and Dickinson, 2003; Wu and Sun, 2005). For many insects in free flight, the translational velocity of the wing varies with time approximately according to a simple harmonic function and the wing rotation is symmetrical (Ellington, 1984c; Ennos, 1989; Dudley and Ellington, 1900a; Willmott and Ellington, 1997a; Fry, Sayaman, and Dickinson, 2005; Liu and Sun, 2008; Walker, Thomas, and Taylor, 2010). Under these conditions, the lift peak at the beginning of the half-stroke would almost disappear, because the acceleration there is not very large, and furthermore the wing is conducting pitching-down rotation which acts to decrease the lift (Sun and Tang, 2002). The lift peak near the end of the stroke would be smaller, because the wing conducts

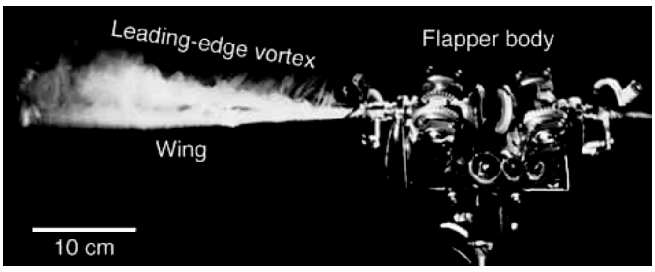


FIG. 5. Flow visualization of the LEV over a model hawk-moth wing (smoke was released from the leading edge). From Ellington, 1999.

rapid pitching-up rotation at a much lower translational speed. Thus most of the aerodynamic force would be produced in the midportion of a half-stroke when translation velocity is relatively high, by the delayed-stall mechanism. This has been confirmed by several experimental and computational investigations (Sun and Du, 2003; Wang, Birch, and Dickinson, 2004; Fry, Sayaman, and Dickinson, 2005; Ramamurit and Sandberg, 2007; Aono, Liang, and Liu, 2008). However, for insects with relatively low stroke amplitude, e.g., for some honeybees, the translational phase, during which the delayed-stall mechanism is acting, is relatively short, and the other mechanisms are also important: measurements on a dynamically scaled robot showed that the kinematics of honeybee wings generate prominent force peaks during the beginning, middle, and end of each half-stroke (Altshuler *et al.*, 2005). For insects in fast maneuvers, different timing of wing rotation for the left and the right wings is possibly employed to provide large control forces and moments, and the other mechanisms might also play an important role in generating the required forces and moments.

The wings of most insects are corrugated and, in flapping motion, they undergo time-varying deformation (Ellington, 1984c; Ennos, 1989; Walker, Thomas, and Taylor, 2010). Researchers have studied the structural properties of corrugated insect wings and have shown that corrugation gives a flapping wing the advantages of low mass, high stiffness, and low membrane stress, and that because of the arrangement of the veins, in general, the flapping wing mainly has camber deformation and spanwise twist deformation (Rees, 1975; Newman and Wootton, 1986; Ennos, 1988), which is confirmed by the observation of freely flying insects (Ellington, 1984c; Ennos, 1989; Walker, Thomas, and Taylor, 2010). Zhao *et al.* (2010) conducted an experimental study on aerodynamic effects of wing deformation, using model wings with "assumed" time-varying wing deformation and showed that the deforming wing could generate forces nearly the same as or even higher than the rigid model wing. Young *et al.* (2009) conducted a computational study, using measured time-varying wing deformation (wing twist and camber) of a tethered locust in a wind tunnel, and showed that the power economy in locust forward flight is significantly increased by wing deformation. Du and Sun (2010) investigated the effect of wing deformation (wing twist and camber) on aerodynamic forces in freely hovering hoverflies, using the data of Walker, Thomas, and Taylor (2010) on realistic wing deformation, and showed that deformation increased the lift by about 10% and drag by about 3%, and decreased the aerodynamic power required to generate the lift by about 5%, compared with those of the rigid flat-plate wing. They also showed that the lift increase is mainly due to wing camber and the power reduction is mainly due to wing twist. Although 10% lift and 3% drag increases do not have a very large effect on flight force balance, the effect on the power economy is not small: a 10% increase in lift, allied with a 5% reduction in aerodynamic power to generate that lift, could significantly enhance flight performance. The results of both Young *et al.* 2009)) and Du and Sun (2010) showed that, although deformation produces some quantitative changes in aerodynamic forces and power requirements, the wing used the same unsteady aerodynamic mechanisms as those of a rigid, flat-plate wing to produce the forces.

In the above studies on deforming wings (Young *et al.*, 2009; Du and Sun, 2010; Zhao *et al.*, 2010), wing corrugations were not included. Du and Sun (2012) added corrugation to the deforming hoverfly wing discussed above and showed the following. When acting alone, the effect of wing deformation is to increase the lift by about 9.7% and decrease the torque (or aerodynamic power) by 5.2%, and the effect of wing corrugation is to decrease the lift by 6.5% and increase the torque by 2.2%. But when acting together, the wing deformation and corrugation increased the lift by only ∼3% and decreased the torque by ∼3%. That is, the combined aerodynamic effect of deformation and corrugation is rather small. Thus, wing corrugation is mainly for structural, not aerodynamic, purposes. In computing or measuring the aerodynamic forces, using a rigid flat-plate wing to model the corrugated deforming hoverfly wing can be a good approximation. In the existing studies on insect flight dynamics, rigid flat-plate wings were employed to model real insect wings.

### C. Aerodynamic models for flight dynamics studies

When studying flight dynamics, one needs to know how the aerodynamic forces and moments vary as functions of wing and body motion, and models for computing aerodynamic forces and moments are required. Aerodynamic models for flight dynamics studies are generally divided into two areas: simple aerodynamic models and CFD models.

Early simple models (Weis-Fogh, 1972) are the same as those used for helicopter rotors and propellers, which are based on quasisteady approximations. According to the quasisteady approximation, the instantaneous aerodynamic forces on a flapping wing are equal to the forces during steady motion of the wing at an identical instantaneous velocity and angle of attack (Ellington, 1984a). According to this method, any time dependence of the aerodynamic forces arises from the time dependence of the kinematics but not the fluid flow itself. These quasisteady models fell short of calculating even the required average lift for hovering, and substantial revision of the quasisteady theory was therefore necessary (Ellington, 1984a). With the newly acquired insights into the unsteady aerodynamics of insects' flapping wings, researchers had developed models which included the key unsteady-flow mechanisms. Sane and Dickinson (2002) developed a revised quasisteady model, which has been used in many flight dynamics studies. In this model, the instantaneous forces generated by a thin, flapping wing are represented as a sum of four force components, each acting normal to the wing surface (frictional force on the surface is neglected):

$$\mathbf{F}_{\text{inst}} = \mathbf{F}_a + \mathbf{F}_{\text{trans}} + \mathbf{F}_{\text{rot}} + \mathbf{F}_{\text{wc}}, \tag{2}$$

where $\mathbf{F}_{\text{inst}}$ is the instantaneous aerodynamic force on the wing, $\mathbf{F}_a$ is the force due to the wing acceleration, i.e., due to the added-mass effect, $\mathbf{F}_{\text{trans}}$ is the instantaneous translational force due to the translational mechanism of delayed stall, $\mathbf{F}_{\text{rot}}$ is the force due to wing rotation, and $\mathbf{F}_{\text{wc}}$ is the force due to wake capture. The first term $\mathbf{F}_a$ is calculated for each blade

element using the existing formula of added-mass force for airfoils and integrated along the span of the wing to estimate the added-mass force on a three-dimensional wing. The second term $\mathbf{F}_{\text{trans}}$ is obtained through the vector addition of the mutually orthogonal lift and drag estimates from the revolving-wing experiment (Dickinson, 1999):

$$C_L(\alpha) = 0.225 + 1.58\sin(2.13\alpha - 7.2), \tag{3}$$

$$C_D(\alpha) = 1.92 - 1.55\cos(2.04\alpha - 9.82), \tag{4}$$

where $\alpha$ is in degrees. For the third term $\mathbf{F}_{\text{rot}}$, a rotational force coefficient is determined by subtracting the measured force of a revolving wing without rotation from that of a revolving wing with rotation, or alternatively determined from the results of thin-airfoil theory (Fung, 1969):

$$\mathbf{F}_{\text{rot}} = \rho U \Gamma_{\text{rot}}, \tag{5}$$

where $\Gamma_{\text{rot}}$ is the rotational circulation, $\rho$ is the fluid density, and $U$ is the translational velocity of the wing section; $\Gamma_{\text{rot}}$ is given by

$$\Gamma_{\text{rot}} = C_{\text{rot}}\omega c^2, \tag{6}$$

where $\omega$ is the angular velocity of the wing section, and the rotational coefficient $C_{\text{rot}}$ is given by

$$C_{\text{rot}} = \pi(0.75 - \hat{x}_0), \tag{7}$$

where $\hat{x}_0$ is the nondimensional axis of rotation. The fourth term $\mathbf{F}_{\text{wc}}$ is not given by Sane and Dickinson (2002); it is not readily determined. Because the effect of wake capture is relatively small and limited to a short time, this term is neglected in flight dynamics studies that employ this model (Dickson, Straw, and Dickinson, 2008; Faruque and Humbert, 2010a, 2010b). Pesavento and Wang (2004) and Berman and Wang (2007) developed a model which is similar to that of Sane and Dickinson (2002), but does not have the wake-capture term and includes a viscous force term.

The above two models rely on experimental data to determine the coefficients of the translational force due to the delayed-stall mechanism. Zbikowski (2002), Yu, Tong, and Ma (2003), Ansari, Zbikowski, and Knowles (2006), and Zbikowski, Ansari, and Knowles (2006) developed semi-analytical models with no empirical fixes. A wing section was represented by a flat plate with separated flow at both leading and trailing edges, and the Laplace equation for unsteady inviscid flow was solved by modeling the wing section as an array of sources or sinks (or alternatively by a conformal-mapping method), while the separated flow was comprised of "free" point vortices. A time-marching algorithm was employed whereby a pair of point vortices—one each at the leading and trailing edges—was introduced at each time step and the wake due to the free vortices was convected (Yu, Tong, and Ma, 2003; Ansari, Zbikowski, and Knowles, 2006). Results of each section were integrated along the span of the wing to obtain a flow solution for a three-dimensional wing (Zbikowski, 2002; Ansari, Zbikowski, and Knowles, 2006). In these semianalytical models, a LEV develops automatically and the added-mass, wing-rotation, and wake-capture effects are included. However, they are much more computationally costly than the simple models discussed above, and furthermore the LEV development may not be very accurately calculated because viscous effects are neglected and the axial flow of the LEV is absent. Thus these models may not be very suitable for flight dynamics analysis. However, because they are analytical in nature and can clearly show the aerodynamic contributions and the underlying flow physics of various flow components, they are powerful in revealing aerodynamic-force mechanisms (Yu, Tong, and Ma, 2003; Ansari, Zbikowski, and Knowles, 2006).

CFD models directly solve the Navier-Stokes equations by numerical methods to determine the aerodynamic forces and moments (Liu and Kawachi, 1998; Wang, 2000a, 2000b; Sun and Tang, 2002). The only assumptions made are that the flow is incompressible and laminar. The flow speed is low (Mach number about 0.02) and the characteristic length of an insect is by about 2 orders of magnitude smaller than the wavelength of the sound generated by the flapping wings, justifying the incompressible-flow assumption. The Reynolds number of the flows around the wing is low (Re = 10 to 3000) and hence at least in the near field the flow is laminar. Thus CFD models capture all the unsteady and viscous flow phenomena and calculate aerodynamic forces and moments with good accuracy. It is interesting to note that CFD methods were originally developed to compute complex flows of aircraft, but because of the lack of a proper turbulence model, separated flows, wake flows, and many other complex flows of aircraft still cannot be calculated. However, they can calculate the flow around an insect wing with good accuracy because there is no turbulence problem. The major disadvantages of CFD models are that they are computationally costly and are difficult to handle.

## III. GOVERNING EQUATIONS AND THEORETICAL MODELS

### A. Governing equations

Equations of motion for a model insect with a body and $N$ rigid wings, with wing motion relative to the body prescribed, were derived by Gebert, Gallmeier, and Evers (2002), but simulations were not presented to validate the efforts. Sun, Wang, and Xiong (2007) noted that the equations of Gebert, Gallmeier, and Evers (2002) contain errors and cannot be used and they rederived the equations. Dickson, Straw, and Dickinson (2008) presented simulation efforts for the flight dynamics of a model fruit fly. Their method used physics engine software (similar to that used to make video games and animated features) to model the body and wings, but equations of motion were not presented. In the derivation by Gebert, Gallmeier, and Evers (2002) and Sun, Wang, and Xiong (2007), three right-handed frames of reference are used in the derivation (Fig. 6): Frame $(x_E, y_E, z_E)$ is an inertial frame (a frame fixed on the Earth); $x_E$ is in the horizontal direction and $z_E$ in the vertical direction. Frame $(x_b, y_b, z_b)$ is a frame fixed on the insect body with its origin at the center of mass of the wingless body; $x_b$ and $z_b$ are in the longitudinal symmetrical plane, and $y_b$ points to the right side of the insect. Frame

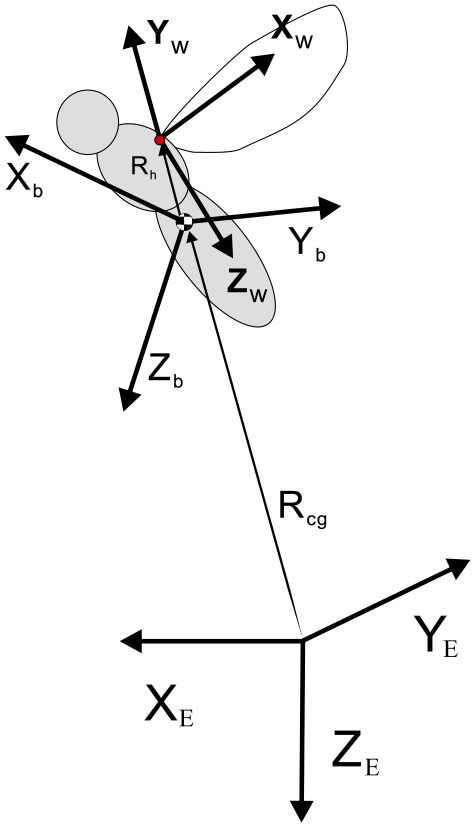


FIG. 6 (color online). Reference frames and sketch of insect body and wings. $(X_E, Y_E, Z_E)$ is a frame fixed on the Earth. $(x_b, y_b, z_b)$ is a frame fixed on the insect body with its origin at the center of mass of the insect body. $(x_w, y_w, z_w)$ is a frame fixed on the wing, with its origin at the wing root, the $x_w$ axis along the wing span and the $z_w$ axis along the chordwise direction. $\mathbf{R}_{cg}$ is the vector of the center of mass of the body relative to the Earth's frame; $\mathbf{R}_h$ is the vector of the wing root relative to the body frame. Adapted from Sun, Wang, and Xiong, 2007.

$(x_w, y_w, z_w)$ is a frame fixed on each of the wings of the insect with its origin at the root of the wing; $x_w$ is in the spanwise direction, pointing to the wing tip, and $z_w$ is in the chordwise direction, pointing to the trailing edge of the wing. With respect to the inertial frame, the center of mass of the wingless body moves at velocity $\mathbf{v}_{cg}$, and the body rotates at angular velocity $\boldsymbol{\omega}_{bd}$ (the angular velocity of the wing relative to the body is prescribed). Let $\mathbf{F}_A$ be the total aerodynamic force, $\mathbf{M}_A$ the total aerodynamic moment about the center of mass of the body, $m$ the total mass of the insect (body mass plus wing mass), $m_{wg}$ the mass of a wing, $\mathbf{I}_{bd}$ the matrix of moments and products of inertia of the body, $\mathbf{R}_{cg}$ the vector of the center of mass of the body relative to the Earth frame, $\mathbf{R}_h$ is the vector from the body center of mass to the root of a wing, $\mathbf{R}_{wg}$ the vector from the wing root to the center of mass of a wing, $\mathbf{g}$ the gravitational acceleration, and $t$ the time. Let ${}_b\mathbf{v}_{cg}$, ${}_b\boldsymbol{\omega}_{bd}$, and ${}_b\mathbf{F}_A$, etc., represent the $x_b$, $y_b$, and $z_b$ components of $\mathbf{v}_{cg}$, $\boldsymbol{\omega}_{bd}$, and $\mathbf{F}_A$, etc., respectively. The equations of motion written in the frame $(x_b, y_b, z_b)$ are (Sun, Wang, and Xiong, 2007)

$$\mathbf{F}_A + m\mathbf{g} = m\left(\frac{d\mathbf{v}_{cg}}{dt} + \boldsymbol{\omega}_{bd} \times \mathbf{v}_{cg}\right) + \mathbf{a}_1 + \mathbf{b}_1, \tag{8}$$

$$\mathbf{M}_A + \sum_{i=1}^{N} \left[m_{wg}\left(\mathbf{R}_h + \mathbf{R}_{wg}\right) \times \mathbf{g}\right]_i = \boldsymbol{\omega}_{bd} \times (\mathbf{I}_{bd} + \mathbf{c})\boldsymbol{\omega}_{bd} + (\mathbf{I}_{bd} + \mathbf{c})\frac{d\boldsymbol{\omega}_{bd}}{dt} + \mathbf{a}_2 + \mathbf{b}_2, \tag{9}$$

where the subscript $b$ of ${}_b\mathbf{v}_{cg}$, ${}_b\boldsymbol{\omega}_{bd}$, and ${}_b\mathbf{F}_A$, etc., has been dropped for simplicity; expressions for $\mathbf{a}_1$, $\mathbf{a}_2$, $\mathbf{b}_1$, $\mathbf{b}_2$, and $\mathbf{c}$ are given in the Appendix: $\mathbf{a}_1$ represents the inertial force of the wing mass due to the rotation and angular acceleration of the body, and $\mathbf{b}_1$ represents the inertial force of the wing mass due to the rotational acceleration of the wings and the gyroscopic force due to the wing and body rotations; $\mathbf{a}_2$ and $\mathbf{b}_2$ represent the corresponding moments; $\mathbf{c}$ represents the time-varying moments and products of inertia of the flapping wings with respect to the body frame $(x_b, y_b, z_b)$. The second term on the left-hand side of Eq. (9) is the moment about the center of mass of the body due to the weight of the wings. Note that when there are no flapping wings, $m_{wg}$, $\mathbf{a}_1$, $\mathbf{a}_2$, $\mathbf{b}_1$, $\mathbf{b}_2$, and $\mathbf{c}$ are zero and Eqs. (8) and (9) become the equations of rigid-body motion that are widely used in aircraft flight dynamics (Johnson, 1980; Etkin and Reid, 1996; Padfield, 1996).

The wing motion (flapping motion) with respective to the body is prescribed. The independent variables in the equations of motion are the velocity of the body center of mass $\mathbf{v}_{cg}$, the angular velocity of the body $\boldsymbol{\omega}_{bd}$, and the angles which determine the orientation of the body; they are called state variables. Because of the flapping motion of the wings, their aerodynamic and inertial forces oscillate with a frequency equal to the wing-beat frequency. Compelled by these forces, the insect body has oscillations around its gross motion (flight path), as observed in freely flying insects ( Ellington, 1984c; Wakeling and Ellington, 1997; Hedrick and Daniel, 2006; Liu and Sun, 2008). Therefore, the system is a nonlinearly time-variant system. Letting $\mathbf{x} = [\mathbf{v}_{cg}\boldsymbol{\omega}_{bd}]^T$, the equations of motion [Eqs. (8) and (9)] are ordinary differential equations of the form

$$d\mathbf{x}/dt = f(\mathbf{x}, t). \tag{10}$$

The aerodynamic force and moment vectors in Eqs. (8) and (9), $\mathbf{F}_A$ and $\mathbf{M}_A$, are determined by the Navier-Stokes equations

$$\nabla \cdot \mathbf{u} = 0, \tag{11}$$

$$\frac{\partial \mathbf{u}}{\partial t} + \mathbf{u} \cdot \nabla \mathbf{u} = -\frac{1}{\rho}\nabla p + \nu \nabla^2 \mathbf{u}, \tag{12}$$

where $\mathbf{u}$ is the fluid velocity, $p$ is the pressure, $\rho$ is the density, $\nu$ is the kinematic viscosity, $\nabla$ is the gradient operator, and $\nabla^2$ is the Laplacian operator.

The motion (equilibrium flight and perturbation motion) of an insect is governed by the equations of motion [Eqs. (8) and (9)] coupled with the Navier-Stokes equations [Eqs. (11) and (12)]. It should be noted that in deriving Eqs. (8) and (9) the insect is assumed to have a rigid body and $N$ rigid wings. For some large insects, e.g., butterflies, there is relative motion between the abdomen and the thorax (Betts and Wootton, 1988; Dudley, 1990), and furthermore the wing deformations

are relatively large (Sunada *et al.*, 1993). In these cases, the equations of motion need rederivation to include these factors.

### B. Averaged model and linear theory

Similarly to a flying insect, a helicopter in forward flight [its blade encounters periodically varying relative velocity and hence produces periodic aerodynamic forces (Johnson, 1980)] or an airplane with wings of high aeroelasticity (Bryson, 1994) is also a nonlinear time-variant dynamic system. For such a system, the oscillating mass distribution and the periodic aerodynamic and inertial forces associated with the oscillating wings (or rotation blades) can couple with the body's natural modes of motion. But if the frequencies of aeroelastic flutter or blade rotation are sufficiently high compared to the aircraft's natural frequencies of motion, such a coupling is unlikely to occur. In this case, the variations in forces at the frequencies of the aeroelastic flutter or blade rotation will then not exhibit resonance with the aircraft's gross motion and one may consider replacing the forces by wing-flutter-cycle (or blade-rotation-angle) average forces, which might vary over the time scale of the gross motion of the aircraft. This is the basis of the averaged model introduced by Hohenemser (1939) to simplify the flight dynamics of helicopters. This model is now commonly used to make problems of stability and control analytically tractable in rotary (Johnson, 1980; Padfield, 1996) and fixed-wing (Bryson, 1994; Etkin and Reid, 1996) aircraft. With this model, the equations of motion become the equations of rigid-body motion, or Euler's equations of motion, which are widely used in aircraft flight dynamics (Etkin and Reid, 1996):

$$\mathbf{F} + m\mathbf{g} = m\frac{d\mathbf{v}}{dt} + \boldsymbol{\omega} \times \mathbf{v}, \tag{13}$$

$$\mathbf{M} = \boldsymbol{\omega} \times \mathbf{I} \times \boldsymbol{\omega} + \mathbf{I}\frac{d\boldsymbol{\omega}}{dt}, \tag{14}$$

where $\mathbf{F}$ and $\mathbf{M}$ represent the aerodynamic force and moment, respectively, and $\mathbf{v}$ is the velocity of the center of mass, $\boldsymbol{\omega}$ is the angular velocity of the body, $m$ is the mass of the body, and $\mathbf{I}$ is the matrix of moments and products of inertia of the body. Now the system becomes an autonomous one, represented by differential equations of the form $dx/dt = f(\mathbf{x})$.

The majority of the existing studies on insect flight dynamics (Taylor and Thomas, 2002, 2003; Schenato, 2003; Sun and Xiong, 2005; Deng, Schenato, and Sastry, 2006a; Zbikowski, Ansari, and Knowles, 2006) have employed the averaged model, assuming that the wing-beat frequency is relatively high compared to the insect's natural frequency of motion, and Eqs. (13) and (14) are used, instead of Eqs. (8) and (9). Using the assumptions of the averaged model, Eqs. (13) and (14) can be derived formally from Eqs. (8) and (9). The derivation clearly shows the simplification process of the averaged model: Let the overbar denote the mean value (wing-beat-cycle average value) and the symbol $\wedge$ denote the difference between the instantaneous and mean values (e.g., $\mathbf{v}_{cg} = \bar{\mathbf{v}}_{cg} + \hat{\mathbf{v}}_{cg}$). Taking the time average (average over the wing-beat-cycle period) of Eqs. (8) and (9) gives (Sun, Wang, and Xiong, 2007)

$$\bar{\mathbf{F}}_A + m\mathbf{g} = m\left(\frac{d\bar{\mathbf{v}}_{cg}}{dt} + \bar{\boldsymbol{\omega}}_{bd} \times \bar{\mathbf{v}}_{cg} + \overline{\hat{\boldsymbol{\omega}}_{bd} \times \hat{\mathbf{v}}_{cg}}\right) + \bar{\mathbf{a}}_1 + \bar{\mathbf{b}}_1, \tag{15}$$

$$\begin{aligned}\bar{\mathbf{M}}_A + \sum_{i=1}^{N}[m_{wg}\bar{\mathbf{R}}_{wg} \times \mathbf{g}]_i = {} & \bar{\boldsymbol{\omega}}_{bd} \times \bar{\mathbf{I}}_{b\text{-}w}\bar{\boldsymbol{\omega}}_{bd} + \overline{\hat{\boldsymbol{\omega}}_{bd} \times \hat{\mathbf{I}}_{b\text{-}w}\hat{\boldsymbol{\omega}}_{bd}} \\ & + \overline{\bar{\boldsymbol{\omega}}_{bd} \times \hat{\mathbf{I}}_{b\text{-}w}\hat{\boldsymbol{\omega}}_{bd}} \\ & + \overline{\hat{\boldsymbol{\omega}}_{bd} \times \hat{\mathbf{I}}_{b\text{-}w}\boldsymbol{\omega}_{bd}} + \bar{\mathbf{I}}_{b\text{-}w}\frac{d\bar{\boldsymbol{\omega}}_{bd}}{dt^+} \\ & + \bar{\mathbf{a}}_2 + \bar{\mathbf{b}}_2,\end{aligned} \tag{16}$$

where $\bar{\mathbf{I}}_{b\text{-}w}$ and $\hat{\mathbf{I}}_{b\text{-}w}$ are the mean and instantaneous values of $\mathbf{I}_{bd} + \mathbf{c}$, respectively. Because $m_{wg}$ is generally about 2 orders of magnitude smaller than $m$ (Ellington, 1984b; Dudley, 2000), compared with the terms of insect weight ($mg$) and inertial force $[m(d\mathbf{v}_{cg}/dt + \boldsymbol{\omega}_{bd} \times \mathbf{v}_{cg})]$, $\bar{\mathbf{a}}_1$ in Eq. (15) can be neglected. Similarly, the moment due to the weight of the wings [the second term on the left-hand side of Eq. (16)] and $\bar{\mathbf{a}}_2$ can be neglected. Because the wing-beat frequency is assumed to be high, the fast oscillation of the body due to the cyclic variations of forces and moments at the wing-beat frequency, $\hat{\mathbf{v}}$ and $\hat{\boldsymbol{\omega}}$, should be very small; thus terms like $\overline{\hat{\boldsymbol{\omega}}_{bd} \times \hat{\mathbf{v}}_{cg}}$ can be neglected; similarly, terms like $\overline{\bar{\boldsymbol{\omega}}_{bd} \times \hat{\mathbf{I}}_{b\text{-}w}\hat{\boldsymbol{\omega}}_{bd}}$ and $\overline{\hat{\boldsymbol{\omega}}_{bd} \times \hat{\mathbf{I}}_{b\text{-}w}\boldsymbol{\omega}_{bd}}$ can also be neglected. Sun, Wang, and Xiong (2007) performed a simulation for the reduced system to quantify these terms. It turns out that each of the product terms is $O(10^{-2})$, meaning the product is $O(10^{-4})$, while the retained terms for the aerodynamic acceleration are $O(10^{-1})$, justifying the elimination of these terms. As for $\bar{\mathbf{b}}_1$ and $\bar{\mathbf{b}}_2$, they represent the mean inertial force and moment, respectively, of the wings due to wing acceleration and gyroscopic effects of the wing and body rotations. There are acceleration and deceleration of the wing within each downstroke (or upstroke), and moreover the rotation of the wing in its upstroke is opposite to that in the downstroke. When averaged over one cycle, the positive wing acceleration and gyroscopic forces and moments approximately cancel out their negative counterparts; thus $\bar{\mathbf{b}}_1$ and $\bar{\mathbf{b}}_2$ should be approximately zero and can be neglected. The same simulation quantified these terms to $O(10^{-6})$. As a result, Eqs. (15) and (16) become

$$\bar{\mathbf{F}}_A + m\mathbf{g} = m\left(\frac{d\bar{\mathbf{v}}_{cg}}{dt} + \bar{\boldsymbol{\omega}}_{bd} \times \bar{\mathbf{v}}_{cg}\right), \tag{17}$$

$$\bar{\mathbf{M}}_A = \bar{\boldsymbol{\omega}}_{bd} \times \bar{\mathbf{I}}_{b\text{-}w}\bar{\boldsymbol{\omega}}_{bd} + \bar{\mathbf{I}}_{b\text{-}w}\frac{d\bar{\boldsymbol{\omega}}_{bd}}{dt}, \tag{18}$$

which are the same as the Euler equations (13) and (14). Let the $x_b$, $y_b$, and $z_b$ axes be so chosen that at equilibrium, the $x_b$ and $y_b$ axes are horizontal; the $x_b$ axis points forward, and the $y_b$ axis points to the right of the insect (Fig. 7). Let the $x_b$, $y_b$, and $z_b$ components of the velocity $\bar{\mathbf{v}}_{cg}$ be $u$, $v$, and $w$, respectively; those of $\bar{\boldsymbol{\omega}}_{bd}$ be $p$, $q$, and $r$, respectively; those of $\bar{\mathbf{F}}_A$ be $X$, $Y$, and $Z$, respectively; those of $\bar{\mathbf{M}}_A$ be $L$, $M$, and $N$, respectively. Let $I_x$, $I_y$, and $I_z$ be the moments of inertia

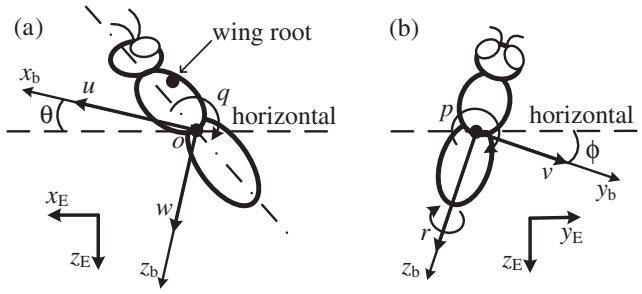


FIG. 7. Definition of the state variables and sketches of the reference frame. (a) Lateral view and (b) back view. $(x_b, y_b, z_b)$ is a frame fixed on the insect body with its origin at the center of mass of the insect body; the $x_b$, $y_b$, and $z_b$ axes are chosen so that at equilibrium, the $x_b$ and $y_b$ axes are horizontal, the $x_b$ axis points forward, and the $y_b$ axis points to the right of the insect. The model insect is shown during a perturbation ( $v, w, p, q, r, \theta$, and $\phi$ are zero at reference flight). Adapted from Zhang and Sun, 2011a.

about the $x_b$, $y_b$, and $z_b$ axes, respectively; $I_{xz}$ is the product of inertia. A system of Euler angles defines the orientation of the body rotation to the Earth and is specified by the angles of right-handed rotation about the three axes in the order $z_b$ (yaw, $\psi$), then $y_b$ (pitch, $\theta$), and then $x_b$ (roll, $\phi$). With these notations, Eqs. (17) and (18) and kinematical equations governing the Euler angles may be expanded as a set of eight coupled nonlinear ordinary differential equations (Etkin and Reid, 1996; Taylor and Thomas, 2003; Zbikowski, Ansari, and Knowles, 2006):

$$\frac{du}{dt} = -(wq - vr) + \frac{X}{m} - g\sin\theta, \tag{19}$$

$$\frac{dv}{dt} = -ru + pw + \frac{Y}{m} + g\cos\theta\sin\phi, \tag{20}$$

$$\frac{dw}{dt} = qu - pv + \frac{Z}{m} + g\cos\theta\cos\phi, \tag{21}$$

$$I_{xx}\frac{dp}{dt} - I_{xz}\frac{dr}{dt} = L + I_{xz}pq + (I_{yy} - I_{zz})qr, \tag{22}$$

$$I_{yy}\frac{dq}{dt} = M - I_{xz}(p^2 - r^2) - (I_{xx} - I_{zz})rp, \tag{23}$$

$$-I_{xz}\frac{dp}{dt} + I_{zz}\frac{dr}{dt} = N + (I_{xx} - I_{yy})pq - I_{xz}qr, \tag{24}$$

$$\dot{\phi} = p + \tan\theta(q\sin\phi + r\cos\phi), \tag{25}$$

$$\dot{\theta} = q\cos\phi - r\sin\phi. \tag{26}$$

The equation governing $\psi$,

$$\dot{\psi} = \frac{1}{\cos\theta}(q\sin\phi + r\cos\phi), \tag{27}$$

is decoupled from the above equations and $\psi$ can be solved after Eqs. (19)–(26) are solved.

Now that an insect has the same equations of motion as those of a rigid airplane, analysis methods used in the flight dynamics of aircraft (Etkin and Reid, 1996; Cook, 1997) can be readily applied to the flight dynamics of insects. The methods use linear theory and the techniques of eigenvalue and eigenvector analyses. The insects' motion is assumed to consist of small disturbances from a reference flight condition of steady motion. The independent, state variables are written as

$$\mathbf{x} = \mathbf{x}_e + \delta\mathbf{x}, \tag{28}$$

where $\mathbf{x}$ is the state vector:

$$\mathbf{x} = [u, v, w, p, q, r, \phi, \theta]^T, \tag{29}$$

the subscript $e$ (for equilibrium) denotes the reference flight condition, and the prefix $\delta$ denotes a small disturbing quantity. Each of the six aerodynamic forces and moments are written in the form

$$X = X_e + \frac{\partial X}{\partial u}\delta u + \frac{\partial X}{\partial v}\delta v + \frac{\partial X}{\partial w}\delta w + \frac{\partial X}{\partial p}\delta p + \frac{\partial X}{\partial q}\delta q + \frac{\partial X}{\partial r}\delta r, \tag{30}$$

where $\partial X/\partial u$, $\partial X/\partial w$, etc., are partial derivatives, referred to as aerodynamic derivatives (e.g., $\partial X/\partial u$ represents the increment in $X$ when there is a unit increment in $u$). Incorporating the small-disturbance notation into Eqs. (19)–(27) and dropping any nonlinear terms in the disturbing quantities give the linearized equations of motion. As a result of the linearization, the longitudinal and lateral small-disturbance equations are decoupled. For horizontal forward flight, the linearized longitudinal-disturbance equations of motion are (Taylor and Thomas, 2003)

$$\begin{bmatrix} \delta\dot{u}^+ \\ \delta\dot{w}^+ \\ \delta\dot{q}^+ \\ \delta\dot{\theta}^+ \end{bmatrix} = \mathbf{A}\begin{bmatrix} \delta u^+ \\ \delta w^+ \\ \delta q^+ \\ \delta\theta \end{bmatrix}, \tag{31}$$

$$\mathbf{A} = \begin{bmatrix} X_u^+/m^+ & X_w^+/m^+ & X_q^+/m^+ & -g^+ \\ Z_u^+/m^+ & Z_w^+/m^+ & Z_q^+/m^+ + u_e^+ & 0 \\ M_u^+/I_y^+ & M_w^+/I_y^+ & M_q^+/I_y^+ & 0 \\ 0 & 0 & 1 & 0 \end{bmatrix}, \tag{32}$$

and the linearized lateral equations of motion are (Faruque and Humbert, 2010b; Xu and Sun, 2013)

$$\begin{bmatrix} \delta\dot{v}^+ \\ \delta\dot{p}^+ \\ \delta\dot{r}^+ \\ \delta\dot{\phi} \end{bmatrix} = \mathbf{A}_1\begin{bmatrix} \delta v^+ \\ \delta p^+ \\ \delta r^+ \\ \delta\phi \end{bmatrix}, \tag{33}$$

$$\mathbf{A}_1=\begin{bmatrix} Y_v^+/m^+ & Y_p^+/m^+ & Y_r^+/m^+-u_e^+ & g^+ \\ (I_z^+L_v^++I_{xz}^+N_v^+)/(I_x^+I_z^+-I_{xz}^{+2}) & (I_z^+L_p^++I_{xz}^+N_p^+)/(I_x^+I_z^+-I_{xz}^{+2}) & (I_z^+L_r^++I_{xz}^+N_r^+)/(I_x^+I_z^+-I_{xz}^{+2}) & 0 \\ (I_{xz}^+L_v^++I_xN_v^+)/(I_x^+I_z^+-I_{xz}^{+2}) & (I_{xz}^+L_p^++I_x^+N_p^+)/(I_x^+I_z^+-I_{xz}^{+2}) & (I_{xz}^+L_r^++I_x^+N_r^+)/(I_x^+I_z^+-I_{xz}^{+2}) & 0 \\ 0 & 1 & 0 & 0 \end{bmatrix}, \quad (34)$$

where the overdot represents differentiation with respect to time ($t$); $u_e$ is the forward-flight speed; $X_u=\partial X/\partial u$, $X_w=\partial X/\partial w$, etc. (in equilibrium flight $\theta$ and $\phi$ are zero). The variables have been nondimensionalized using $c$, $U$, and $c/U$ as reference length, velocity, and time, respectively ($c$ is the mean chord length of a wing; $U$ is the mean flapping velocity at the radius of the second moment of wing area $r_2$ and is defined as $U=2\Phi nr_2$, where $\Phi$ is the stroke amplitude and $n$ is the wing-beat frequency): $X^+=X/0.5\rho U^2S_t$ ($S_t$ is the area of two wings and $\rho$ is the fluid density); $Y^+=Y/0.5\rho U^2S_t$; $Z^+=Z/0.5\rho U^2S_t$; $L^+=L/0.5\rho U^2S_tc$; $M^+=M/0.5\rho U^2S_tc$; $N^+=N/0.5\rho U^2S_tc$; $t^+=tU/c$; $m^+=m/0.5\rho S_tc$; $g^+=gc/U^2$ ($g$ is the gravitational acceleration); $I_x^+=I_x/0.5\rho S_tc^3$; $I_y^+=I_y/0.5\rho S_tc^3$; $I_z^+=I_z/0.5\rho S_tc^3$; $I_{xz}^+=I_{zz}/0.5\rho S_tc^3$; $u^+=u/U$; $v^+=v/U$; $w^+=w/U$; $p^+=pc/U$; $q^+=qc/U$; and $r^+=rc/U$. Aerodynamic derivatives can be computed by solving the Navier-Stokes equations [Eqs. (11) and (12)] or using the simple aerodynamic models, or alternatively measured experimentally using mechanical flappers. Setting $u_e$ in Eqs. (31)–(34) to zero gives the linearized disturbance equations of motion for hovering flight.

Equations (31) and (33) are solved using the techniques of eigenvalue and eigenvector analyses to yield insights into the dynamic flight stability (Etkin and Reid, 1996; Taylor and Thomas, 2003). Letting $\mathbf{x}(t)$ represent the vector $[\delta u^+ \quad \delta w^+ \quad \delta q^+ \quad \delta\theta]^T$ or $[\delta v^+ \quad \delta p^+ \quad \delta r^+ \quad \delta\phi]^T$, the general solution of Eq. (31) or (33) can be written in the following form:

$$\mathbf{x}(t)=\sum_{j=1}^{4}c_j\mathbf{q}_je^{\lambda_jt}, \quad (35)$$

where $\lambda_j$ and $\mathbf{q}_j$ $(j=1,2,3,4)$ are the eigenvalues and eigenvectors of $\mathbf{A}$ (or $\mathbf{A}_1$), respectively, and $c_j$ $(j=1,2,3,4)$ are constants determined by the initial conditions (i.e., initial disturbances). A real eigenvalue and the corresponding eigenvector (or a conjugate pair of complex eigenvalues and the corresponding eigenvector pair) represent a simple motion called the natural mode of motion of the system. The disturbance motion represented by Eq. (35) is a linear combination of the natural modes of motion. To know the dynamic stability properties of the system, one needs only to examine the motions represented by the natural modes of motion. In a natural mode of motion, the real part of the eigenvalue determines the time rate of growth of the disturbed quantities and the eigenvector determines the magnitudes and phases of the disturbed quantities relative to each other. A positive real eigenvalue results in an exponential growth of each of the disturbed quantities, so the corresponding natural mode is dynamically unstable (this is termed an unstable divergent mode). A negative real eigenvalue results in an exponential decay of the disturbed quantities and the corresponding natural mode is dynamically stable (called a stable subsidence mode). A pair of complex conjugate eigenvalues, e.g., $\lambda_{1,2}=\hat{n}\pm\hat{\omega}i$, results in oscillatory time variation of the disturbed quantities with $\hat{\omega}$ as its angular frequency; the motion decays when $\hat{n}$ is negative (dynamically stable, a stable oscillatory mode) but grows when $\hat{n}$ is positive (dynamically unstable, an unstable oscillatory mode).

In Secs. IV–VII, the stability and control properties of flying insects based on the above averaged model and linear theory are examined, and a test of assumptions in the model and theory by numerically solving the complete equations of motion [Eqs. (8) and (9)] coupled with the Navier-Stokes equations is discussed.

## IV. HOVERING-FLIGHT STABILITY ANALYSIS

### A. Aerodynamic derivatives and natural modes of motion

Sun and colleagues applied the averaged model and linear theory to a study of the longitudinal stability in several hovering insects (hoverfly, crane fly, dronefly, bumblebee, and hawk moth) and the lateral stability in the hovering dronefly and hawk moth (Sun and Xiong, 2005; Sun, Wang, and Xiong, 2007; Zhang and Sun, 2010b). The mass of the insects ranged from 11 to 1648 mg and the wing-beat frequency from 26 to 157 Hz. They used the CFD method to compute the aerodynamic derivatives which, to a large extent, determine the dynamic properties of a flying insect.

The computed aerodynamic derivatives have the following features. For longitudinal derivatives, $X_u^+$ and $Z_w^+$ are negative, their magnitude is large, and $M_u^+$ is positive and large; the other derivatives $Z_u^+$, $X_w^+$, $M_w^+$, $X_q^+$, $Z_q^+$, and $M_q^+$ are very small. For lateral derivatives $Y_v^+$, $L_p^+$, and $N_r^+$ are negative and their magnitude is large, and $L_v^+$ is positive and large; the others $N_v^+$, $Y_p^+$, $N_p^+$, $Y_r^+$, and $L_r^+$ are very small. These results show that a longitudinal-disturbance motion mainly produces a pitch moment ($M_u^+\delta u^+$), a horizontal damping force ($X_u^+\delta u^+$), and a vertical damping force ($Z_w^+\delta w^+$), and a lateral-disturbance motion mainly produces a roll moment ($L_v^+\delta v^+$) and a damping force and two moments: a side damping force ($Y_v^+\delta v^+$), a roll damping moment ($L_p^+\delta p^+$), and a yaw damping moment ($N_r^+\delta r^+$). Different insects have similar nondimensional aerodynamic derivatives.

Some of the force and moment derivatives are very different from those of airplanes and helicopters (Johnson, 1980; Bryson, 1994; Etkin and Reid, 1996; Padfield, 1996). For example, $M_u^+$ of an airplane is zero, but for a hovering insect, it is rather large; $L_v^+$ of an airplane is negative, while for a hovering insect, it is positive. Both an airplane and an insect have three damping force derivatives and three damping moment derivatives, but they produce the derivatives by different mechanisms. Detailed discussions of how the

derivatives are produced can be found in work by Sun and Xiong (2005), Hedrick, Cheng, and Deng (2009), Zhang and Sun (2010b), Cheng *et al.* (2010), and Cheng and Deng (2011). As an example, discussion of how the $u$ derivatives are produced (Sun and Xiong, 2005; Cheng and Deng, 2011) is given here. In equilibrium flight (hovering), the stroke plane is almost horizontal. When the insect moves forward with $\Delta u^+$, in the downstroke, the wing experiences a larger relative velocity than that in the reference, or equilibrium, flight and its drag is larger than the reference value, giving a decrease in $X^+$. In the upstroke, the wing experiences a smaller velocity than that in the reference flight and its drag is smaller than the reference value, also giving a decrease in $X^+$. This explains the negative $X_u^+$, one of the damping-force derivatives. As for the vertical force caused by the above changes in the relative velocity, compared to the reference value, there is an increase in lift in the downstroke, which gives a decrease in $Z^+$, and a decrease in lift in the upstroke, which gives an increase in $Z^+$, resulting in little change in $Z^+$. This explains the small $Z_u^+$. Because the wing is above the mass center, the decrease in $X^+$ results in a nose-up pitch moment, and because of the unsteady-flow effects, the increase in $Z^+$ in the downstroke and the decrease in $Z^+$ in the upstroke produce a couple, which is also a nose-up pitch moment (Sun and Xiong, 2005), explaining the large positive $M_u^+$. This discussion also serves to explain why different insects have similar nondimensional aerodynamic derivatives: they have similar aerodynamic configuration and wing kinematics, i.e., the wings flap back and forth in a horizontal plane and the center of mass is below the stroke plane.

As seen next, the two moment derivatives with respect to translation velocity, $M_u^+$ and $L_v^+$, the damping-force derivative $Z_w^+$ and the two lateral damping-moment derivatives $L_p^+$ and $N_r^+$ are the major stability derivatives that determine the natural modes of motion of a hovering insect. $M_u^+$ and $L_v^+$ cause longitudinal and lateral instabilities, respectively. The damping-moment derivatives make the instabilities weaker, but they are not large enough to stabilize the unstable modes.

The computed eigenvalues are shown in Table I. Three longitudinal natural modes of motion are identified for the five insects: one unstable slow oscillatory mode, one stable fast subsidence mode and one stable slow subsidence mode; and three lateral natural modes of motion are identified for the dronefly, bumblebee, and hawk moth: one unstable slow divergence mode, one stable slow oscillatory mode, and one stable fast subsidence mode. Despite the 1500-fold weight difference, the insects have similar natural modes of motion. Because of the unstable modes, the hovering flight of the insects is dynamically unstable. Based on the eigenvalues, the time for the initial disturbances to double (a time scale of the instability) is 46–60 ms for the hoverfly, dronefly, and crane fly and about 100 ms for the bumblebee and hawk moth (when nondimensionalized by the wing-beat period, the time for the initial disturbances to double is about 9–15 for the hoverfly, dronefly, and bumblebee; about 2.5 for the crane fly and the hawk moth).

From the computed eigenvectors, they observed that for the longitudinal motion, the unstable oscillatory mode and the fast subsidence mode has only forward-backward translation and pitch rotation, and the slow subsidence mode has only vertical translation. For the lateral motion, the unstable slow divergence mode and the stable slow oscillatory mode has only side translation and roll rotation, and the stable fast subsidence mode has only yaw and roll rotations. That is, for the longitudinal motion, the horizontal and pitching motions are decoupled from the vertical motion. For the lateral motion, in two of the three modes, side translation and roll rotation are decoupled from yaw rotation and in the other mode, yaw and roll rotations are decoupled from side translation. These properties can be used for exploring the underlying physics of the disturbed motion; we return to this in Sec. IV.B.

Also applying the averaged-model theory, Faruque and Humbert (2010a, 2010b) studied the dynamic stability in a hovering fruit fly, and Cheng and Deng (2010, 2011) studied the dynamic stability in several hovering insects (fruit fly, stalk-eyed fly, bumblebee, and hawk moth). Unlike Sun and colleagues, they estimated the aerodynamic derivatives using the simple aerodynamic model of Sane and Dickinson (2002), discussed in Sec. II.C. Arguing that the "translational lift" is the largest component, approximately 65%–85%, of an insect's lift production in hover and the most straightforward of the lift mechanisms known to be active, they neglected the added-mass, wing-rotation, and wake-capture terms of Eq. (2).

For the longitudinal motion of the model insects, the same three natural modes of motion as those revealed by Sun and colleagues were identified: one unstable oscillatory mode, one stable fast subsidence mode, and one stable slow subsidence mode; hence the longitudinal motion is unstable.

For the lateral motion, the natural modes of motion are as follows: one stable slow subsidence mode, one stable slow oscillatory mode, and one stable fast subsidence mode. The first mode (a stable slow subsidence mode) is different from that given by Sun and colleagues (an unstable slow divergence mode). Thus, Faruque and Humbert (2010a, 2010b) and

TABLE I. Wing-beat-frequency nondimensionalized eigenvalues $\lambda$ of hovering flight. HF, DF, BB, CF, and HM represent hoverfly, dronefly, bumblebee, crane fly, and hawk moth, respectively. Results are from Sun and Xiong (2005), Sun, Wang, and Xiong (2007), Zhang, Wu, and Sun (2012), and Xu and Sun (2013).

| | Longitudinal modes | | | Lateral modes | | |
|---|---|---|---|---|---|---|
| | $\lambda_{1,2}$ (1/s) | $\lambda_3$ (1/s) | $\lambda_4$ (1/s) | $\lambda_1$ (1/s) | $\lambda_{2,3}$ (1/s) | $\lambda_4$ (1/s) |
| HF | $0.074 \pm 0.144i$ | −0.171 | −0.020 | | | |
| DF | $0.073 \pm 0.139i$ | −0.165 | −0.015 | 0.08 | $-0.09 \pm 0.06i$ | −0.51 |
| BB | $0.045 \pm 0.129i$ | −0.197 | −0.012 | 0.09 | $-0.12 \pm 0.07i$ | −0.69 |
| CF | $0.330 \pm 0.733i$ | −0.865 | −0.110 | | | |
| HM | $0.269 \pm 0.608i$ | −0.747 | −0.092 | 0.26 | $-0.57 \pm 0.26i$ | −5.68 |

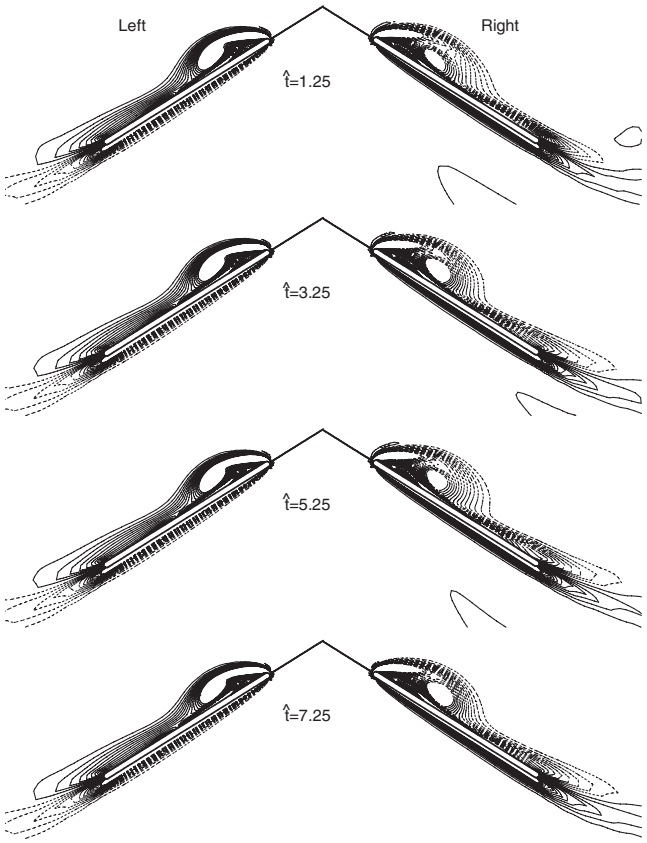


FIG. 8. Vorticity plots at the $0.7R$ wing section at various times for the left and right wings (solid and dashed lines indicate positive and negative vorticities, respectively; the magnitude of the nondimensional vorticity at the outer contour is 2 and the contour interval is 3). Left column: results of the left wing; right column: results of the right wing. The insect moves to its right at $\Delta v/U = 0.1$. The "lateral wind" due to the side motion of the insect increases the axial velocity of the LEV on the left wing and decreases that on the right wing, causing the LEV of the left wing to be more concentrated than that of the right wing. Adapted from Zhang, Wu, and Sun, 2012.

Cheng and Deng (2010, 2011) predicted that the lateral motion was stable, while, as seen above, Sun and colleagues predicted that the lateral motion was unstable (Zhang and Sun, 2010b; Zhang, Wu, and Sun, 2012). The $L_v$ derivative (the roll moment produced by unit side translation) calculated by Sun and colleagues using the Navier-Stokes code is positive (Zhang and Sun, 2010b; Zhang, Wu, and Sun, 2012), but that calculated by Faruque and Humbert (2010b) and Cheng and Deng (2011) using the simple aerodynamic model is negative. A recent analysis by Xu and Sun (2013) showed that it is the difference in the sign of $L_v$ that has caused the difference in the first lateral mode between the study of Sun and colleagues and those of Faruque and Humbert (2010b) and Cheng and Deng (2011). Xu and Sun (2013) also explained what caused the sign difference in $L_v$. When there is a side slip ($\delta v$), the insect experiences a lateral wind. The chordal component of the lateral wind (the component of the lateral wind that is perpendicular to the spanwise axis of a wing) changes the relative velocity of a wing section. The change in relative velocity of a section of the left wing is different from that of the corresponding section of the right wing, resulting in different aerodynamic forces on the left and right wings. This is called the "changing-relative-velocity" effect. On the other hand, the spanwise component of the lateral wind (the component of the lateral wind that is parallel to the spanwise axis of a wing) will change the axial velocity of the LEV of the wing, increasing the axial velocity of the LEV on one wing and decreasing that on the other. This will make the LEV of one wing more concentrated than that of the other wing (Fig. 8), also resulting in different aerodynamic forces on the left and right wings. This is called the "changing-LEV-axial-velocity" effect. The changing-relative-velocity effect gives a negative contribution, and the changing-LEV-axial-velocity effect gives a positive contribution to $L_v$. Because the positive contribution by the changing-LEV-axial-velocity effect is larger than the negative contribution by the changing-relative-velocity effect, $L_v$ is positive. The simple aerodynamic model used by Faruque and Humbert (2010b) and Cheng and Deng (2011) can take the changing-relative-velocity effect into account, but not the changing-LEV-axial-velocity effect; thus their $L_v$ is negative, resulting in the stable slow subsidence mode. Xu and Sun (2013) suggested that if the simple aerodynamic model was modified to include the changing-LEV-axial-velocity effect, $L_v$ would be positive and the resulting first lateral mode would be an unstable divergence mode.

### B. Reduced-order equations and physical interpretation of the natural modes of motion

Of particular interest in the work of Sun and colleagues is their notion that some of the natural modes of motion are decoupled from the others (Sun and Xiong, 2005; Sun, Wang, and Xiong, 2007; Zhang and Sun, 2010b). As a result of the decoupling, the order of the equations of motion can be reduced and approximate analytical expressions for the eigenvalues can be obtained. The analytical expression of an eigenvalue can clearly show the physics underlying the corresponding natural mode of motion.

The longitudinal unstable oscillatory mode and the stable fast subsidence mode have only forward-backward translation and pitch rotation (Sun and Xiong, 2005; Sun, Wang, and Xiong, 2007). Therefore, the vertical component of the force equation can be neglected, $\delta w$ in other equations can be set to zero, and the longitudinal equations of motion [Eq. (31)] can be simplified to

$$\begin{bmatrix} \delta\dot{u}^+ \\ \delta\dot{q}^+ \\ \delta\dot{\theta} \end{bmatrix} = \begin{bmatrix} X_u^+/m^+ & X_u^+/m^+ & -g^+ \\ M_u^+/I_y^+ & M_q^+/I_y^+ & 0 \\ 0 & 1 & 0 \end{bmatrix} \begin{bmatrix} \delta u^+ \\ \delta q^+ \\ \delta\theta \end{bmatrix}, \tag{36}$$

where the characteristic equation is

$$\lambda^3 - \left(\frac{X_u^+}{m^+} + \frac{M_w^+}{I_y^+}\right)\lambda^2 + \left(\frac{X_u^+ M_q^+}{m^+ I_y^+} - \frac{M_u^+ X_q^+}{m^+ I_y^+}\right)\lambda + \frac{g^+ M_u^+}{I_y^+} = 0. \tag{37}$$

The longitudinal stable slow subsidence mode has only vertical translation and the equation of motion [Eq. 31] can be simplified to

$$\delta\dot{w}^+ = \frac{Z_w^+}{m^+}\delta w^+, \tag{38}$$

where the characteristic equation is

$$\lambda - Z_w^+/m^+ = 0. \tag{39}$$

Solving Eqs. (37) and (39) and dropping some higher-order small terms, they obtained the approximate analytical expressions for the longitudinal roots as

$$\lambda_{1,2} = \hat{n} \pm i\hat{\omega}, \tag{40}$$

where

$$\hat{n} \approx \frac{1}{2}\sqrt[3]{\frac{M_u^+ g^+}{I_y^+}}(1-2j), \tag{41}$$

$$\hat{\omega} \approx \frac{\sqrt{3}}{2}\sqrt[3]{\frac{M_u^+ g^+}{I_y^+}}, \tag{42}$$

and

$$\lambda_3 \approx -\sqrt[3]{\frac{M_u^+ g^+}{I_y^+}}(1+j), \tag{43}$$

with

$$j = -\frac{1}{3}\left(\frac{M_q^+}{I_y^+} + \frac{X_u^+}{m^+}\right) \Big/ \sqrt[3]{\frac{M_u^+ g^+}{I_y^+}}, \tag{44}$$

$$\lambda_4 \approx Z_w^+/m^+. \tag{45}$$

They further showed that $j$ is considerably smaller than 1, i.e., the contributions of the damping moment $M_q$ and damping force $X_u$ are negligibly small.

Equations (40)–(44) indicate that $\sqrt[3]{M_u g/I_y}$ plays a major role in determining the longitudinal roots $\lambda_{1,2}$ $(=\hat{n} \pm i\hat{\omega})$ and $\lambda_3$. That is, the unstable slow oscillatory mode and the stable fast subsidence mode are mainly determined by the parameters $M_u$, $g$, and $I_y$. The physical interpretation of these two natural modes of motion are as follows (Sun and Xiong, 2005; Sun, Wang, and Xiong, 2007). First, we look at the unstable slow oscillatory mode. Based on information given by the eigenvectors, in this mode, $\delta u$ and $\delta q$ have the same sign most of the time, and they lag $\delta\theta$ by a phase angle of about 100° (Sun and Xiong, 2005; Sun, Wang, and Xiong, 2007). Suppose that at the beginning $\delta\theta$ is zero and the insect moves forward and pitches up, i.e., $\delta u$ and $\delta q$ are positive [Fig. 9(a)]; a positive moment (pitch-up moment) $M_u\delta u$ will be produced. This moment will aid the pitching up: $\delta\theta$ increases to some positive value, tilting the vertical force $F_0$ backward ($F_0$ equals the insect weight $mg$) and resulting in a negative horizontal force $-F_0\sin(\delta\theta)$ [Fig. 9(b)]. The negative horizontal force will decrease the forward-motion velocity. After $\delta u$ is decreased to zero, it continues to become negative because the negative horizontal force $-F_0\sin(\delta\theta)$ is still in action [Fig. 9(c)]. With $\delta u$ being negative (the insect moving backward), a negative moment (pitch-down moment) $M_u\delta u$ will be produced [Fig. 9(c)], which will make the insect pitch down; that is, $\delta\theta$ decreases [Fig. 9(d)]. When $\delta\theta$ decreases to zero, the horizontal force becomes zero and the magnitude of the negative $\delta u$; hence the pitch-down moment $M_u\delta u$ reaches its maximum [Fig. 9(e)]. Afterward, $\delta\theta$ becomes negative, tilting the vertical force $F_0$ forward, resulting in a positive horizontal force $F_0\sin(-\delta\theta)$ [Fig. 9(f)]. The positive horizontal force will first decrease the backward-motion velocity to zero and then make the insect move forward again [Figs. 9(f) and 9(g)]. This explains why the motion is oscillatory. As seen above, the pitch-up rotation is accompanied by a forward translation ($\delta u$ positive) and the pitch-down rotation is accompanied by a backward translation ($\delta u$ negative). The forward translation will produce a pitch-up moment ($M_u\delta u$ positive) that enhances the pitch-up rotation and the backward translation will produce a pitch-down moment ($M_u\delta u$ negative) that enhances the pitch-down rotation. This causes the instability. Next, we look at the stable fast subsidence mode. In this mode, $\delta u$ and $\delta q$ are out of phase (Sun and Xiong, 2005; Sun, Wang, and Xiong, 2007): when the insect moves forward, it pitches down and vice versa. Suppose that at the beginning the insect has a positive $\delta\theta$, moves forward, and pitches down ($\delta u$ positive and $\delta q$ negative). The positive moment produced by $\delta u$ $(M_u\delta u > 0)$ tends to decrease the pitch-down motion; the negative horizontal force $-F_0\sin(\delta\theta)$ will decrease the forward-motion velocity, making the magnitudes of $\delta u$, $\delta q$, and $\delta\theta$ decrease monotonically, explaining why this mode is stable.

From Eq. (45), it is seen that the stable slow subsidence mode mainly depends on $Z_w$ and $m$. The physical interpretation of why this mode is stable is straightforward: $Z_w$ is negative (vertical damping), a positive $\delta w$ disturbance (insect moving downward) will produce a negative vertical force, which opposes the downward motion, stabilizing the motion.

For the lateral natural modes of motion, similar derivation gives the following simple expressions of the eigenvalues (Zhang and Sun, 2010b):

$$\lambda_1 \approx \sqrt[3]{\frac{L_v^+ g^+}{I_x^+ - I_{xz}^{+2}/I_z^+}} + \frac{L_p^+}{3(I_x^+ - I_{xz}^{+2}/I_z^+)}, \tag{46}$$

$$\lambda_{2,3} = \hat{n} \pm i\hat{\omega}, \tag{47}$$

where

$$\hat{n} \approx \frac{-1}{2}\sqrt[3]{\frac{L_v^+ g^+}{I_x^+ - I_{xz}^{+2}/I_z^+}} + \frac{L_p^+}{3(I_x^+ - I_{xz}^{+2}/I_z^+)}, \tag{48}$$

$$\hat{\omega} \approx \frac{\sqrt{3}}{2}\sqrt[3]{\frac{L_v^+ g^+}{I_x^+ - I_{xz}^{+2}/I_z^+}}, \tag{49}$$

$$\lambda_4 \approx \frac{1}{2}\left(\frac{L_p^+}{I_x^+ - I_{xz}^{+2}/I_z^+} + \frac{N_r^+}{I_z^+ - I_{xz}^{+2}/I_x^+}\right) + \frac{I_{xz}^+\sqrt{L_p^+ N_r^+}}{I_x^+ I_z^+ - I_{xz}^{+2}}. \tag{50}$$

For the lateral unstable slow divergence mode, the expression of $\lambda_1$ [Eq. (46)] shows that $L_v$, $g$, and $L_p$ play major roles in

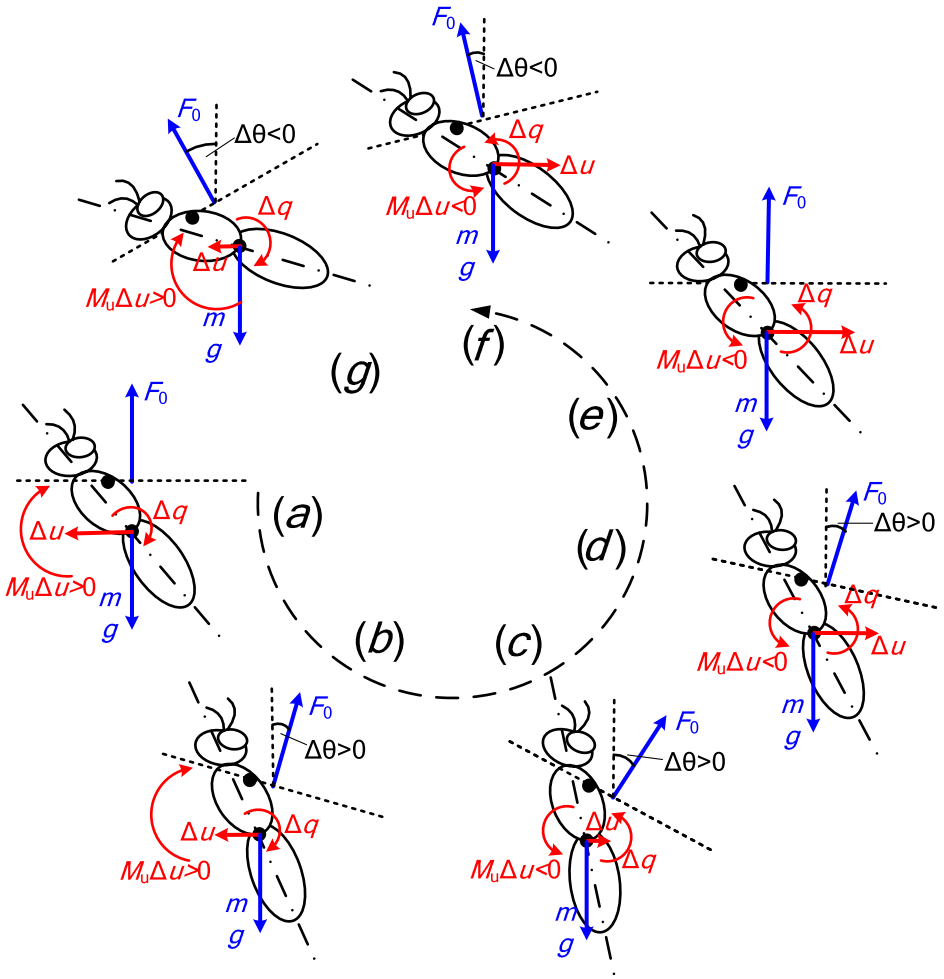


FIG. 9 (color online). Diagram (side view) of the body attitude ($\Delta\theta$), forward-backward translation speed ($\Delta u$), pitch rate ($\Delta q$), and the forces and moments, during the first cycle of the disturbed motion when the unstable slow oscillatory mode is excited. $F_0$ is the total aerodynamic force at equilibrium, $F_0 = mg$. The forward translation produces a pitch-up moment ($M_u\Delta u$ positive) that enhances the pitch-up rotation and the backward translation produces a pitch-down moment ($M_u\Delta u$ negative) that enhances the pitch-down rotation, causing the instability. Adapted from Sun and Xiong, 2005, and Sun, Wang, and Xiong, 2007.

this mode. $L_v$ and $g$ are both positive; hence $\sqrt[3]{L_v g}$ is positive, giving a destabilizing contribution (note that $I_x - {I_{xz}}^2/I_z$ is positive); $L_p$, the roll damping, is negative, giving a stabilizing contribution. The physical reason for the destabilizing effects of $\sqrt[3]{L_v g}$ can be explained as follows (Zhang and Sun, 2010b). $L_v$ is the roll moment produced by side-motion velocity, and $g$ represents the weight or vertical aerodynamic force. In this mode, based on information given by the eigenvectors, the insect conducts horizontal side motion with its body tilted in the same direction as that of the side motion (Zhang and Sun, 2010b). Suppose that at the beginning the insect moves and tilts to the right, as illustrated by Fig. 10. The side motion ($\delta v > 0$) will produce a moment $L_v\delta v$ ($> 0$) that will enhance the roll and at the same time, the roll will tilt the vertical force (equal to $mg$) to the right, which will enhance the side motion, producing the destabilizing effect (the case of translating and rolling to the left can be similarly explained). The physical reason for the stabilizing effect of $L_p$ is obvious: $L_p$ gives a damping moment. From the above discussion, we see that because of the roll moment produced by the horizontal side motion and the side force produced by the roll rotation, the motion is unstable, and because of the effect of the roll damping moment, the instability becomes relatively weak (i.e., the divergence is relatively slow).

For the lateral stable slow oscillatory mode, the expression of the real part of $\lambda_{2,3}$ [Eqs. (47)–(49)] is similar to that of $\lambda_1$, except that the term involving $L_v$ and $g$ is negative (multiplied by $-1/2$). Thus, in this mode, $L_v$ and $g$, as well as $L_p$, give a stabilizing contribution. Unlike in the unstable slow divergence mode, in this mode the insect conducts horizontal side motion with its body rolled to the opposite direction of the side motion. Thus the moment produced by the side velocity is in the opposite direction of the roll and the side force produced by the roll is in the opposite direction of the side motion, stabilizing the motion.

For the lateral stable fast subsidence mode, $\delta p$ and $\delta r$ are the main variables. As seen from the expression for $\lambda_4$ [Eq. (50)], $L_p$ and $N_r$ are both negative; hence each term in the expression for $\lambda_4$ produces a stabilizing effect (note that $I_{xz}$ is negative). The physical reason is clear: $L_p$ and $N_r$ give damping moments. They also explained why this mode is relatively fast. Based on information given by the

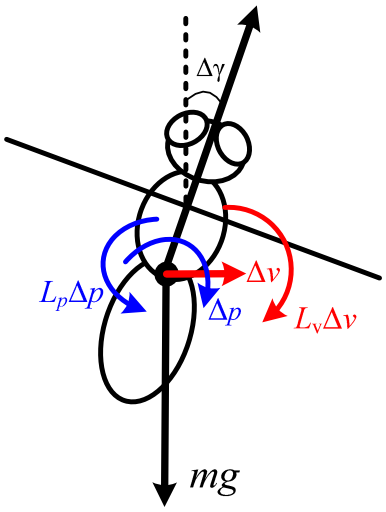


FIG. 10 (color online). Diagram of the body attitude (roll angle $\Delta\gamma$), side translation speed ($\Delta v$), and roll rate ($\Delta p$), and the forces and moments during the disturbed motion when the lateral unstable slow divergence mode is excited (insect moving to the right, back view). $F_0$ is the total aerodynamic force at equilibrium, $F_0 = mg$. The side motion ($\Delta v > 0$) produces a moment $L_v\Delta v$ ($> 0$) that will enhance the roll and at the same time, the roll tilts the vertical force ($F_0$) to the right, which will enhance the side motion, producing the destabilizing effects. Adapted from Zhang and Sun, 2010b.

eigenvectors, in this mode the insect rotates about the long axis of its body ($\delta p$ and $\delta r$ have approximately the same magnitude but opposite sign, and the $x_b$ axis is about 45° from the long axis of the body; hence the resultant angular velocity is about the long axis of the body). The moment of inertia about the long axis of the body is relatively small, while the damping moments, represented by $L_p$ and $N_r$, are relatively large. This results in large decelerations in $\delta p$ and $\delta r$, causing $\delta p$ and $\delta r$ to die out very fast.

### C. Test of the averaged model by direct numerical simulation

Numerical solution of the complete equations of motion coupled with the Navier-Stokes equations can provide data to test the validity of the averaged-model theory and the linearization; moreover, it can extend the stability analysis to nonlinear ranges. Requisite solution methods and codes have been developed by Wu and Sun (2009), Liu *et al.* (2010), and Zhang and Sun (2010b).

Zhang and Sun (2010b) and Zhang, Wu, and Sun (2012) simulated the disturbed motions of two hovering model insects and compared the results with the analytical solutions given by the averaged model and by linear theory. They considered only small disturbance motions so that the nonlinear effect would not appear in the direct numerical simulation. Thus any discrepancy between the analytical and numerical solutions is due to the averaged-model assumption. The two model insects were a model dronefly and a model hawk moth. The model dronefly represents insects with relatively high wing-beat frequency (its wing-beat frequency is about 160 Hz) and the model hawk moth those with relatively low wing-beat frequency (its wing-beat frequency is about 26 Hz). Typical results are presented in Fig. 11. The averaged-model theory works well for the dronefly [Fig. 11(a)]. But for the hawk moth, quantitative differences exist between the theory and the simulation [Fig. 11(b)]. They suggested that this is because the time scale of the gross motion of the hawk moth is not much larger than the period of the wing beat (based on Table I, the ratio of

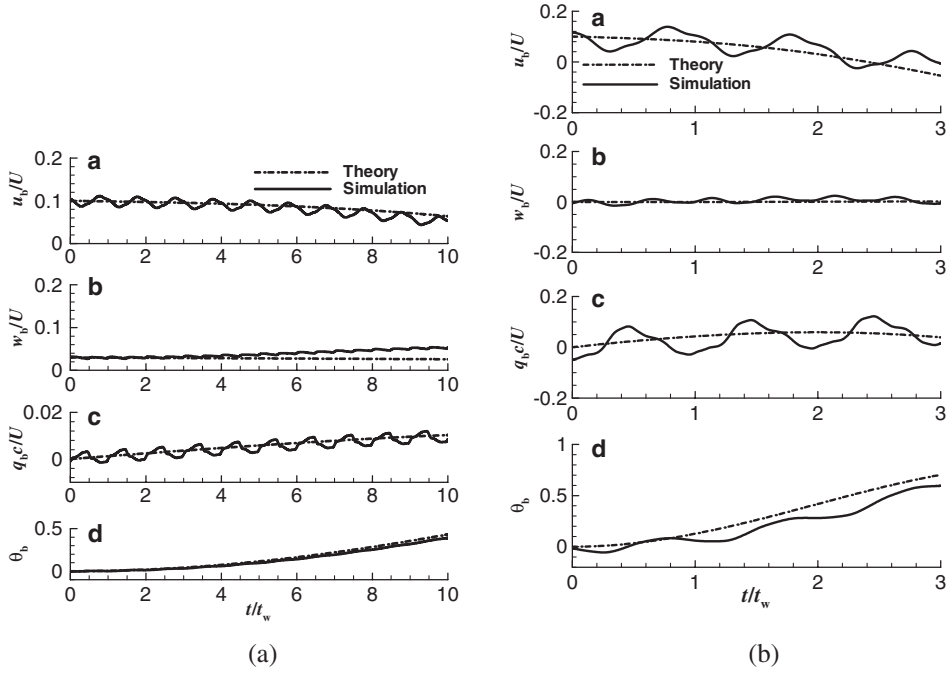


(a) (b)

FIG. 11. Curves showing the comparison between simulation and the averaged-model theory for the longitudinal-disturbance motion of (a) the model dronefly and (b) the model hawk moth. The initial disturbances are $\Delta u = 0.1$ and $\Delta w = \Delta q = \Delta\theta = 0$, which simulate a horizontal longitudinal gust ($U$ is the mean flapping velocity). Adapted from Zhang and Sun, 2010b.

the period of the unstable oscillatory mode to the period of the wing beat is only about 10 for the hawk moth; it is about 45 for the dronefly). Nevertheless, the theory still correctly predicts the trend of the dynamic properties of the motion of the hawk moth. Compared with many other insects, the wing-beat frequency of the hawk moth is relatively low and the characteristic times of the natural modes of motion of the body divided by the wing-beat period are relatively large. The fact that the theory based on the averaged model can correctly predict the trend of the dynamic properties of the hawk moth suggests that it could do so for many insects.

Another approach to testing the validity of the averaged model is to compare the solution given by the averaged model and linear theory with that given by Floquet theory, which does not average out the high-frequency oscillation. This is discussed in Sec. IV.D.

### D. Floquet stability analysis

As previously mentioned, because of the periodically varying aerodynamic and inertial forces of the flapping wings, an insect hovering or flying at a constant speed is a cyclically forcing system, and generally the flight is not in a fixed-point equilibrium but in a cyclic-motion equilibrium. Thus, when studying the flight stability of an insect, in principle, one should consider the stability of the periodic solution that represents the "equilibrium flight." But in the averaged model used in the above studies, the cyclic-motion equilibrium was reduced to a fixed-point equilibrium, and stability with respect to this equilibrium point was considered.

Taylor and Zbikowski (2005) studied the dynamic flight stability of locusts without assuming the equilibrium as a fixed point. They used instantaneous force and moment measurements from tethered locusts to parametrize the equations of motion and developed a nonlinear time-periodic model of the locusts. By numerically integrating the nonlinear equations in the model, they explored the stability problem of the locusts. Because forces and moments measured from real insects were used, some control responses were necessarily included in the model. As a result, the results they obtained were for a controlled system not for an open-loop system. Therefore, their model cannot provide information on the inherent stability of an insect. Moreover, by numerical simulation, the study gave specific solutions only for given initial data, while the general stability properties cannot be obtained.

Wu and Sun (2012) treated the flight as a cyclic-motion equilibrium and used the Floquet theory to analyze the longitudinal stability of insect flight. Again, the hovering flights of a model dronefly and a model hawk moth were considered. The former has a relatively high wing-beat frequency and a small ratio of wing mass to body mass, and hence a very small amplitude of body oscillation, while the latter has a relatively low wing-beat frequency and a large ratio of wing mass to body mass, and hence a relatively large amplitude of body oscillation (Wu, Zhang, and Sun, 2009). They first numerically solved the complete equations of motion coupled with the Navier-Stokes equations to obtain the periodic solution of the hovering flight. Then they perturbed the equations of motion about the periodic solution and linearized, obtaining a system of linear ordinary differential equations with periodic coefficients:

$$\frac{d}{dt}\begin{bmatrix}\delta u\\ \delta w\\ \delta q\\ \delta\theta\end{bmatrix} = \mathbf{A}(t)\begin{bmatrix}\delta u\\ \delta w\\ \delta q\\ \delta\theta\end{bmatrix}, \tag{51}$$

where $\mathbf{A}(t)$ is the system matrix and each element of $\mathbf{A}(t)$ is a periodic function of time with a period $T$ ($T = 1/n$, the wing-beat period of the insect). On the basis of the Floquet theory (Rugh, 1996), the general solution of Eq. (51) can be written in the following form:

$$\mathbf{x}(t) = \sum_{j=1}^{4} a_j \mathbf{p}_j(t) e^{\rho_j t}, \tag{52}$$

where $a_j$ ($j = 1, 2, 3, 4$) are constants, $\mathbf{p}_j(t)$ ($j = 1, 2, 3, 4$) are periodic vector functions with $T$ as the period, and $\rho_j$ ($j = 1, 2, 3, 4$) are the characteristic exponents of the system. The stability of the periodic solution or the hovering flight is determined by the sign of the real part of $\rho_j$ ($j = 1, 2, 3, 4$). Their computed values of $\rho_j$ ($j = 1, 2, 3, 4$) showed that for each of the two model insects there is a pair of complex characteristic exponents ($\rho_{1,2}$) with positive real part and two negative real characteristic exponents ($\rho_3$ and $\rho_4$). Because the real part of $\rho_{1,2}$ is positive, the periodic solution, or the hovering flight, of the two model insects is unstable.

For comparison, they also made an analysis using the averaged-model theory (fixed-point stability analysis). For each of the insects, there are a pair of complex eigenvalues ($\lambda_{1,2}$) with positive real part and two negative real eigenvalues ($\lambda_3$ and $\lambda_4$). Thus the Floquet theory and the averaged-model theory predict three similar natural modes of motion: one unstable slow oscillatory mode, one stable fast subsidence mode, and one stable slow subsidence mode. There are only quantitative differences between the two theories for the model hawk moth: the growth and decay rates of the modes obtained by the Floquet theory [(real) $\rho_{1,2} = 0.199$, $\rho_3 = -0.747$, and $\rho_4 = -0.103$] are different from those of the averaged-model theory [(real) $\lambda_{1,2} = 0.253$, $\lambda_3 = -0.715$, and $\lambda_4 = -0.094$] by 4%–21%. For the model dronefly, the two theories give almost identical results.

These results further show that the averaged model works well for the dronefly, and that for the hawk moth, although there are quantitative differences in results between the averaged-model theory and the Floquet theory, the averaged-model theory can correctly predict the trend of the dynamic properties of the disturbed motion.

### E. Applicability of the linearization

Besides averaging over the wing-beat cycle, another major simplification in the stability theories discussed earlier is the linearization of the equations of motion. In the linearization, each of the six aerodynamic forces and moments is approximated by a linear function of the disturbed-state variables, and nonlinear terms in the disturbed quantities are dropped from the equations. In principle, the small-disturbance theory

should work only for calculations where the disturbances are infinitesimal. But in practice it has been found to give good results for calculations where the disturbances are not very small (Dickson *et al.*, 2010; Zhang and Sun, 2010b, 2010c; Cheng, Deng, and Hedrick, 2011). For example, comparison between the theory and simulation using complete equations of motion coupled with Navier-Stokes equations shows that under a horizontal gust of velocity equal to $0.3U$ (30% of the mean flapping velocity), results of the theory are still in good agreement with those of the simulation (Zhang and Sun, 2010b). Experiments by Dickson *et al.* (2010) and Cheng and Deng (2011), using a dynamically scaled, flapping winged robotic model, showed that the aerodynamic torques vary linearly with each of the three angular velocities, even at a rather high value of the angular velocity, e.g., 35° per wing stroke. This partially explains the above results.

A systematic study on why the theory gives good results for motion under a relatively large disturbance should be conducted in future work.

### F. The effect of wing deformation

The model employed in the above analyses of insect flight stability and control assume rigid flat-plate wings (Sun and Xiong, 2005; Hedrick, Cheng, and Deng, 2009; Faruque and Humbert, 2010a, 2010b). As far as the present author knows, there is no formal quantitative study or even qualitative discussion about the effect of wing deformation on flight dynamics stability. However, examination of the existing data on wing deformation could shed light on the problem. Because of the arrangement of the veins of a wing (or the pattern of wing corrugation), in general, a flapping insect wing mainly has camber deformation and spanwise twist deformation (Rees, 1975; Newman and Wootton, 1986; Ennos, 1988). Quantitative measurement in freely flying droneflies and dragonflies (Wang, Zeng, and Yin, 2002; Walker, Thomas, and Taylor, 2010) and computation by fluid and structure coupling in hovering hawk moths (Nakata and Liu, 2012) showed that in the midportion of a downstroke or upstroke, where the major part of the aerodynamic force is produced, the camber is less than 8% of the wing chord, and that along the outer 80% of the wing length the twist is less than 25°. That is, at equilibrium flight the deformation is relatively small. During small-disturbance motion, the aerodynamic force on the wing has changes of small order and the inertial force of the wing mass does not change (Sun and Xiong, 2005; Faruque and Humbert, 2010a, 2010b; Cheng and Deng, 2011). As a result, the changes in deformation during disturbed motion are small at a higher order. Therefore, deformation produces negligibly small variations in aerodynamic force during the disturbed motion and hence cannot affect the stability properties.

## V. FORWARD-FLIGHT STABILITY ANALYSIS

The majority of the present studies on insect flight stability are for hovering flight, and there are only limited works on forward-flight stability. An obvious reason for this is that hovering flight is a very important type of flight and is relatively simple, yet representative of insect flight. Another possible reason is that complete wing kinematic descriptions of free forward flight are very few. Bumblebees and hawk moths are the only insects in which the most complete wing kinematic descriptions of free forward flight have been measured (Dudley and Ellington, 1990b; Willmott and Ellington, 1997a). It should be noted that even in these cases, the angle of attack of a wing and its variations along the wing span (i.e., wing twist) at stroke reversal were not accurately measured.

Taylor and Thomas (2003) studied dynamic flight stability in the desert locust *Schistocerca gregaria* at one flight speed, employing the averaged-model theory. This was the first attempt to conduct a formal quantitative study of the dynamic stability in a flapping-flying animal. They measured the aerodynamic forces and moments of the locust tethered in a wind tunnel to obtain the aerodynamic derivatives. They identified three natural modes of motion: one stable subsidence mode, one unstable divergence mode, and one stable oscillatory mode. Because their experimental approach (i.e., using real insects) necessarily included some control responses, the aerodynamic derivatives they measured are not the inherent (or passive) stability derivatives, but stability derivatives with some control effects. As a result, these natural modes of motion are unlikely to represent the inherent stability properties of the forward-flying locust. Nevertheless, their work pioneered a formal quantitative analysis of dynamic stability in a flying insect.

Xiong and Sun (2008, 2009) applied the averaged-model theory to investigate the longitudinal flight dynamics of level forward flight in a bumblebee. The stability analysis was conducted at various flight speeds, ranging from 0 to 4.5 m/s (the advance ratio $J$ ranging from 0 to 0.57; $J$ is defined as the ratio of flight speed to the mean tip speed of the wing in the flapping motion). Wing kinematics of freely flying bumblebees measured by Dudley and Ellington (1990b) were used for the equilibrium flight at each flight speed. The CFD method was used to compute the aerodynamic derivatives in the system matrices. The computed eigenvalues show the following. At slow forward-flight speeds of less than 1.0 m/s, the natural modes of motion are qualitatively similar to those of the hovering flight: one unstable oscillatory mode, one stable fast subsidence mode, and one stable slow subsidence mode. Because of the unstable oscillatory mode, the flight is unstable. At medium forward-flight speeds of 2.5 and 3.5 m/s, the eigenvalues exist in two pairs and both have negative real parts of very small magnitude. The flight is approximately neutrally stable in longitudinal motion. Finally, at a high speed of 5.7 m/s, the modal structure contains four real eigenvalues: two stable and two unstable, and the magnitude of one of the positive eigenvalues is quite large. The flight is strongly unstable (the initial disturbance doubles its value in only 3.5 wing beats). Furthermore, they found no decoupling between the natural modes of motion in forward flight. The results differ from those presented by Taylor and Thomas (2003), which predicted a modal structure identical to that in the hovering flight. As noted, the Taylor and Thomas (2003) results may not represent the inherent stability properties of the forward-flying locust.

Xu and Sun (2013) extended the above work on bumblebees to a lateral stability analysis. At slow forward-flight

speeds of less than 1.0 m/s, the natural modes of motion are qualitatively similar to those of a hovering flight: one unstable slow divergence mode, one stable slow oscillatory mode, and one stable fast subsidence mode. Because of the unstable slow divergence mode, the flight is unstable. At medium forward-flight speeds of 2.5 and 3.5 m/s, the modal structure is similar to those at the lower speeds, but the eigenvalue of the first mode is close to zero. The flight becomes approximately neutrally stable in lateral motion. At a high speed of 5.7 m/s, the modal structure is also similar to those at the lower speeds, but the first eigenvalue becomes negative or the first mode becomes a stable slow subsidence mode. The flight is stable in lateral motion. Similarly to the case of longitudinal motion, they found no decoupling between the lateral modes. As discussed, the instability at hovering is mainly caused by the roll moment produced by a sideways wind made by the lateral movement of the bee; Xu and Sun (2013) showed that as the bee flies faster, the wings "bend" toward the back of the body, reducing the effect of the sideways wind and increasing the stability of its flight.

In summary, these investigations on bumblebee forward flight show that, at low forward-flight speeds, flight is weakly unstable (because both longitudinal and lateral disturbance motions have a slow unstable mode); at medium forward-flight speeds, flight is approximately neutrally stable; at high forward-flight speeds, the flight is strongly unstable (because one of the longitudinal modes is strongly unstable, even if the other longitudinal modes and all lateral modes are stable). It is interesting to note that bumblebees are more unstable when they hover than when they fly forward at low to medium speeds.

Because there is no decoupling between the natural modes of motion in forward flight, approximate analytical expressions for the eigenvalues like those for hovering flight are not available for interpretation of the physics of the stability properties. Other approaches should be explored in the future to give insight into the underlying physics of the natural modes of motion.

Unlike the case of hovering flight for which a stability analysis has been made for a number of species by several groups, analyses on forward-flight stability at a series of flight speeds have been made only for bumblebees. For other insects, the modal structure and its variation as functions of flight speed could be different. For instance, when examining the effect of aerial turbulence on forward-flight performance and maximum flight speed in wild orchid bees, Combes and Dudley (2009) found that the bees' flight exhibits severe lateral instability at high flight speeds; however, for bumblebees at high flight speeds, the above stability analysis predicts strong longitudinal instability. Further studies on flight dynamic stability at forward flight are required in the future.

## VI. STABILIZATION CONTROL ANALYSIS

The stability studies described showed that for many insects at hovering flight and for bumblebees at hovering or at each of the forward-flight speeds considered, there exists at least one unstable, or neutrally stable, natural mode of motion. As a result, the flight is generally inherently unstable. If the insects did not use sensory information to control their inherent flight dynamics, they would quickly crash. The main advantage of being inherently unstable is that this enhances maneuverability, but it also requires the insect to have a fast response and move its controls constantly to stabilize the flight. In fact, one of the functions of an insect's control systems is to provide stability (Dudley, 2000; Balint and Dickinson, 2001; Taylor, 2001).

### A. Controllability analysis

A few research groups added control-force terms into the linearized disturbance equations of motion [Eqs. (31) and (33)] and studied the controllability (or reachability) of hovering flight (Sun and Wang, 2007; Cheng and Deng, 2010; Humbert and Faruque, 2011; Zhang and Sun, 2011a). Controllability characterizes the amount of control one has over the state of a system through the choice of input.

When control is applied, the expression for each of the six forces and moments is changed from Eq. (30) to

$$X = X_e + \frac{\partial X}{\partial u}\delta u + \frac{\partial X}{\partial v}\delta v + \cdots + \frac{\partial X}{\partial c1}\delta c1 + \frac{\partial X}{\partial c2}\delta c2 + \cdots, \tag{53}$$

where $c1$, $c2$, etc., refer to the control variables and $\partial X/\partial c1$, $\partial X/\partial c2$, etc., are partial derivatives and termed control derivatives (e.g., $\partial X/\partial c1$, denoted as $X_{c1}$, is the increment in $X$ when there is a unit increment in $c1$). For the longitudinal motion the disturbance equations of motion become (Taylor and Thomas, 2003)

$$\begin{bmatrix} \delta\dot{u}^+ \\ \delta\dot{w}^+ \\ \delta\dot{q}^+ \\ \delta\dot{\theta}^+ \end{bmatrix} = \mathbf{A}\begin{bmatrix} \delta u^+ \\ \delta w^+ \\ \delta q^+ \\ \delta\theta \end{bmatrix} + \mathbf{Bc}, \tag{54}$$

where $\mathbf{c}$ is the control vector, $\mathbf{c} = [c1, c2, \ldots,]^T$, and

$$\mathbf{B} = \begin{bmatrix} X^+_{c1}/m^+ & X^+_{c2}/m^+ & \cdots \\ Z^+_{c1}/m^+ & Z^+_{c2}/m^+ & \cdots \\ M^+_{c1}/I^+_y & M^+_{c2}/I^+_y & \cdots \\ 0 & 0 & \cdots \end{bmatrix}. \tag{55}$$

Many freely flying insects have been observed to control their flight by changing stroke amplitude ($\Phi$), mean stroke angle ($\bar{\phi}$), downstroke ($\alpha_d$) and upstroke ($\alpha_u$) angles of attack, wing-rotation time ($\Delta t_r$), and rotation timing (Ellington, 1984b; Ennos, 1989; Fry, Sayaman, and Dickinson, 2003; Zhang and Sun, 2010a). Freely flying fruit flies were observed to control their flight by changing the stroke-plane angle ($\beta$) in addition to $\Phi$, $\bar{\phi}$, $\alpha_d$, $\alpha_u$, $\Delta t_r$, and wing-rotation timing (Fry, Sayaman, and Dickinson, 2005). Thus the longitudinal control changes are $\delta\Phi$, $\delta\bar{\phi}$, $\delta\alpha_1$, $\delta\alpha_2$, etc. ($\delta\Phi$ and $\delta\bar{\phi}$ represent changes in $\Phi$ and $\bar{\phi}$ from their equilibrium values, respectively; $\delta\alpha_1$ represents an equal change in $\alpha_d$ and $\alpha_u$ from their equilibrium values and $\delta\alpha_2$ represents a differential change in $\alpha_d$ and $\alpha_u$ from their respective equilibrium values). The lateral control changes are $\delta\Phi_a$, $\delta\alpha_{1a}$, $\delta\alpha_{2a}$, etc. $\delta\Phi_a$ represents

an asymmetrical change in $\Phi$ of the left and right wings, e.g., $\delta\Phi_a = 10°$ means that $\Phi$ of the left wing increases by 5° and that of the right wing decreases by 5° from the equilibrium value. $\delta\alpha_{1a}$ represents the following variation in wing angle of attack: $\alpha_d$ and $\alpha_u$ of the left wing both increase by $|\delta\alpha_{1a}|/2$ and those of the right wing decrease by $|\delta\alpha_{1a}|/2$ from their respective equilibrium values. $\delta\alpha_{2a}$ represents the following variation in wing angle of attack: for the left wing, $\alpha_d$ increases and $\alpha_u$ decreases by $|\delta\alpha_{2a}|/2$ from their respective equilibrium values; for the right wing, $\alpha_d$ decreases and $\alpha_u$ increases by $|\delta\alpha_{2a}|/2$ from their respective equilibrium values.

Control derivatives with respect to each control variable can be measured using a dynamically scaled robotic model [as by Dickson *et al.* (2010)], or computed using the CFD method [as by Sun and Wang (2007)] or the simple aerodynamic model discussed in Sec. II.C [as by Humbert and Faruque (2011)]. The measured (Dickson *et al.*, 2010) and computed (Sun and Wang, 2007; Cheng and Deng, 2011; Humbert and Faruque, 2011; Zhang and Sun, 2011a) longitudinal control derivatives at a normal hovering condition indicate that a change in stroke amplitude ($\delta\Phi$) and/or an equal change in the angles of attack of the downstroke and upstroke ($\delta\alpha_1$) mainly produces a change in vertical force (the magnitude of $Z_\Phi^+$ is much greater than those of $X_\Phi^+$ and $M_\Phi^+$ and the magnitude of $Z_{\alpha_1}^+$ is much greater than those of $X_{\alpha_1}^+$ and $M_{\alpha_1}^+$), a change in mean stroke angle ($\delta\bar{\phi}$) mainly produces a change in pitching moment, and a differential change in the angles of attack of the downstroke and upstroke ($\delta\alpha_2$) mainly produces a change in horizontal force. The corresponding lateral control derivatives show that an antisymmetrical change in stroke amplitude ($\delta\Phi_a$) or an antisymmetrical change in angle of attack with equal change in $\alpha_d$ and $\alpha_u$ ($\delta\alpha_{1a}$) mainly produces a change in roll moment, and an antisymmetrical change in angles of attack with differential change in $\alpha_d$ and $\alpha_u$ ($\delta\alpha_{2a}$) mainly produces a change in the yaw moment. These results tell us that at normal hovering each control variable mainly produces a force or a moment in one direction, i.e., the control variables are approximately uncoupled.

With control derivatives determined, the flight controllability was then analyzed by using the modal decomposition method. In this method (Bryson, 1994; Stevens and Lewis, 2003), a linearly dynamic system is transformed into modal coordinates. When the system is in modal coordinates one can immediately see whether or not a mode can be controlled, and if it can, by which controls. Sun and Wang (2007), Cheng and Deng (2011), and Zhang and Sun (2011a) studied the controllability of hovering flight in hoverflies, fruit flies, and droneflies. $\Phi$, $\bar{\phi}$, and $\alpha$ were taken as control variables, and the results were as follows. For longitudinal motion, the unstable slow oscillatory mode can be controlled by $\delta\bar{\phi}$ or $\delta\alpha_2$ and the stability of the weakly stable mode can be augmented by $\delta\Phi$ and $\delta\alpha_1$. For lateral motion, the unstable mode can be controlled and the stability of the weakly stable mode can be augmented by any two of $\delta\Phi_a$, $\delta\alpha_{1a}$, and $\delta\alpha_{2a}$. Humbert and Faruque (2011) studied the longitudinal controllability of a hovering fruit fly. They took $\delta\Phi$, $\delta\bar{\phi}$, $\delta\beta$, $\delta\alpha_1$, and $\delta\alpha_2$ as control variables and demonstrated that controllability is achieved through the choice of two of these control inputs.

Liu *et al.* (2010), by numerically solving the complete equations of motion coupled with the Navier-Stokes equations and by trial and error, showed that a cycle-by-cycle manipulation of just three wing-kinematical parameters ($\Phi$, $\bar{\phi}$, and $\beta$) could stabilize longitudinal flight.

These controllability analyses show that although unstable, the hovering flight of insects is controllable, and that there are redundant control variables. The studies discussed above are limited to hovering flight. Formal quantitative studies on controllability at forward flight need to be made in the future.

### B. Closed-loop control analysis

Controllability considers only the "outer" open-loop dynamics of the insects [the equations of motion, e.g., Eq. (31), modeled only the dynamics and aerodynamics of the body and wings and contained no information on the sensors, neural circuits, and muscles]. These studies show only whether or not the flight is controllable, and which control variables can best control an unstable or weakly stable mode, but cannot tell us how the controls are applied to stabilize the flight. How an insect stabilizes its flight is determined by the coupling between its "inner" control systems (sensory system and neuron-motor control system) and the outer dynamics. At present, wing and body aerodynamics and dynamics are relatively well understood and modeled (as seen in Secs. II–V), but it is not so for the inner control systems. Insect sensors are well studied and are well understood in physiological detail, but not at a broader functional level (Dudley, 2000; Land and Nilsson, 2002; Taylor and Krapp, 2007). Many components of the internal control system, e.g., neural circuitry and wing-hinge mechanics, are still poorly understood (Dickson, Straw, and Dickinson, 2008) and are being actively investigated (Balint and Dickinson, 2001; Tammero and Dickinson, 2002; Sherman and Dickinson, 2003; Kern *et al.*, 2005; Sane *et al.*, 2007; Straw, Lee, and Dickinson, 2010; Rohrseitz and Fry, 2011; Krishnan *et al.*, 2012). Despite these limitations, some attempts have been made to understand how flying insects control and stabilize their flight, by combining recordings of insects' closed-loop free-flight behaviors and the open-loop dynamics with simple models of sensory systems and sensory-motor responses (Dickson, Straw, and Dickinson, 2008; Ristroph *et al.*, 2010; Cheng and Deng, 2011).

Dickson, Straw, and Dickinson (2008) presented a framework for simulating the flight dynamics and control strategies of flies, which consisted of five main components: a model of body dynamics, a model of aerodynamic forces and moments, a sensory systems model, a control model, and an environment model (see the block diagram in Fig. 12). In modeling the body dynamics, the two-winged insect was represented by a system of three rigid bodies connected by a pair of actuated ball joints (similar to that shown in Fig. 6). For the aerodynamic model, a simple aerodynamic model of Sane and Dickinson (2002) discussed in Sec. II.C was employed. The sensory model focused on two key sensory systems, the visual system and the halteres, with the former proving information concerning the presence of approaching obstacles or distant targets (navigation) and the latter providing

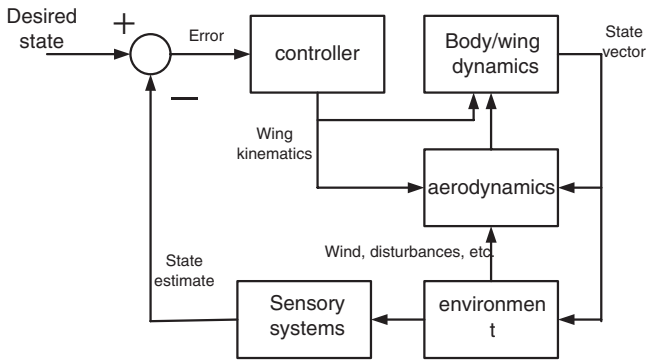


FIG. 12. Block diagram illustrating the overall architecture of the simulation framework which simulates the flight dynamics and control strategies of flies. The framework consists of five main components: a model of body dynamics, a model of aerodynamic forces and moments, a sensory systems model, a control model, and an environment model. Adapted from Dickson, Straw, and Dickinson, 2008.

information on the rate of change of key variables such as pitch, roll, and yaw angles. The control model consisted of a set of control laws specifying the behavior of the insect with regard to sensory inputs, providing a means by which the outputs of the sensory system modulated the wing kinematics. In the environment model, arbitrary visual surroundings were simulated by a computer graphics engine, and physical features such as wind gusts could be added; the model provided input to both the sensory systems and the aerodynamic model. Because the flight control mechanisms and neuron-motor physiology in real insects are poorly understood at present, the control model in the framework is coarsely represented. Nevertheless, this simulation framework is valuable in that it provides a quantitative test bed for examining the possible control strategies employed by flying insects. Similar work have been done to model a micromechanical flying insect (Schenato, 2003; Deng, Schenato, and Sastry, 2006a, 2006b), a small fixed-wing aircraft (Beyeler *et al.*, 2006), and a hovercraft (Serres *et al.*, 2006).

Ristroph *et al.* (2010) studied the stabilization control of fruit flies at near hover by combining thoughtful experiment and model simulation. This work can be considered as an example of application of the simulation framework given by Dickson, Straw, and Dickinson (2008). First, they applied yaw-torque impulses to freely flying fruit flies (*Drosophila melanogaster*) in slow-speed flight and measured the body yaw-angle and wing-motion variation using high-speed video and a motion tracking method (Ristroph *et al.*, 2009), obtaining the overall response properties of the insects. Then they formed a simulation model that included the body dynamics, wing aerodynamics, angular rate sensing system, and a controller that specified the relation between the output of sensory systems and the input to the wing-motion system. Finally, by comparing the measured closed-loop behaviors with the results of the simulation model, they tested some of the uncertain components of the simulation model and determined the time constant in the model of the sensory system and the parameters in the model of neural circuitry.

In the behavioral-response measurement, at $t = 0$, the yaw-torque impulse was applied for about one wing beat (the wing-beat period is 4.5 ms). They found that at about 3.5 wing beats the fly experiences its maximal deflection in yaw angle ($\psi$), and then $\psi$ decreases from its maximal deflection to approximately zero monotonically, in about 6.5 wing beats. Measured wing-kinematical data show that the recovery is controlled by asymmetrically adjusting the angles of attack of the left and right wings, i.e., using control input $\delta\alpha_{2a}$. The control starts at $t \approx 2.5$ wing beats, showing that the delay time of the sensory-motor response (neural latency and inertia of the sensors and motor) is about 10 ms.

In the simulation model, only the yaw rotation (rotation about a vertical axis passing the center of mass of the body) was considered and other motions were neglected. The body yaw dynamics was described by

$$I\ddot{\psi} = N_{\text{aero}} + N_{\text{ext}}, \tag{56}$$

where $I$ was the yaw moment of inertia of the insect body, $N_{\text{aero}}$ was the aerodynamic yaw torque, and $N_{\text{ext}}$ was the applied torque impulse. $N_{\text{aero}}$ had two parts: One was due to the disturbed motion and could be written as $N_{\dot{\psi}}\dot{\psi}$, where $N_{\dot{\psi}}$ was the yaw damping derivative. The other was due to active control by adjusting the wing angle of attack, and can be written as $N_\alpha \delta\alpha_{2a}$, where $N_\alpha$ was the control derivative representing the yaw moment produced by a unit asymmetrical change in the angles of attack of the left and right wings. Equation (56) can be written as

$$I\ddot{\psi} = N_{\dot{\psi}}\dot{\psi} + N_\alpha \delta\alpha_{2a} + N_{\text{ext}}. \tag{57}$$

The wing aerodynamic model used to compute $N_{\dot{\psi}}$ and $N_\alpha$ was the simple aerodynamic model of Sane and Dickinson (2002), the same as that used by Dickson, Straw, and Dickinson (2008). The sensory system for the stabilization control was considered to be the halteres for the following reasons. As observed from the measured data, the body motion was a yaw rotation and the delay time of the sensory-motor response was very short (only about 10 ms). Anatomical, mechanical, and behavioral evidence indicated that the halteres serve as detectors of body angular velocity that quickly trigger muscle action (Pringle, 1948; Sandeman and Markl, 1980; Dickinson, 1999). Here the input of the halteres was the yaw rate $\dot{\psi}$. The controller, which related the sensed yaw rate $\dot{\psi}$ to the change in wing kinematics ($\delta\alpha_{2a}$), was modeled and tested as follows. They first modeled it by a minimal linear-control model containing a term proportional to the integral over time of $\dot{\psi}$:

$$\delta\alpha_{2a} = K_1\psi(t - \Delta t), \tag{58}$$

where $\Delta t$ was the response delay time and its value was known from the measurement (2.5 wing-beat periods or about 10 ms). They found that this control law [Eq. (58)] was used, the simulation model failed to match the yaw data. They then changed to a proportional-plus-derivation (PD) scheme:

$$\delta\alpha_{2a} = K_1\psi(t - \Delta t) + K_2\dot{\psi}(t - \Delta t). \tag{59}$$

With this control law, they arrived at a good match to the yaw data.

This study shows that in its stabilization of the yaw motion, the sensory-motor circuit of the fruit flies can be modeled by a linear-control model with a PD scheme that feeds back to all state variables (here $\psi$ and $\dot{\psi}$) with a delay time. It should be noted that in the study the delay times for $\psi$ and $\dot{\psi}$ were assumed to be the same. This may not be appropriate: Fruit flies are known to use their halteres to sense angular velocity, but sensing of angular orientation is likely visual (Dickinson, 1999; Taylor and Krapp, 2007). The latency of the visual system is much higher than that of mechanosensor-based biological gyroscopes. There is another problem with the modeling: only the yaw rotation (rotation about the vertical axis) was considered in the model. The applied yaw moment and the yaw moment produced by the wings' $\delta\alpha_{2a}$ were about the vertical axis. Because the vertical axis is not a principal axis of the body (the vertical axis is about 30° from the long axis of the body, which is very close to a principal axis), the yaw moments would produce, in addition to the yaw rotation, rotations in other directions. Neglect of these rotations needs justification.

Cheng, Deng, and Hedrick (2011) studied the stabilization control of hovering hawk moths, using an approach similar to that of Bergou *et al.* (2010). They took advantage of the hawk moths' natural behavior of hovering to feed. They first applied a visual stimulus to disturb hawk moths which freely hovered in front of an artificial flower. The disturbed motion was approximately longitudinal and mainly contained pitch rotation and horizontal translation. The results of the behavioral-response measurement are as follows: After being startled, the hovering moth began to pitch up and move backward simultaneously, and the backward velocity was close to maximum when the moth reached the largest pitch angle (about 60°; the initial hovering pitch angle was 35°). Next the moth began to pitch down while it was still moving backward, typically overpitching down to about 15° below the initial hovering pitch angle. Last, the moth began to pitch up again but at a slower rate, returning to the equilibrium flight (hovering). The recovery time, the period between the time when the insect is at the largest pitch angle and the time when hovering is recovered, is about 360 ms (11 wing beats). The simultaneously measured wing kinematics shows that the recovery is controlled by a differential change in the down-stroke and upstroke angles of attack of the wings ($\delta\alpha_2$ control).

In this simulation model, the dynamics of the pitch rotation and horizontal translation of the body is described by

$$m_b\ddot{x} = X_u\dot{x} - m_b g\sin\delta\theta + X_c, \tag{60}$$

$$I_{yy}\ddot{\theta} = M_q\dot{\theta} - M_u\dot{x} + M_c, \tag{61}$$

where $m_b$ is the body mass; $I_{yy}$ is the pitch moment of inertia of the body; $\dot{x}\,(=u)$ and $\ddot{x}$ are the horizontal-translation velocity and acceleration, respectively; $\theta$ is the pitch angle; and $\boldsymbol{\delta}\theta$ is the difference between $\theta$ and its value at hovering. $X_u$, $M_q$, and $M_u$ are aerodynamic derivatives; and $X_c$ and $M_c$ are the control force and moment, respectively. They model the controller using a linear-control model with PD scheme:

$$X_c = -K_u\dot{x}(t), \tag{62}$$

$$M = -K_\theta\delta\theta(t-\tau_1) - K_{\dot{\theta}}\delta\dot{\theta}(t-\tau_2), \tag{63}$$

where $K_u$, $K_\theta$, and $K_{\dot{\theta}}$ are constants, and $\tau_1$ and $\tau_2$ are the response delay times for the visual sensing system and the mechanosensor-based sensing system, respectively [recent studies showed that hawk moths' antennae may be involved in the inertial sensing of rotations, in addition to sensing airflow (Sane *et al.*, 2007; Krishnan *et al.*, 2012)]. Experiments employing dynamically scaled robotic wings (Zhao *et al.*, 2010) were used to estimate the force and moment derivatives. They found that the above controller model gave a good match to the measured behavioral response for plausible sensory delays ($\tau_1$ and $\tau_2$) for one to two wing beats. In recomputing the closed-loop flight dynamics coefficients with different assumed sensory delays, they found that increasing the sensory delay parameters increased the feedback gain required for the best fit to the observed data; this is also true in the case of yaw motion in fruit flies (Elzinga, Dickson, and Dickinson, 2012). The study also showed that hawk moths rely largely on passive damping to reduce the body translation but use feedback control based on pitch angle and angular velocity to control their orientation.

In the control-force model Eq. (62), the translation-velocity feedback $-K_u\dot{x}$ does not have a time delay and they did not explain why it could be so. Furthermore, only the translation velocity ($\dot{x}$), but not the horizontal position ($x$), is fed back for the stabilization control. A hawk moth hovering in front of a flower tends to maintain contact with the flower (Sprayberry and Daniel, 2007), and the horizontal position might need to be fed back for the stabilization control.

Both studies discussed (Ristroph *et al.*, 2010; Cheng, Deng, and Hedrick, 2011) indicate that the insect's sensory-motor system can be modeled by a PD controller with delay times. Tanaka and Kawachi (2006) and Graetzel, Nelson, and Fry (2010) studied an insect's sensory-motor system using frequency-domain approaches. Frequency-response characteristics of tethered bumblebees (Tanaka and Kawachi, 2006) and fluit flies (Graetzel, Nelson, and Fry, 2010) to vertical visual oscillations were measured and analyzed. By tethering the insect and measuring its control responses to a properly designed stimulus, the active controls that stabilize the inherent instability of flying insects can be separated from the natural flight dynamics of the insect and analyzed (Taylor *et al.*, 2008). They measured the vertical force of the insects at various oscillation frequencies. They summarized the response characteristics in terms of amplitude and phase differences. In the low-frequency domain, the amplitude was almost constant, whereas the phase gradually lagged with increasing frequency. This indicates that the vertical force is directly proportional to the apparent vertical displacement and there is a delay time (Graham and McRuer, 1961; Tischler and Remple, 2006). That is, the controller is a proportional ($P$) controller with a delay time. Further studies are required to explore why for the case of vertical motion (Tanaka and Kawachi, 2006; Graetzel, Nelson, and Fry, 2010) the controller is a $P$ controller with a delay time, but for the case of yaw rotation (Ristroph *et al.*, 2010), or a combination of pitch

rotation and horizontal translation (Cheng, Deng, and Hedrick, 2011), it is a PD controller with delay times.

Earlier on, some researchers obtained the overall response properties of freely flying hawk moths by presenting oscillating visual stimuli at a range of different frequencies, taking advantage of their natural behavior of maintaining contact with the flower where they are feeding. Farina, Varju, and Zhou (1994) investigated how well the diurnal hawk moth *Macroglossum stellatarum* performed when a (dummy) flower was moved toward and away from the animal. The hawk moth successfully tracked the dummy flower at frequencies from 0.15 to 5 Hz, indicating that the system behaved as a bandpass filter with corner frequencies of 0.15 and 5 Hz. The same group also investigated the result of oscillating the wider visual environment but with the flower stationary, and similar frequency-response properties were shown in the hawk moth *Macroglossum stellatarum* (Farina, Kramer, and Varju, 1995). This group further investigated the case of combined translational and rotational pattern motion (Kern and Varju, 1998). They found that oscillatory translational and rotational pattern motion leads to compensatory responses that peak in the frequency range between 2 and 4 Hz. Similar behavior was demonstrated in the crepuscular hawk moth *Manduca sexta* (Moreno, Tu, and Daniel, 2000). Sprayberry and Daniel (2007) investigated the effect of frequency and the direction of flower motion on tracking performance in the hawk moth *Manduca sext*, and found that while *M. sexta* appeared equally capable of tracking flowers moving in the horizontal and vertical axes, they demonstrated poor ability to track flowers moving in the looming axis. These studies (Farina, Varju, and Zhou, 1994; Farina, Kramer, and Varju, 1995; Kern and Varju, 1998; Moreno, Tu, and Daniel, 2000; Sprayberry and Daniel, 2007) identified the overall response properties of the hawk moths, but did not break the system down into subsystems representing the effects of active control and of the natural flight dynamics. If the overall response study is combined with the natural flight dynamics model, the subsystem representing the effects of active control can be identified. This approach is recommended for future studies.

## VII. STEADY-STATE CONTROL

Steady-state control is the constant control required for changing the flight system from one equilibrium flight to another. Theoretical and experimental investigations have been done on changing from hovering to small-speed flight. But only experimental investigations have been done on forward flight (changing from one flight speed to another).

### A. Steady-state control for changing from hovering to small-speed flight

Ellington (1984c) and Ennos (1989) made high-speed films of many insects hovering and flying slowly inside flight chambers. Their films revealed that insects changing from hovering to small-speed flight are simply controlled by tilting the stroke plane, as for a helicopter: Going from hovering to forward flight is always preceded by a forward tilt of the stroke plane, and backward tilt gives backward flight. Similarly, flight in lateral directions is accompanied by a roll of the stroke plane. Roll can be affected by increasing the flapping amplitude and/or angle of attack of the outside wing (i.e., $\delta\Phi_a$ and/or $\delta\alpha_{1a}$ controls). Pitching results from a fore or aft shift of the center of lift, which pitches the body and hence the stroke plane; the shift can be realized by changing the fore or aft extent of the flapping motion (i.e., a $\delta\bar{\phi}$ control) and/or the angle of attack over a half-stroke (i.e., a $\delta\alpha_2$ control).

Wu and Sun (2009) and Zhang and Sun (2011b) made a formal quantitative analysis of the steady-state control for changing from hovering to small-speed flight in a model dronefly, using the linear theories of stability and control. They solved the steady-state equations of motion to determine the required steady-state control. Based on experimental observation of dronefly flight (Ellington, 1984a; Ennos, 1989), $\delta\Phi$, $\delta\bar{\phi}$, $\delta\alpha_1$, and $\delta\alpha_2$ were taken as longitudinal control variables, and $\delta\Phi_a$, $\delta\alpha_{1a}$, and $\delta\alpha_{2a}$ as lateral control variables. Setting the time-derivative terms on the left-hand side of the equations of motion with control force and moment terms [Eq. (54)] to zero gives

$$\mathbf{A}\begin{bmatrix}\delta u^+\\ \delta w^+\\ \delta q^+\\ \delta\theta\end{bmatrix}+\mathbf{B}\begin{bmatrix}\delta\Phi\\ \delta\alpha_1\\ \delta\bar{\phi}\\ \delta\alpha_2\end{bmatrix}=0 \tag{64}$$

for longitudinal motion. For lateral motion the corresponding equation is

$$\mathbf{A}_1\begin{bmatrix}\delta v^+\\ \delta p^+\\ \delta r^+\\ \delta\gamma\end{bmatrix}+\mathbf{B}_1\begin{bmatrix}\delta\Phi_a\\ \delta\alpha_{1a}\\ \delta\alpha_{2a}\end{bmatrix}=0. \tag{65}$$

Equations (64) and (65) determine the small-speed steady-state motion under given small controls: Without controls (i.e., $\delta\Phi$, $\delta\alpha_1$, etc., are zero), one obtains the reference flight (hovering: $\delta u^+$, $\delta w^+$, $\delta q^+$, $\delta\theta$, $\delta v^+$, $\delta p^+$, $\delta r^+$, and $\delta\gamma$ are zero). With small controls (some of $\delta\Phi$, $\delta\alpha_1$, etc., are not zero), some of the motion variables are nonzero, giving small-speed steady-state motions. The solutions of Eqs. (64) and (65) are

$$(\delta q^+=0,\quad \delta p^+=0), \tag{66}$$

$$\delta u^+=1.73\delta\bar{\phi}-0.28\delta\alpha_2, \tag{67}$$

$$\delta w^+=-1.47\delta\Phi-2.17\delta\alpha_1, \tag{68}$$

$$\delta\theta=-1.61\delta\bar{\phi}-1.80\delta\alpha_2, \tag{69}$$

$$\delta v^+=-2.77\delta\Phi_a-4.29\delta\alpha_{1a}, \tag{70}$$

$$\delta r^+=-2.47\delta\alpha_{2a}, \tag{71}$$

$$\delta\gamma=-1.62\Phi_a-2.91\delta\alpha_{1a}. \tag{72}$$

Supposing that a control $\delta\bar{\phi}$ is applied (i.e., $\delta\bar{\phi}\neq 0$ and the other controls are zero), the above equations give

$$\delta u^+=1.73\delta\bar{\phi}, \tag{73}$$

$$\delta\theta=-1.61\delta\bar{\phi}, \tag{74}$$

$$\delta w^+ = \delta v^+ = \delta p^+ = \delta q^+ = \delta r^+ = \delta\gamma = 0. \quad (75)$$

That is, a change in the mean stroke angle ($\delta\bar{\phi}$) results in a horizontal forward or backward flight at velocity $\delta u^+$ [see Eq. (73)] with the body tilted forward or backward from its hovering attitude by an angle $\delta\theta$ [see Eq. (74)]. This is consistent with observations by Ellington (1984c) and Ennos (1989). Similarly, from Eqs. (66)–(72) the following can be shown: A change in the stroke amplitude ($\delta\Phi$) or an equal change in the downstroke and upstroke angles of attack ($\delta\alpha_1$) results in a vertical climb or descent at velocity $\delta w^+ = -1.47\delta\Phi$ (or $-2.17\delta\alpha_1$). An antisymmetrical change in the stroke amplitudes of the contralateral wings ($\delta\Phi_a$), and/or an antisymmetrical change in the angles of attack of the contralateral wings, with the downstroke and upstroke angles of attack of a wing having equal change ($\delta\alpha_{1a}$), results in a side translation at velocity $\delta v^+ = -2.77\delta\Phi_a$ (or $-4.29\delta\alpha_{1a}$) with the body tilted to the same side by an angle. A proper combination of these controls can give a flight of any small speed in any desired direction.

Equations (66)–(72) also show that an antisymmetrical change in the angles of attack of the contralateral wings, with the downstroke and upstroke angles of attack of a wing having differential change ($\delta\alpha_{2a}$), results in a constant-rate yaw rotation at rotational speed $\delta r^+ = -2.47\delta\alpha_{2a}$ [see Eq. (71)]. The only possible steady-state rotational motion is a constant-rate yaw rotation (steady-state pitch or roll rotation could not be realized), which agrees with observations.

It should be noted that the above results are the steady-state (or long-term) effects of the controls. The initial (or short-term) effects of a control can sometimes be opposite to the steady-state effects. The initial effects of a control are to start a motion, and its exact analysis needs to solve the complete equations of motion. An example of this is the analysis of the starting of yaw maneuvers of a fruit fly by Bergou *et al.* (2010). We return to their analysis in Sec. VIII. Here, we examine the initial (or short-term) effects of the controls qualitatively by simple physical reasoning. We first consider the $\delta\alpha_{2a}$ control (an antisymmetrical change in the angles of attack of the contralateral wings, with the downstroke and upstroke angles of attack of a wing having differential change). When a positive $\delta\alpha_{2a}$ control is applied, a negative yaw moment $N_{\alpha_{2a}}\,\delta\alpha_{2a}$ [$N_{\alpha_{2a}}$ is the yaw moment derivative with respect to $\delta\alpha_{2a}$ and is negative (Cheng and Deng, 2011; Zhang and Sun, 2011a)] will result, which makes the insect start yawing to the left and gradually increases the yaw-rotation velocity. The left-yawing velocity ($\delta r < 0$) produces a positive moment $Nr\delta r$ [$Nr$ is the yaw moment derivative with respect to $\delta r$ and is negative, a damping moment (Cheng and Deng, 2011; Zhang and Sun, 2011a)]. As the magnitude of the yawing velocity becomes large enough, $Nr\delta r$ and $N_{\alpha_{2a}}\,\delta\alpha_{2a}$ become balanced and the steady-state flight (left-yawing rotation) is reached. Here both the initial and steady-state effects of the $\delta\alpha_{2a}$ control are to make the insect yaw to the left. We thus see that the initial (short-term) and steady-state (long-term) effects of a $\delta\alpha_{2a}$ control are similar. However, this is not true for the case of $\delta\Phi_a$ control (an antisymmetrical change in the stroke amplitudes of the contralateral wings): When a positive $\delta\Phi_a$ control is applied, a positive roll moment $L_{\Phi_a}\,\delta\Phi_a$ [$L_{\Phi_a}$ is the roll moment derivative with respect to $\delta\Phi_a$ and is positive (Cheng and Deng, 2011; Zhang and Sun, 2011a)] will result. This moment makes the insect start rolling to the right and a positive roll angle $\delta\gamma$ results. This angle $\delta\gamma$ tilts the vertical force $F_0\,(=mg)$ to the right, giving a positive side force $F_0\delta\gamma$, which makes the insect move to the right (i.e., have a positive $\delta v$). That is, the initial effect of the positive $\delta\Phi_a$ control is to make the insect start a horizontal right-side translation. But, as discussed, the steady-state effect of the positive $\delta\Phi_a$ control is to maintain a left-side translation. Thus, we see that the initial and steady-state effects of a $\delta\Phi_a$ control are quite contrary. For a steady-state horizontal side translation that requires a positive $\delta\Phi_a$ control, the insect needs to use a negative $\delta\Phi_a$ control as the initial control, and vice versa. For example, to have a steady-state left-side translation, the insect needs a positive $\delta\Phi_a$ control (increasing the stroke amplitude of the left wing and decreasing that of the right wing) to maintain the steady-state flight, but it needs a negative $\delta\Phi_a$ control (decreasing the stroke amplitude of the left wing and increasing that of the right wing) to start the flight.

### B. Control for changing from one forward-flight speed to another

Differences in wing-kinematical parameters between two flight speeds can be taken as the constant controls required for changing from one flight speed to the other. Using high-speed cinematography, Dudley and Ellington (1990a, 1990b) and Cooper (1993) measured the wing and body kinematics of bumblebees in a wind tunnel, over a flight speed range of 0 to 4.5 m/s (the advance ratio, the ratio of the flight speed to the mean flapping speed at the wing tip, ranged from 0 to 0.57). They found that as flight speed increases from 0 to 1 m/s, then to 2.5 m/s, and finally to 4.5 m/s, the stroke-plane angle ($\beta$) invariably increases and the body angle ($\chi$) concomitantly decreases, with the angle between the stroke plane and the longitudinal body axis ($\beta+\chi$), remaining approximately constant for any particular insect. The increasing tilt of the stroke plane with forward speed results in increasing tilt of the mean force vector of the wings, providing a larger thrust required for the increased flight speed, and at the same time, the decreasing body angle results in smaller body drag coefficient. The wing kinematical data showed that as air speed increases, the differential change in the angles of attack of the downstroke and upstroke increased, but no systematic change in wing-beat frequency, stroke amplitude, or mean stroke angle was observed. Willmott and Ellington (1997a, 1997b) made similar measurements in hawk moths over a flight speed range of 0 to 5 m/s (advance ratio ranging from 0 to 1.12). Similar to the case of bumblebees, as flight speed increases, the stroke-plane angle increases and the body angle decreases. The wing kinematical data showed that the changes in flight speed and body attitude resulted from an increase of the mean stroke angle and a differential change of the downstroke and upstroke angles of attack. At lower flight speeds (between hovering and 3 m/s), the change in mean stroke angle is pronounced and at higher flight speeds (between 3 and 5 m/s), the change in downstroke and upstroke angles of attack is pronounced. No systematic change in wing-beat frequency with airspeed was observed, similarly to the case of bumblebees.

These data indicate that the insects mainly use a change in mean stroke angle ($\delta\bar{\phi}$) and a differential change in the downstroke–upstroke angles of attack ($\delta\alpha_{2a}$) to go from one flight speed to another. Up to now, wing and body kinematics of free flight has been measured over the entire speed range only for bumblebees and hawk moths. Other insects might use different controls for changing flight speed.

## VIII. MANEUVER CONTROL

Many insects perform maneuvers as often as they hover or fly at constant speed along a straight line (Dudley, 2000; Grimaldi and Engel, 2005). Typical maneuvers include takeoff and landing, fast change in flight speed and/or flight direction, body saccades (brisk right-angle turns at or near hovering), etc. (Govind and Dandy, 1972; Land and Collett, 1974; Collett and Land, 1975; Ruppell, 1989; Dudley, 2000; Wang *et al.*, 2003; Card and Dickinson, 2008). For most of these maneuvers, there have been many photographs and descriptions of body motion, but detailed wing kinematics during the maneuvers are not available. As a result, controls applied to achieve the maneuvers cannot be analyzed. There is one typical maneuver, the saccade of flies, for which the body motion and the corresponding change in wing motion (i.e., the control) have been studied in detail. Body motion and wing motion during the maneuver saccades of fruit flies (Fry, Sayaman, and Dickinson, 2003; Bergou *et al.*, 2010) and droneflies (Zhang and Sun, 2010a) are measured using three-dimensional, high-speed videograph, and aerodynamic forces produced by the wings are measured by "replaying" the wing kinematics on a dynamically scaled robotic model (Fry, Sayaman, and Dickinson, 2003), or computed by using the simple aerodynamic model discussed in Sec. II.C (Bergou *et al.*, 2010) or by the CFD method (Zhang and Sun, 2010a).

Previously it was assumed that inertia plays a minor role in the dynamics of even large fly species (Reichardt and Poggio, 1976). If so, during a saccade a fly would apply a positive (or negative) control continuously to produce torque of the same sign to overcome the friction force acting on its body. However, studies on fruit flies *Drosophila melanogaster*, which are very small in size, showed that the flies need to apply a control to start the turn and an opposite one to stop it; thus it is the inertia, not friction, that dominates the flight dynamics of the flies (Fry, Sayaman, and Dickinson, 2003). The flies rotate by 90° within 50 ms, completing the maneuver within 10 wing beats.

Similar experiments were conducted with droneflies (Zhang and Sun, 2010a), which are about 4.5 times as large as fruit flies. It was surprising to find that the number of wing beats taken to make the turn (about 10 wing beats) is approximately the same as, and the turning time (about 55 ms) is only a little different from, that of the fruit flies, even though the mass of a dronefly is more than 100 times that of a fruit fly. The reason for this is that, although the moment of inertia increases as $R^5$ ($R$ is the wing length), so does the aerodynamic moment (Zhang and Sun, 2010a).

During a saccade, although the body rotation is mainly about a vertical axis, the moment vector required for the turn is not along the vertical axis, since it is not a principal axis of the body. Because the moment of inertia of the body about the axis perpendicular to the long axis of the body is much larger than that about the long axis, a moment around an axis that is almost perpendicular to the long axis is needed for the turn, and this axis is about 30° from the vertical axis for droneflies (Zhang and Sun, 2010a). The moment is mainly produced by changes in wing angles of attack (Bergou *et al.*, 2010; Zhang and Sun, 2010a): in a right turn, for example, the dronefly lets its right wing have a rather large angle of attack in the downstroke (generally larger than 50°) and a small one in the upstroke to start the turn, and lets its left wing do so to stop the turn. Although the stroke amplitude, mean stroke angle, and elevation angle have some variations during the turn, they were shown to not be responsible for the turning moment generation; the wing-beat frequency does not change during the turn (Bergou *et al.*, 2010; Zhang and Sun, 2010a). It is believed that variations in the stroke and elevation angles are used to stabilize the turning motion.

In the study of Bergou *et al.* (2010) of fruit-fly saccade, they also considered the wing-hinge mechanics, or how the variations of the wing angles of attack (the controls) were generated. They inverted the equations of motion of wings to determine the torque exerted by the fly at the wing hinge, $\tau_p$. Body and wing inertial forces and moments in the equations were determined using the measured kinematics and morphological data. The aerodynamic torque in the equations was computed using the simple aerodynamic model. Thus the torque of the fly exerted to pitch the wing (to maintain or change the angle of attack) could be determined. Examining the $\tau_p$ vs $\psi_w$ (wing pitch angle) plot, which was an elliptical curve whose major axis had a negative slope, suggested that the hinge acted like a damped torsional spring. They found that this hinge model matched the experimental data well. They concluded that the wing hinge acted as a torsional spring that passively resisted the wing's tendency to flip in response to aerodynamic and inertial forces. To change the pitch angle (angle of attack) of the wing (e.g., for initiating a turn), the insects simply changed the spring rest angle. In this way, the wing pitch control becomes rather simple. Animals take advantage of mechanical properties of their bodies to simplify the complex actuation necessary to move (Dickinson *et al.*, 2000; Liao *et al.*, 2003); the wing-hinge mechanism provides a concrete example of this.

Saccades of flies are made during or near hovering flight. There is one study on turning maneuvers in free forward flight of dragonflies in which detailed wing motion (control) is measured. Wang *et al.* (2003) used a projected comb-fringe technique combined with the natural landmarks on dragonflies (*Polycanthagyna melanictera*) to determine the wing kinematics, body position, and attitude of the dragonflies. Kinematical parameters, including wing-beat frequency, stroke angle, angle of attack, torsional angle, and camber deformation, were measured. Their data showed that during the turn there were large asymmetries between the stroke amplitudes of the left and right wings, while asymmetries in other parameters were generally small, implying that the dragonflies use asymmetries between the stroke amplitudes of the left and right wings to make a turn. This is different from the behavior of fruit flies and droneflies, which use asymmetries between the angles of attack of the left and right wings to make a turn. Unfortunately, aerodynamic forces and

moments were not computed or measured. It is desirable to have these forces and moments to provide a quantitative analysis of this type of turning maneuver.

## IX. CONCLUDING REMARKS

Aerodynamic models for flight dynamics studies are generally divided into two types: simple aerodynamic models and CFD models. Computational fluid dynamics models capture all the unsteady and viscous flow phenomena of a flapping insect wing and can accurately calculate the aerodynamic derivatives needed in the flight dynamics analysis. But they are computationally costly and difficult to handle. Simple models by Sane and Dickinson (2002) and Berman and Wang (2007) capture the essential unsteady and viscous flow phenomena (delayed-stall and added-mass effects). For longitudinal motion, they can predict aerodynamic derivatives with reasonably good accuracy. But for lateral motion, they encounter difficulties when predicting some of the aerodynamic derivatives, because they do not take the changing-LEV-axial-velocity effect into account. This raises a need for modifying these models to include the changing-LEV-axial-velocity effect.

Current stability and control analyses of insect flight are based on the averaged-model theory and treat hovering flight or forward flight as a fixed-point equilibrium. With this model, well-developed stability and control theories and analysis methods for aircraft can be applied to insect flight dynamics. Verifications using Floquet theory and direct numerical simulation (solving the complete equations of motion coupled with the Navier-Stokes equations) show that the averaged model is a good approximation for many insects, even for relatively large insects, such as hawk moths for which the wing-beat frequency is relatively low and characteristic times of the natural modes of motion of the body divided by the wing-beat period are relatively large compared with many other insects.

Stability analysis shows that for hovering flight there exist three longitudinal natural modes of motion: one unstable slow oscillatory mode, one stable fast subsidence mode, and one stable slow subsidence mode, and three lateral natural modes of motion: one unstable slow divergence mode, one stable slow oscillatory mode, and one stable fast subsidence mode. Approximate analytical expressions of the eigenvalues identify the speed derivative $M_u$ (the pitch moment produced by unit forward-backward speed) as the primary source of the longitudinal unstable mode, and the speed derivative $L_v$ (the roll moment produced by unit side speed) as the primary source of the lateral unstable mode. Coupling between horizontal forward-backward motion and pitch rotation through $M_u$ causes longitudinal instability, and coupling between horizontal side motion and roll rotation through $L_v$ causes lateral instability. Because of the unstable modes, the hovering flight of the insects is dynamically unstable. As for forward flight, only one study on one species (bumblebee *Bombus terrestris*) has been made. It was shown that for bumblebees at hovering and at each of the forward-flight speeds considered, there exists at least one unstable, or neutrally stable, natural mode of motion, and thus the flight is not dynamically stable. Further studies on flight dynamic stability at level forward flight and straight-line flight in other directions (climbing flight, vertical flight, etc.) are required in the future. Dragonflies and butterflies often glide. No studies have been made on dynamic flight stability in gliding in insects. It is of interest to investigate this problem in the future.

The advantage of being inherently unstable or neutrally stable is that this enhances maneuverability. But it also requires the insect to have fast response and move its controls constantly to stabilize the flight. To achieve stable flight, an unstable natural mode of motion needs to be stabilized, and a neutrally stable or weakly stable mode requires stability enhancement. For hovering flight, controllability analyses show the following: The longitudinal unstable mode (the unstable slow oscillatory mode) can be controlled by a change in mean stroke angle and/or a differential change in angles of attack of the downstroke and upstroke; the longitudinal weakly stable mode (the stable slow subsidence mode) can be controlled by a change in stroke amplitude and/or an equal change in angles of attack of the downstroke and upstroke. The lateral unstable mode (the unstable slow divergence mode) and weakly stable mode (the stable slow oscillatory mode) can be controlled through the choice of two of the following control inputs: an asymmetrical change in stroke amplitude of the left and right wings, an asymmetrical change in angles of attack of the left and right wings (for each wing, downstroke and upstroke angles of attack have an equal change), and an asymmetrical change in angles of attack of the left and right wings (for each wing, downstroke and upstroke angles of attack have a differential change). That is, although hovering flight is inherently unstable, it is controllable, and furthermore there are redundant control variables. A controllability analysis has not been made for forward flight. It is of great interest to conduct the analysis because the maximum flight speed might be limited by flight stability.

The flight control of animals is a result of closed-loop flight dynamics, i.e., the combination of the passive open-loop dynamics (dynamic flight stability and controllability), sensory systems, and feedback control responses. As the first step, these subsystems have been studied individually. But recently, in a few pioneering works, researchers have taken the approach of combining these interacting dynamical subsystems (Dickson, Straw, and Dickinson, 2008; Ristroph *et al.*, 2010; Cheng, Deng, and Hedrick, 2011). Stabilization controls of fruit flies and hawk moths have been studied in these works. Fruit flies flying at low speed, when disturbed by an impulsive yaw torque, asymmetrically adjust the angles of attack of the left and right wings to stabilize the flight. The flight course is recovered in about 6.5 wing beats (30 ms). Hawk moths hovering to feed in front of an artificial flower, after a pitching-up and backward-moving disturbance, use a differential change in the downstroke and upstroke angles of attack of the wings to stabilize the flight, and hovering is recovered in about 11 wing beats (360 ms). Using measurements of these overall response properties and simple models for the passive open-loop dynamics it has been shown that the insects' sensory-motor systems can be modeled by a PD controller with delay times. The results are interesting, but it should be noted that in these studies overly simplified models of passive open-loop dynamics were used and morphological data, such as body and wing moments of inertia and location

of the center of mass, were roughly estimated. These approximations might affect the accuracy of the models of the sensory-motor systems. The results could be improved when more accurate models of the passive open-loop dynamics are employed. At present, the passive open-loop flight dynamics of insects is relatively well understood and modeled. Insect sensors for flight control have been intensively studied and are well understood in physiological detail, but not at a broader functional level. Many components of the internal control system, e.g., neural circuitry and wing-hinge mechanics, are still poorly understood and are being actively investigated. Simultaneous examination of several of these research areas may lead to rapid progress in understanding how insects control and stabilize their flights and how each subsystem works. Future research in this direction is strongly recommended.

## ACKNOWLEDGMENTS

I thank M. W. Chen, B. Liang, X. G. Meng, and N. Xu and for their help, and D. Du, Y. P. Liu, J. H. Wu, and Y. L. Zhang for useful comments. I acknowledge financial support from the National Science Foundation of China through Grants No. 10232010, No. 10472008, No. 10732030, and No. 11232030, and the Ph.D. Student Foundation of the Chinese Ministry of Education through Grants No. 20110006022 and No. 30400002011105001.

## APPENDIX

Expressions $\mathbf{a}_1$, $\mathbf{a}_2$, $\mathbf{b}_1$, $\mathbf{b}_2$, and $\mathbf{c}$ in Eqs. (8) and (9) are given here:

$$\mathbf{a}_1 = m_{\mathrm{wg}} \sum_{i=1}^{N} \left\{ \frac{d\boldsymbol{\omega}_{\mathrm{bd}}}{dt} \times (\mathbf{R}_h + \mathbf{R}_{\mathrm{wg}}) + \boldsymbol{\omega}_{\mathrm{bd}} \times [\boldsymbol{\omega}_{\mathrm{bd}} \times (\mathbf{R}_h + \mathbf{R}_{\mathrm{wg}})] \right\}_i, \tag{A1}$$

$$\mathbf{b}_1 = m_{\mathrm{wg}} \textstyle\sum_{i=1}^{N} \left[ \left( \mathbf{E}_{w\to b}\, \tilde{\mathbf{E}}_{b\to w}\, \boldsymbol{\omega}_{\mathrm{bd}} + \mathbf{E}_{w\to b} \frac{d_w \boldsymbol{\omega}_{\mathrm{wg0}}}{dt} \right) \times \mathbf{R}_{\mathrm{wg}} + (\boldsymbol{\omega}_{\mathrm{bd}} + \boldsymbol{\omega}_{\mathrm{wg0}}) \times (\boldsymbol{\omega}_{\mathrm{wg0}} \times \mathbf{R}_{\mathrm{wg}}) + \boldsymbol{\omega}_{\mathrm{wg0}} \times (\boldsymbol{\omega}_{\mathrm{bd}} \times \mathbf{R}_{\mathrm{wg}}) \right]_i, \tag{A2}$$

$$\mathbf{a}_2 = m_{\mathrm{wg}} \sum_{i=1}^{N} \left\{ (\mathbf{R}_h + \mathbf{R}_{\mathrm{wg}}) \times \frac{d\mathbf{v}_{\mathrm{cg}}}{dt} + \mathbf{v}_{\mathrm{cg}} \times [\boldsymbol{\omega}_{\mathrm{bd}} \times (\mathbf{R}_h + \mathbf{R}_{\mathrm{wg}})] + \boldsymbol{\omega}_{\mathrm{bd}} \times [(\mathbf{R}_h + \mathbf{R}_{\mathrm{wg}}) \times \mathbf{v}_{\mathrm{cg}}] \right\}_i, \tag{A3}$$

$$\begin{aligned} \mathbf{b}_2 = \sum_{i=1}^{N} \Bigg\{ & m_{\mathrm{wg}} \mathbf{R}_h \times \left[ \frac{d\boldsymbol{\omega}_{\mathrm{wg0}}}{dt} \times \mathbf{R}_{\mathrm{wg}} + (\boldsymbol{\omega}_{\mathrm{wg0}} + \boldsymbol{\omega}_{\mathrm{bd}}) \times (\tilde{\mathbf{E}}_{w\to b}\, {}_w\mathbf{R}_{\mathrm{wg}}) \right] + \tilde{\mathbf{E}}_{w\to b}\, {}_w\mathbf{I}_{\mathrm{wg}} ({}_w\boldsymbol{\omega}_{\mathrm{wg0}} + \mathbf{E}_{b\to w}\, \boldsymbol{\omega}_{\mathrm{bd}}) \\ & + \mathbf{E}_{w\to b}\, {}_w\mathbf{I}_{\mathrm{wg}} \frac{d_w \boldsymbol{\omega}_{\mathrm{wg0}}}{dt} + \boldsymbol{\omega}_{\mathrm{bd}} \times (\mathbf{E}_{w\to b}\, {}_w\mathbf{I}_{\mathrm{wg}\,w}\boldsymbol{\omega}_{\mathrm{wg0}}) + \mathbf{E}_{w\to b}\, {}_w\mathbf{I}_{\mathrm{wg}} \tilde{\mathbf{E}}_{b\to w}\, \boldsymbol{\omega}_{\mathrm{bd}} + m_{\mathrm{wg}} \boldsymbol{\omega}_{\mathrm{bd}} \times [\mathbf{R}_h \times (\boldsymbol{\omega}_{\mathrm{wg0}} \times \mathbf{R}_{\mathrm{wg}})] \\ & + m_{\mathrm{wg}} (\tilde{\mathbf{E}}_{w\to b}\, {}_w\mathbf{R}_{\mathrm{wg}}) \times (\mathbf{v}_{\mathrm{cg}} + \boldsymbol{\omega}_{\mathrm{bd}} \times \mathbf{R}_h) + m_{\mathrm{wg}} \mathbf{v}_{\mathrm{cg}} \times (\boldsymbol{\omega}_{\mathrm{wg0}} \times \mathbf{R}_{\mathrm{wg}}) \Bigg\}_i, \end{aligned} \tag{A4}$$

$$\mathbf{c} = \sum_{i=1}^{N} [\mathbf{E}_{w\to b}\, {}_w\mathbf{I}_{\mathrm{wg}}\, \mathbf{E}_{b\to w} - m_{\mathrm{wg}} (\tilde{\mathbf{R}}_h + \tilde{\mathbf{R}}_{\mathrm{wg}}) \tilde{\mathbf{R}}_h - m_{\mathrm{wg}} \tilde{\mathbf{R}}_h \tilde{\mathbf{R}}_{\mathrm{wg}}]_i, \tag{A5}$$

where $\mathbf{I}_{\mathrm{wg}}$ represents is the moments and products of the inertial of a wing with respect to the wing frame $(x_w, y_w, z_w)$; ${}_w\mathbf{I}_{\mathrm{wg}}$ represents the $x_w$, $y_w$, and $z_w$ components of $\mathbf{I}_{\mathrm{wg}}$; $\boldsymbol{E}_{w\to b}$ and $\boldsymbol{E}_{b\to w}$ are matrices of direction cosines (determined by the flapping angles), representing the transformation from wing frame to body frame and body frame to wing frame, respectively; the symbol "~" is defined as follows: let $\boldsymbol{a} = [a_1 \quad a_2 \quad a_3]^T$ be a vector, and the $\tilde{\boldsymbol{a}}$ denotes the following matrix (Etkin and Reid, 1996):

$$\tilde{\boldsymbol{a}} = \begin{bmatrix} 0 & -a_3 & a_2 \\ a_3 & 0 & -a_1 \\ -a_2 & a_1 & 0 \end{bmatrix}. \tag{A6}$$

## REFERENCES

Altshuler, D. L., W. B. Dickson, J. T. Vance, S. P. Roberts, and M. H. Dickinson, 2005, "Short-amplitude high frequency wing strokes determine the aerodynamics of honeybee flight," Proc. Natl. Acad. Sci. U.S.A. **102**, 18 213.

Ansari, S. A., R. Zbikowski, and K. Knowles, 2006, "Aerodynamic modeling of insect-like flapping flight for micro air vehicles," Prog. Aerosp. Sci. **42**, 129.

Aono, H., F. Liang, and H. Liu, 2008, "Near- and far- field aerodynamics in insect hovering flight: and integrated computational study," J. Exp. Biol. **211**, 239.

Balint, C. N., and M. H. Dickinson, 2001, "The Correlation Between Wing Kinematics and Steering Muscle Activity in the Blowfly Calliphora Vicina," J. Exp. Biol. **204**, 4213.

Bender, J. A., and M. H. Dickinson, 2006, "Comparison of visual and haltere-mediated feedback in the control of body saccades in Drosophila melanogaster," J. Exp. Biol. **209**, 4597.

Bergou, A. J., L. Ristroph, J. Guckenheimer, I. Cohen, and Z. J. Wang, 2010, "Fruit flies modulate passive wing pitching to generate in-flight turns," Phys. Rev. Lett. **104**, 148101.

Berman, G. J., and Z. J. Wang, 2007, "Energy-minimizing kinematics in hovering insect flight," J. Fluid Mech. **582**, 153.

Betts, C. R., and R. J. Wootton, 1988, "Wing shape and flight behaviour in butterflies (Lepidoptera: Papilionoidea and Hesperioidea): a preliminary analysis," J. Exp. Biol. **138**, 271.

Beyeler, A., C. Mattiussi, J. Zufferey, and D. Floreano, 2006, "Vision based altitude and pitch estimation for ultra-light indoor aircraft," *IEEE International Conference on Robotics and Automation (ICRA 2006)* (IEEE, Picataway, NJ).

Birch, J. M., and M. H. Dickinson, 2003, "The influence of wing-wake interactions on the production of aerodynamic forces in flapping flight," J. Exp. Biol. **206**, 2257.

Bomphrey, R. J., J. L. Nicholas, J. H. Nicholas, G. K. Taylor, and A. L. R. Thomas, 2005, "The aerodynamics of Manduca sexta: digital particle image velocimetry analysis of the leading-edge vortex," J. Exp. Biol. **208**, 1079.

Bryson, A. E., 1994, *Control of Spacecraft and Aircraft* (Princeton University Press, Princeton, NJ).

Card, G., and M. H. Dickinson, 2008, "Performance trade-offs in the flight initiation of Drosophila," J. Exp. Biol. **211**, 341.

Cheng, B., and X. Deng, 2010, "Near-hover dynamics and attitude stabilization of an insect model," in *Proceedings of the 2010 American Control Conference* (IEEE, Baltimore, MD).

Cheng, B., and X. Deng, 2011, "Translational and Rotational Damping of Flapping Flight and Its Dynamics and Stability at Hovering," IEEE. Trans. Robot. **27**, 849.

Cheng, B., X. Deng, and T. L. Hedrick, 2011, "The mechanics and control of pitching manoeuvres in a freely flying hawkmoth (Manduca sexta)," J. Exp. Biol. **214**, 4092.

Cheng, B., S. N. Fry, Q. Huang, and X. Deng, 2010, "Aerodynamic damping during rapid flight maneuvers in the fruit fly Drosophila", J. Exp. Biol. **213**, 602.

Collett, T. S., and M. F. Land, 1975, "Visual control of flight behaviour in the house fly Synitta pipiens L." J. Comp. Physiol. **99**, 1.

Combes, S. A., and R. Dudley, 2009, "Turbulence-driven instabilities limit insect flight performance," Proc. Natl. Acad. Sci. U.S.A. **106**, 9105.

Cook, M. V., 1997, *Flight Dynamics: Principles* (Arnold, London).

Cooper, A. J., 1993, "Limitations on bumblebee flight performance," Ph.D thesis, Cambridge University.

Davis, W. R, 1996, "Micro air vehicle for optical surveillance, The Lincoln Laboratory Journal **9**, 197.

Deng, X., L. Schenato, and S. S. Sastry, 2006a, "Flapping flight for biomimetic robotic insects: part I, system modeling," IEEE. Trans. Robot. **22**, 776.

Deng, X., L. Schenato, and S. S. Sastry, 2006b, "Flapping flight for biomimetic robotic insects: part II, flight control design." IEEE. Trans. Robot. **22**, 789.

Dickinson, M. H., 1994, "The Effects of wing rotation on unsteady aerodynamic performance at low Reynolds numbers," J. Exp. Biol. **192**, 179.

Dickinson, M. H., 1999, "Haltere-mediated equilibrium reflexes of the fruit fly, Drosophila melanogaster," Phil. Trans. R. Soc. B **354**, 903.

Dickinson, M. H., 2006, "Insect flight," Curr. Biol. **16**, R309.

Dickinson, M. H., C. T. Farley, R. J. Full, M. A. R. Koehl, R. Kram, and S. Lehman, 2000, "How animal move: an integrative view," Science **288**, 100.

Dickinson, M. H., F. O. Lehman, and K. G. Götz, 1993, "The active control of wing rotation by Drosophila," J. Exp. Biol. **182**, 173.

Dickinson, M. H., F. O. Lehman, and S. P. Sane, 1999, "Wing rotation and the aerodynamic basis of insect flight," Science **284**, 1954.

Dickson, W. B., P. Polidoro, M. M. Tanner, and M. H. Dickinson, 2010 "A linear systems analysis of the yaw dynamics of a dynamically scaled insect model," J. Exp. Biol. **213**, 3047.

Dickson, W. B., A. D. Straw, and M. H. Dickinson, 2008, "Integrative model of Drosophila flight," AIAA J. **46**, 2150.

Du, G., and M. Sun, 2010, "Effects of wing deformation on aerodynamic forces in hovering hoverflies," J. Exp. Biol. **213**, 2273.

Du, G., and M. Sun, 2012, "Aerodynamic effects of corrugation and deformation in flapping wings of hovering hoverflies," J. Theor. Biol. **300**, 19.

Dudley, R., 1990, "Biomechanics of flight in neotropical butterflies: Morphometrics and kinematics," J. Exp. Biol. **150**, 37.

Dudley, R., 2000, *The Biomechanics of Insect Flight: Form, Function, Evolution* (Princeton University Press, Princeton, NJ).

Dudley, R., and C. P. Ellington, 1990a, "Mechanics of forward flight in bumblebees. I. Kinematics and morphology," J. Exp. Biol. **148**, 19.

Dudley, R., and C. P. Ellington, 1990b, "Mechanics of forward flight in bumblebees. II. Quasi-steady lift and power requirements," J. Exp. Biol. **148**, 53.

Ellington, C. P., 1984a, "Aerodynamics of hovering insect flight. I. The quasi-steady analysis," Phil. Trans. R. Soc. B **305**, 1.

Ellington, C. P., 1984b, "The aerodynamics of hovering insect flight. II. Morphological parameters," Phil. Trans. R. Soc. B **305**, 17.

Ellington, C. P., 1984c, "Aerodynamics of hovering insect flight. III. Kinematics," Phil. Trans. R. Soc. B **305**, 41.

Ellington, C. P., 1984d, "The aerodynamics of hovering insect flight. IV. Aerodynamic mechanisms," Phil. Trans. R. Soc. B **305**, 79.

Ellington, C. P., 1984e, "The aerodynamics of hovering insect flight. VI. Lift and power requirements," Phil. Trans. R. Soc. B **305**, 145.

Ellington, C. P., 1991, "Aerodynamics and the origin of insect flight," Adv. Insect Physiol. **23**, 171.

Ellington, C. P., 1995, "Biological fluid dynamics," edited by C. P. Ellington and T. J. Pedley, Symp. Soc. Exp. Biol. **49**, 109.

Ellington, C. P., 1999, "The novel aerodynamics of insect flight: applications to micro-air vehicles," J. Exp. Biol. **202**, 3439.

Ellington, C. P., K. E. Machin, and T. M. Casey, 1990, "Oxygen consumption of bumblebees in forward flight," Nature (London) **347**, 472.

Ellington, C. P., C. van den Berg, A. P. Willmott, and A. L. R. Thomas, 1996, "Leading edge vortices in insect flight," Nature (London) **384**, 626.

Elzinga, M. J., W. B. Dickson, and M. H. Dickinson, 2012, "The influence of sensory delay on the yaw dynamics of a flapping insect," J. R. Soc. Interface **9**, 1685.

Ennos, A. R., 1988, "The importance of torsion in the design of insect wings," J. Exp. Biol. **140**, 137.

Ennos, A. R., 1989, "The kinematics and aerodynamics of the free flight of some Diptera," J. Exp. Biol. **142**, 49.

Etkin, B., and L. D. Reid, 1996, *Dynamics of Atmospheric Flight* (John Wiley and Sons, Inc., New York).

Farina, W. M., D. Kramer, and D. Varju, 1995, "The response of the hovering hawk moth Macroglossum stellatarum to translatory pattern motion," J. Comp. Physiol. A **176**, 551.

Farina, W. M., D. Varju, and Y. Zhou, 1994, "The regulation of distance to dummy flowers during hovering flight in the hawk moth Macroglossum stellatarum," J. Comp. Physiol. A **174**, 239.

Faruque, I., and J. S. Humbert, 2010a "Dipteran insect flight dynamics. Part 1: Longitudinal motion about hover," J. Theor. Biol. **264**, 538.

Faruque, I., and J. S. Humbert, 2010b, "Dipteran insect flight dynamics. Part 2: Lateral-directional motion about hover," J. Theor. Biol. **265**, 306.

Fontaine, E. I., F. Zabala, M. H. Dickinson, and J. W. Burdick, 2009, "Wing and body motion during flight initiation in Drosophila revealed by automated visual tracking," J. Exp. Biol. **212**, 1307.

Fry, S. N., R. Sayaman, and M. H. Dickinson, 2003, "The aerodynamics of free-flight maneuvers in Drosophila," Science **300**, 495.

Fry, S. N., R. Sayaman, and M. H. Dickinson, 2005, "The aerodynamics of hovering flight in Drosophila," J. Exp. Biol. **208**, 2303.

Fung, Y. C., 1969, *An Introduction to the Theory of Aeroelasticity* (Dover, New York).

Gebert, G., P. Gallmeier, and J. Evers, 2002, "Equations of motion for flapping flight," AIAA paper 2002-4872..

Govind, C. K., and J. W. T. Dandy, 1972, "Non-fibrillar muscles and the start and cessation of flight in the milkweed bug, Oncopeltus," J. Comp. Physiol. **77**, 398.

Graetzel, C. F., B. J. Nelson, and S. N. Fry, 2010, "Frequency response of lift control in Drosophila," J. R. Soc. Interface **7**, 1603.

Graham, D., and D. T. McRuer, 1961, *Analysis of nonlinear control systems* (Wiley, New York).

Grimaldi, D., and M. S. Engel, 2005, *Evolution of the insects* (Cambridge University Press, Cambridge, England).

Hedrick, T. L., B. Cheng, and X. Deng, 2009, "Wingbeat Time and the Scaling of Passive Rotational Damping in Flapping Flight," Science **324**, 252.

Hedrick, T. L., and T. L. Daniel, 2006, "Flight control in the hawkmoth Manduca sexta: the inverse problem of hovering," J. Exp. Biol. **209**, 3114.

Hohenemser, K., 1939, "Dynamic stability of a helicopter with hinged rotor blades," NACA TM 907.

Humbert, J., and I. Faruque, 2011, "Analysis of insect-inspired wingstroke kinematic perturbations for longitudinal control," J. Guid. Control **34**, 618.

Johnson, W., 1980, *Helicopter theory* (Dover Publications, New York).

Kern, R., J. van Hateren, C. Michaelis, J. Lindemann, and M. Egelhaaf, 2005, "Function of a Fly Motion-Sensitive Neuron Matches Eye Movements During Free Flight," PLoS Biol. **3**, e171.

Kern, R., and D. Varju, 1998, "Visual position stabilization in the hummingbird hawk moth, Macroglossum stellatarum L. I. Behavioral analysis," J. Comp. Physiol. A **182**, 225.

Krishnan, A., S. Prabhakar, S. Sudarsan, and S. P. Sane, 2012, "The neural mechanisms of antennal positioning in flying moths," J. Exp. Biol. **215**, 3096.

Lan, S. L., and M. Sun, 2001, "Aerodynamic properties of a wing performing unsteady rotational motions at low Reynolds number," Acta Mech. **149**, 135.

Land, M. F., and T. S. Collett, 1974, "Chasing behaviour of house flies (Fannia canicularis), A description and analysis," J. Comp. Physiol. **89**, 331.

Land, M. F., and D. E. Nilsson, 2002, *Animal Eyes* (Oxford University Press, Oxford).

Liao, J. C., D. N. Beal, G. V. Lauder, and M. S. Triantafyllou, 2003, "Fish exploiting vortices decrease muscle activity," Science **302**, 1566.

Lighthill, M. J., 1973, "On the Weis-Fogh mechanism of lift generation," J. Fluid Mech. **60**, 1.

Liu, H., C. P. Ellington, K. Kawachi, C. van den Berg, and A. P. Willmott, 1998, "A computational fluid dynamic study of hawkmoth hovering," J. Exp. Biol. **201**, 461.

Liu, H., and K. Kawachi, 1998, "A numerical study of insect flight," J. Comput. Phys. **146**, 124.

Liu, H., T. Nakata, N. Gao, M. Maeda, H. Aono, and W. Shyy, 2010, "Micro air vehicle-motivated computational biomechanics in bio-flights: aerodynamics, flight dynamics and maneuvering stability," Acta Mech. Sin. **26**, 863.

Liu, Y. P., and M. Sun, 2008, "Wing kinematics measurement and aerodynamics of hovering drone-flies," J. Exp. Biol. **211**, 2014.

Ma, K. Y., P. Chirarattananon, S. B. Fuller, and R. J. Wood, 2013, "Controlled flight of a biologically inspired, insect-scale robot," Science **340**, 603.

Maxworthy, T., 1979, "Experiments on the Weis-Fogh mechanism of lift generation by insects in hovering flight," J. Fluid Mech. **93**, 47.

Moreno, C., M. Tu, and T. Daniel, 2000, "Visualmotor feedback in the tracking behavior of hovering Manduca sexta," American Zoologist **40**, 1138.

Mou, X. L., Y. P. Liu, and M. Sun, 2011 "Wing motion measurement and aerodynamics of hovering true hoverflies," J. Exp. Biol. **214**, 2832.

Nakata, T., and H. Liu, 2012 "Aerodynamic performance of a hovering hawkmoth with flexible wings: a computational approach," Proc. R. Soc. B **279**, 722.

Newman, D. J. S., and R. J. Wootton, 1986, "An approach to the mechanics of pleating in dragonfly wings," J. Exp. Biol. **125**, 361.

Norberg, R. A., 1975, "Hovering flight of the dragonfly Aeschna juncea L., kinematics and aerodynamics," *Swimming and Flying in Nature* edited by T. Y. Wu, C. J. Brokaw, and C. Brennen (Plenum Press, NewYork), pp. 763–781.

Okamoto, M., K. Yasude, and A. Azuma, 1996, "Aerodynamic characteristics of the wings and body of a dragonfly," J. Exp. Biol. **199**, 281.

Padfield, G. D., 1996, *Helicopter Flight Dynamics* (Blackwell Science Ltd, Oxford).

Pesavento, U., and Z. J. Wang, 2004, "Falling paper: Navier-Stokes solutions, model of fluid forces, and center of mass elevation," Phys. Rev. Lett. **93**, 144501.

Pringle, J. W. S., 1948, "The gyroscopic mechanism of the halteres of Diptera," Phil. Trans. R. Soc. B **233**, 347.

Ramamurit, R., and W. C. Sandberg, 2002, "A three-dimensional computational study of the aerodynamic mechanisms of insect flight," J. Exp. Biol. **205**, 1507.

Ramamurit, R., and W. C. Sandberg, 2007, "A computational investigation of the three-dimensional unsteady aerodynamics of Drosophila hovering and maneuvering," J. Exp. Biol. **210**, 881.

Rees, C. J. C., 1975, "Form and function in corrugated insect wings," Nature (London) **256**, 200.

Reichardt, W., and T. Poggio, 1976 "Visual control of orientation behaviour in the fly: Part I. A quantitative analysis" Q. Rev. Biophys. **9**, 311.

Ristroph, L., A. J. Bergou, G. Ristroph, K. Coumes, G. J. Berman, J. Guckenheimer, Z. J. Wang, and I. Cohen, 2010, "Discovering the Flight Auto-stabilizer of Fruit flies by Inducing Aerial Stumbles," Proc. Natl. Acad. Sci. U.S.A. **107**, 4820.

Ristroph, L., G. J. Berman, A. J. Bergou, Z. J. Wang, and I. Cohen, 2009, "Automated hull reconstruction motion tracking (HRMT) applied to sideways maneuvers of free-flying insects," J. Exp. Biol. **212**, 1324.

Rohrseitz, N., and S. N. Fry, 2011, "Behavioural system identification of visual light speed control in Drosophila melanogaster." J. R. Soc. Interface **8**, 171.

Rugh, W. J., 1996, *Linear system theory* (Prentice-Hall, Inc., Upper Saddle River, NJ).

Ruppell, G., 1989, "Kinematical analysis of semmetrical flight manoeuvers of odonata," J. Exp. Biol. **144**, 13.

Sandeman, D. C., and H. Markl, 1980, "Head movements in flies (Calliphora) produced by deflexion of the halteres," J. Exp. Biol. **85**, 43.

Sane, S. P., 2003, "The aerodynamics of insect flight," J. Exp. Biol. **206**, 4191.

Sane, S. P., and M. H. Dickinson, 2001, "The control of flight force by a flapping wing: lift and drag production," J. Exp. Biol. **204**, 2607.

Sane, S. P., and M. H. Dickinson, 2002, "The aerodynamic effects of wing rotation and a revised quasi-steady model of flapping flight," J. Exp. Biol. **205**, 1087.

Sane, S. P., A. Dieudonne, M. A. Willis, and T. L. Daniel, 2007, "Antennal mechanosensors mediate flight control in moths," Science **315**, 863.

Schenato, L., 2003, "Analysis and control of flapping flight: from biological to robotic insects," Ph.D. thesis, Electrical Engineering and Computer Science, University of California at Berkeley.

Serres, J., F. Ruffier, S. Viollet, and N. Franceschini, 2006, "Toward optic flow regulation for wall-following and centering behaviors," International Journal of Advanced Robotic Systems **3**, 147.

Sherman, A., and M. H. Dickinson, 2003, "A comparison of visual and haltere-mediated equilibrium reflexes in the fruit fly Drosophila melanogaster," J. Exp. Biol. **206**, 295.

Shyy, W., H. Aono, S. K. Chimakurthi, P. Trizila, C. K. Kang, C. E. S. Cesink, and H. Liu, 2010, "Recent progress in flapping wing aerodynamics and aeroelasticity," Prog. Aerosp. Sci. **46**, 284.

Shyy, W., M. Berg, and D. Ljungqvist, 1999, "Flapping and flexible wings for biological and micro air vehicles," Prog. Aerosp. Sci. **35**, 455.

Sprayberry, J. D. H., and T. L. Daniel, 2007, "Flower tracking in hawkmoths: behavior and energetics," J. Exp. Biol. **210**, 37.

Stevens, B. L., and Lewis, F. L. (2003), *Aircraft control and simulation* (John Wiley and Sons, Inc, Hoboken, NJ).

Straw, A. D., S. Lee, and M. H. Dickinson, 2010, "Visual control of altitude in flying Drosophila," Curr. Biol. **20**, 1550.

Sun, M., and G. Du, 2003, "Lift and power requirements of hovering insect flight," Acta Mech. Sin. **19**, 458.

Sun, M., and J. Tang, 2002, "Unsteady aerodynamic force generation by a model fruit-fly wing," J. Exp. Biol. **205**, 55.

Sun, M., and J. K. Wang, 2007, "Flight stabilization control of a hovering model insect," J. Exp. Biol. **210**, 2714.

Sun, M., J. K. Wang, and Y. Xiong, 2007, "Dynamic flight stability of hovering insects," Acta Mech. Sin. **23**, 231.

Sun, M., and J. H. Wu, 2004, "Large aerodynamic force generation by a sweeping wing at low Reynolds number," Acta Mech. Sin. **20**, 24.

Sun, M., and Y. Xiong, 2005, "Dynamic flight stability of a hovering bumblebee," J. Exp. Biol. **208**, 447.

Sunada, S., K. Kawachi, I. Watanabe, and A. Azuma, 1993, "Performance of a butterfly in take-off flight," J. Exp. Biol. **183**, 249.

Tammero, L. F., and M. H. Dickinson, 2002, "The influence of visual landscape on the free flight behavior of the fruit fly Drosophila melanogaster," J. Exp. Biol. **205**, 327.

Tanaka, K., and K. Kawachi, 2006, "Response characteristics of visual altitude control system in Bombus terrestris," J. Exp. Biol. **209**, 4533.

Taylor, G. K., 2001, "Mechanics and aerodynamics of insect flight control," Biol. Rev. Camb. Philos. Soc. **76**, 449.

Taylor, G. K., M. Bacic, R. J. Bomphrey, A. C. Carruthers, J. Gillies, S. M. Walker, and A. L. R. Thomas, 2008, "New experimental approaches to the biology of flight control systems," J. Exp. Biol. **211**, 258.

Taylor, G. K., and H. G. Krapp, 2007, "Sensory systems and flight stability: what do insects measure and why?," *Insect Mechanics and Control, 34 of Advances in Insect Physiology* edited by J. Casas, and S. J. Simpson (Academic Press, London), pp. 231–316.

Taylor, G. K., and A. L. R. Thomas, 2002, "Animal flight dynamics. II. Longitudinal stability in flapping flight," J. Theor. Biol. **214**, 351.

Taylor, G. K., and A. L. R. Thomas, 2003, "Dynamic flight stability in the desert locust Schistocerca gregaria," J. Exp. Biol. **206**, 2803.

Taylor, G. K., and R. Zbikowski, 2005, "Nonlinear time-periodic models of the longitudinal flight dynamics of desert locusts Schistocerca gregaria," J. R. Soc. Interface **2**, 197.

Tischler, M. B., and R. K. Remple, 2006, *Aircraft and rotorcraft system identification: Engineering methods with flight-test examples* (AIAA, Reston, VA).

Usherwood, J. R., and C. P. Ellington, 2002a, "The aerodynamics of revolving wings. I. Model hawkmoth wings," J. Exp. Biol. **205**, 1547.

Usherwood, J. R., and C. P. Ellington, 2002b, "The aerodynamics of revolving wings. II. Propeller force coefficients from mayfly to quail," J. Exp. Biol. **205**, 1565.

van den Berg, C., and C. P. Ellington, 1997a, "The vortex wake of a 'hovering' model hawkmoth," Phil. Trans. R. Soc. B **352**, 317.

van den Berg, C., and C. P. Ellington, 1997b, "The three-dimensional leading-edge vortex of a 'hovering' model howkmoth. Phil. Trans. R. Soc. B **352**, 329.

Vogel, S., 1966, "Flight in Drosophila. I. Flight performance of tethered flies," J. Exp. Biol. **44**, 567.

Vogel, S., 1967a, "Flight in Drosophila. II. Variations in stroke parameters and wing contour," J. Exp. Biol. **46**, 383.

Vogel, S., 1967b, " Flight in Drosophila. III. Aerodynamic characteristics of fly wings and wing models," J. Exp. Biol. **46**, 431.

Wagner, H., 1925, "Über die Entstehung des dynamischen Äuftriebes von Tragflügeln," Z. Angew. Math. Mech. **5**, 17.

Wakeling, J. M., and C. P. Ellington, 1997 "Dragonfly flight, II. velocities, accelerations and kinematics of flapping flight," J. Exp. Biol. **200**, 557.

Walker, P. B., 1931, " Experiments on the growth of circulation about a wing and an apparatus for measuring fluid motion," Rep. Memo. Aeronaut. Res. (Great Britain) No. 1402.

Walker, S. M., A. L. R. Thomas, and G. K. Taylor, 2010, "Deformable wing kinematics in free-flying hoverflies," J. R. Soc. Interface **7**, 131.

Wang, H., L. Zeng, H. Liu, and C. Yin, 2003, "Measuring wing kinematics, flight trajectory and body attitude during forward flight and turning maneuvers in dragonflies," J. Exp. Biol. **206**, 745.

Wang, H., L. J. Zeng, and C. Y. Yin, 2002 "Measuring the body position, attitude and wing deformation of a free-flight dragonfly by combining a comb fringe pattern with sign points on the wing," Meas. Sci. Technol. **13**, 903.

Wang, Z. J., 2000a, "Vortex shedding and frequency selection in flapping flight," J. Fluid Mech. **410**, 323.

Wang, Z. J., 2000b, "Two dimensional mechanism for insect hovering," Phys. Rev. Lett. **85**, 2216.

Wang, Z. J., 2005, "Dissecting Insect Flight," Annu. Rev. Fluid Mech. **37**, 183.

Wang, Z. J., J. M. Birch, and M. H. Dickinson, 2004, "Unsteady forces and flows in low Reynolds number hovering flight: two-dimensional computations vs robotic wing experiments," J. Exp. Biol. **207**, 449.

Wang, Z. J., and D. Russell, 2007, "Effect of forewing and hindwing interactions on aerodynamic forces and power in hovering dragonfly flight," Phys. Rev. Lett. **99**, 148101.

Weis-Fogh, T., 1972, "Energetics of hovering flight in hummingbirds and in Drosophila," J. Exp. Biol. **56**, 79.

Weis-Fogh, T., 1973, "Quick estimates of flight fitness in hovering animals, including novel mechanisms for lift production," J. Exp. Biol. **59**, 169.

Weis-Fogh, T., and M. Jensen, 1956, "Biology and physics of locust flight. I. Basic principles of insect flight. A critical review," Phil. Trans. R. Soc. B **239**, 415.

Willmott, A. P., and C. P. Ellington, 1997a, "The mechanics of flight in the hawkmoth Manduca Sexta. I. Kinematics of hovering and forward flight," J. Exp. Biol. **200**, 2705.

Willmott, A. P., and C. P. Ellington, 1997b, "The mechanics of flight in the hawkmoth Manduca sexta. II. Aerodynamic consequences of kinematic and morphological variation," J. Exp. Biol. **200**, 2723.

Wilson, J., 2001, "Micro Warfare," Popular Mechanics **2**, 62.

Wootton, R. J., 1981, "Palaeozoic insects," Annu. Rev. Entomol. **26**, 319.

Wu, J. C., 1981, "Theory for aerodynamic force and moment in viscous flow," AIAA J. **19**, 432.

Wu, J. H., and M. Sun, 2004, "Unsteady aerodynamic forces of a flapping wing," J. Exp. Biol. **207**, 1137.

Wu, J. H., and M. Sun, 2005, "The influence of the wake of a flapping wing on the production of aerodynamic forces," Acta Mech. Sin. **21**, 411.

Wu, J. H., and M. Sun, 2009, "Control for going from hovering to small speed flight of a model insect," Acta Mech. Sin. **25**, 295.

Wu, J. H., and M. Sun, 2012, "Floquet stability analysis of the longitudinal dynamics of two hovering model insects," J. R. Soc. Interface **9**, 2033.

Wu, J. H., Y. L. Zhang, and M. Sun, 2009, "Hovering of model insects: simulation by coupling equations of motion with Navier-Stokes equations," J. Exp. Biol. **212**, 3313.

Wu, T. Y., 2011, "Fish swimming and bird/insect flight," Annu. Rev. Fluid Mech. **43**, 25.

Xiong, Y., and M. Sun, 2008, "Dynamic flight stability of a bumblebee in forward flight" Acta Mech. Sin. **24**, 25.

Xiong, Y., and M. Sun, 2009, "Stabilization control of a bumble bee in hovering and forward flight," Acta Mech. Sin. **25**, 13.

Xu, N., and M. Sun, 2013, "Lateral dynamic flight stability of a model bumblebee in hovering and forward flight," J. Theor. Biol. **319**, 102.

Young, J., S. M. Walker, R. J. Bomphrey, G. K. Taylor, and L. R. Thomas, 2009, "Details of insect wing design and deformation enhance aerodynamic function and flight efficiency," Science **325**, 1549.

Yu, Y., B. Tong, and H. Ma, 2003, "An analytic approach to theoretical modeling of highly unsteady viscous flow excited by wing flapping in small insects," Acta Mech. Sin. **19**, 508.

Zanker, J. M., 1990, "The wing beat of Drosophila melanogasterI. Kinematics," Phil. Trans. R. Soc. B **327**, 1.

Zbikowski, R., 2002, "On aerodynamic modelling of an insect-like flapping wing in hover for micro air vehicles," Phil. Trans. R. Soc. A **360**, 273.

Zbikowski, R., S. A. Ansari, and K. Knowles, 2006, "On mathematical modelling of insect flight dynamics in the context of micro air vehicles," Bioinsp. Biomim. **1**, R26.

Zhang, Y., and M. Sun, 2010a, "Wing kinematics measurement and aerodynamics of free-flight maneuvers in drone-flies," Acta Mech. Sin. **26**, 371.

Zhang, Y. L., and M. Sun, 2010b, "Dynamic of flight stability a hovering model insect: lateral motion," Acta Mech. Sin. **26**, 175.

Zhang, Y. L., and M. Sun, 2010c, "Dynamic flight stability of hovering model insects: theory vs. simulation using equations of motion coupled with Navier-Stokes equations," Acta Mech. Sin. **26**, 509.

Zhang, Y., and M. Sun, 2011a, "Stabilization control of a hovering model insect: lateral motion," Acta Mech. Sin. **27**, 823.

Zhang, Y., and M. Sun, 2011b, "Control for small-speed lateral flight in a model insect," Bioinsp. Biomim. **6**, 036003.

Zhang, Y., J. H. Wu, and M. Sun, 2012, "Lateral dynamic flight stability of hovering insects: theory vs. numerical simulation," Acta Mech. Sin. **28**, 221.

Zhao, L., Q. F. Huang, X. Y. Deng, and S. P. Sane, 2010, "Aerodynamic effects of flexibility in flapping wings," J. R. Soc. Interface **7**, 485.